

Magnetolectric laminated composites and devices

By

Junyi Zhai

Dissertation submitted to the faculty of the
Virginia Polytechnic Institute and State University
in partial fulfillment of the requirement for the degree of
Doctor of Philosophy
in
Materials Science and Engineering

Dwight D. Viehland (Chair)
Jie-Fang Li
Alex Aning
Yu Wang
Shashank Priya

Feb 10th 2009
Blacksburg, Virginia

Keywords: Magnetolectric, piezoelectric, magnetostrictive, devices, laminates,
composites, energy harvester.

© Copyright 2009, Junyi Zhai

Magnetolectric laminated composites and devices

Junyi Zhai

ABSTRACT

Since the turn of the millennium, giant magnetolectric (ME) effects have been found in laminated composites of piezoelectric and magnetostrictive layers. Compared to ME single phase and two phase particulate composites, laminated composites have much higher ME coefficients and are also readily fabricated. In this thesis, I have investigated ME effect in laminated composites including materials, structures, fundamental properties and devices.

Giant permeability Metglas was incorporated in ME laminates. The piezomagnetic coefficient of the Metglas is larger than that of widely used magnetostrictive materials, such as Terfenol-D or nickel ferrite. The experimental results show that Metglas based ME laminates have giant ME voltage coefficients and small required DC magnetic biases. Besides, the laminates have a good directional dependence of the magnetic field: it can only sense the magnetic field along its longitudinal direction. Symmetric bimorph and differential mode magnetolectric laminates have been designed to reject (decrease) thermal and vibration noise sources, respectively. The mechanism for the noise cancellation capability is that the laminate operates in a bending (or longitudinal) mode, whereas the noise is contained in the other mode.

The ME susceptibility (α_{me}) is the fundamental property that describes the coupling between the polarization and magnetization of a ME media. It is a complex

quantity (α_{me}^*). I discuss the relationship of the ME susceptibility between the magnetic permeability, dielectric permittivity of the materials, and the widely used ME voltage coefficient. The shape of the magnetic layer has a large impact on the giant permeability due to shape demagnetization effects. A long, thin and narrow shape increases the ME voltage coefficient and decreases the required optimum DC bias. The resonance frequency of Terfenol-D/PZT laminates can be continuously tuned by magnetic field over a wide range. This large tunability is due to the large magnetostriction of Terfenol-D. It results in a dramatic increase in the bandwidth over which devices might take advantage of the resonance enhanced ME coefficient.

Four device applications have also been studied based on the giant ME effect of laminate composites. (i) ME laminates offer much potential for low-frequency (10^2 to 10^3 Hz) detection of minute magnetic fields (10^{-12} Tesla or below) in a passive mode of operation. With a wrapped active coil, the Metglas/PZT laminates are also capable of detecting changes of 0.8 nano-Tesla in DC magnetic fields without an applied DC bias. (ii) A geomagnetic field sensor is shown to have high sensitivity to variations in Earth's field of $H_{DC}=0.8$ nano-Tesla. It could offer potential applications in global positioning. (iii) Under electro-mechanical resonance drive conditions, ME laminates have been shown to have a high gyration effect. These findings indicate the potential existence of a fifth fundamental network element. (iv) A multimodal system has been developed for simultaneously harvesting mechanical vibration and magnetic energies.

To my parents, sister and wife,

Acknowledgements

I would like to express my sincere gratitude to my advisors Dr. Dwight Viehland and Dr. Jiefang Li for their faith, guidance and support throughout the course of my Ph.D. research and also for giving me the opportunity to work on these interesting projects. .

I am deeply indebted to my advisor, Dr. Dwight Viehland, for his constant guidance, support, allowance of freedom during the entire course of this work. I would like to thank him for his trust in my abilities and his continuous efforts to bring the best out of me. The improvements that he has brought in me over the years will help me for the rest of my career. His professional and personable attitude has guided me in a variety of ways and has made my stay at Virginia Tech a very rewarding and memorable experience.

Equally important, Jiefang has given me great help in almost all equipment and facilities setup. She generously shared all her knowledge and experience in experimental techniques. Without her help, my research would not be so successful.

I am grateful to Dr. Alex Aning, Dr. Shashank Priya and Dr. Yu Wang for serving as my thesis reading committee and their part in guiding and supporting this work.

In particular, I would like to acknowledge the tremendous help that Dr. Shuxiang Dong had provided for a long time, who greatly helped me to develop expertise in magnetoelectric materials and devices.

I would like to thank Dr. M.I. Bichurin for all the valuable discussion we held on magnetoelectric susceptibility and gyrator as related to this dissertation.

I would like to thank Mr. Zengping Xing, who will be Dr. Xing very soon in our group. We shared a lot in this project and I learned detailed analysis to noise from him during my study here.

I am grateful to David Berry and Dr. Carlos Suchicital for help with the experiments and insightful discussions.

I would like to thank Feiming Bai, Hu Cao, Li Yan, Yaodong Yang, Chris DeVreugd and Junqi Gao, whom are students in our research group. We have had very close cooperation and discussions we held in the view of real application of current

project. I thank all other group members: it will be always a good memory to work with these guys.

Last, but most importantly, I wish to express my deepest appreciation to my family. I am eternally indebted to my parents, Yuzhang Zhai and Yinjie Liu, for their wholehearted and endless support over the years. I would also like to thank my sister, Suwan Zhai for her understanding, patience and encouragement when it was most required. I would like to express my gratitude to my wife, Juan Liu. She have been constantly providing faith, encourage and enjoyment during my Ph.D study.

Table of contents

ABSTRACT.....	ii
DEDICATION.....	iv
ACKNOWLEDGEMENTS.....	v
TABLE OF CONTENTS.....	vii
LIST OF TABLES.....	ix
LIST OF FIGURES.....	x
1. INTRODUCTION.....	1
1.1 Magnetolectric effect.....	1
1.2 Piezoelectric and magnetostrictive materials.....	3
1.2.1 Piezoelectricity and piezoelectric materials.....	3
1.2.2 Magnetostriction and magnetostrictive materials.....	7
1.3 Magnetolectric laminated composites.....	12
1.3.1 All ceramic ME laminated composites.....	12
1.3.2 Ceramic/alloy ME composites.....	17
1.3.3 Working mode of ME laminates.....	18
1.3.4 Quasi-static Calculation.....	27
1.3.5 Frequency dependent response - an equivalent circuit method.....	29
1.4 Section summary.....	32
2. PURPOSE OF THIS THESIS.....	33
3. MAGNETOELECTRIC LAMINATED COMPOSITES AND STRUCTURES..	36
3.1 Introduction.....	36
3.2 New Metglas-based ME laminates.....	37
3.2.1 Metglas/PVDF.....	39
3.2.2 Metglas/PZT fiber.....	45
3.3 New ME structure designs.....	49
3.3.1 Symmetric bimorph design.....	51
3.3.2 Differential mode.....	57
3.4 Section summary.....	61
4. FUNDAMENTAL ME PROPERTIES.....	65
4.1 ME susceptibility.....	65

4.2 Demagnetization (shape) and magnetization distribution (position) effects...	76
4.3 Magnetic field tunability of resonance frequency: enhanced effective bandwidth.....	84
4.4 Section summary.....	92
5. MAGNETOELECTRIC DEVICES AND APPLICATIONS.....	94
5.1 Ultra-sensitive magnetic field sensors.....	94
5.1.1 Passive AC magnetic sensor.....	95
5.1.2 Active DC magnetic sensor.....	103
5.2 Geomagnetic sensor.....	106
5.3 Gyration.....	113
5.4 Energy harvester.....	121
5.5 Section summary.....	129
6. CONCLUSION AND FUTURE WORK.....	131
6.1 Conclusion.....	131
6.2 Suggested future work.....	133
REFERENCE.....	135

LIST OF TABLES

Table 1.1 Properties of piezoelectric materials.....	8
Table 1.2 Properties of magnetostrictive materials.....	12
Table 1.3 ME voltage coefficient of different mode.....	23
Table 4.1 Modules of the ME susceptibility for various ME laminate composites, and different mode configurations.....	68

LIST OF FIGURES

Figure 1.1 Direct piezoelectric effect.....	4
Figure 1.2 Converse piezoelectric effect.....	5
Figure 1.3 Domain rotate under applied magnetic field.....	9
Figure 1.4 Schematic graph of magnetoelectric laminated composites.....	12
Figure 1.5 Transverse ME voltage coefficient at room temperature as a function of static magnetic field H for a two-layer structure consisting of 200-nm films of NFO and PZT.....	15
Figure 1.6 (a) An optical and (b) scanning electron micrograph of the fractured surface of the sandwiched PZT/NiF ₂ O ₄ /PZT ceramics.....	16
Figure 1.7 (a) Induced ME voltages as a function of DC magnetic field of Terfenol-D/PZT/Terfenol-D trilayers. The polarization direction of PZT and is along the longitudinal direction. (b) Frequency dependence of the ME voltage coefficient for 1 f <math><100</math> kHz. These data were taken using a <math>h_{dc}=550< <math>h_{ac}="1</math>" and="" math>="" oe="" oe.....<="" td=""> <td style="text-align: right;">19</td> </math>h_{dc}=550<>	19
Figure 1.8 Schematic illustration of the various ME coupling modes (a) L-L; (b) T-L; (c) L-T; and (d) T-T.....	21
Figure 1.9 Schematic illustration of the various ME coupling mode push-pull mode.....	24
Figure 1.10 Schematic illustration of the various ME coupling ring modes (a) L-T; and (b) 4 parts push-pull.....	25
Figure 1.11 Schematic illustration of the various ME coupling mode (a) Unimorph mode; and (b) Three phase unimorph mode.....	28
Figure 1.12 ME equivalent circuit under free-free boundary conditions.....	31
Figure 3.1 (a) Photograph of a Metglas/PVDF unimorph laminate; and the structure of (b) the unimorph configuration, and (c) the 3-layer L-T sandwich configuration. In both configurations, the Metglas layer(s) were longitudinally magnetized, whereas the piezoelectric ones were transversely poled.....	40
Figure 3.2. (a) DC magnetic field dependence of the ME voltage coefficient and phase for a Metglas/PVDF 3-layer laminate, measured at 1 kHz and <math>h_{ac} (b)<="" 1<="" =="" math>="" oe;="" td=""> <td></td> </math>h_{ac}>	

magnetostriction (closed square) and piezomagnetic coefficient (open dot) for a Metglas (2605 SA1) layer in the L-T mode.....42

Figure 3.3 Frequency dependence ($10^2 < f < 10^5$ Hz) of the ME voltage coefficient of both 3-layer Metgals(SA1)/PVDF and unimorph Metglas(CO)/PVDF laminates measured under $H_{dc}=80e$ and $H_{ac}=10e$. The inset shows the ME voltage coefficient of both laminate types at low frequencies, illustrating a bending-mode enhancement in the unimorph at 110Hz.....44

Figure 3.4. Illustration of the FeBSiC/piezofiber (*L-L*) laminate configuration. It consists of a (1-3) piezoelectric active fiber/epoxy composited (AFC) thin layer where the fibers are oriented along the longitudinal axis, which is laminated between two FeBSiC layers. Insulating Kapton films with inter-digitated (ID) electrodes were placed between layers. Each piezo-fiber had numerous alternating symmetric longitudinally-poled ('push-pull' units) that were each $2l_p=1mm$ in length, as shown in the inset.....46

Figure 3.5. Magnetolectric characterizations of FeBSiC/piezofiber laminates: (a) the (*L-L*) ME voltage coefficient $\alpha_{ME}^{(L-L)}$ as a function of H_{dc} for both short (30mm) and long (100mm) laminates; (b) $\alpha_{ME}^{(L-L)}$ as a function of frequency illustrating a strong enhancement at the electromechanical resonance frequency, where the inset shows a flat response over the quasi-static frequency range.....48

Figure 3.6 anisotropy of α_{ME} for H_{ac} applied along the length ($\alpha_{ME}^{(L-L)}$), width ($\alpha_{ME}^{(T1-L)}$) and thickness ($\alpha_{ME}^{(T2-L)}$) of the laminate.....50

Figure 3.7 Schematic of the symmetric bimorph mode laminate with U shape DC magnetic biases.....52

Figure 3.8. Frequency dependence ($10^2 < f < 10^5$ Hz) of the ME voltage coefficient for the symmetric bimorph and LT modes. These laminates have the same dimensions and were constructed from Terfenol-D and PZT layers of the same size.....54

Figure 3.9 Time dependence of the voltage induced by an ac magnetic field of $H_{ac}=1.2 \times 10^{-7}$ Tesla ($f=1$ Hz) for (a) this symmetric bimorph, and (b) a LT

mode laminate. At time $t=6.5s$, temperature increased $1^{\circ}C$ by thermoelectric plate.....56

Figure 3.10 The schematic graph of the vibration differential design. The insert 2 layers are PZT fiber layer. The inset figure shows structure of each section. The small square is the electrodes. The arrow is the poling direction of the PZT fiber.....58

Figure 3.11 Demonstration of vibration noise cancellation by differential mode. Signal 1 and 2 are the voltages generated by vibration of top and bottom PZT layer respectively, the line in the center is the differential result of signal 1 and 2..60

Figure 3.12 Voltages of the top and bottom PZT layer in the differential mode by applied magnetic field. The green line shows the differential result of the voltage 1 and voltage 2.....64

Figure 4.1 The real (left-hand side) and imaginary (right-hand side) components of the ME susceptibility as a function of frequency for (a) a L-L mode configuration consisting of PZT layers laminated together with Terfenol-D ones; (b) a L-T configuration consisting of PZT layers laminated together with Terfenol-D ones; and (c) a L-T configuration consisting of PZT layers laminated together with $NiFe_2O_4$ ones. The insets show Cole-Cole or Argand-type plots of the real and imaginary components. These measurements were performed under an ac magnetic field of $H_{ac}=1Oe$, and dc magnetic bias of $H_{dc}=500Oe$71

Figure 4.2 Demonstration showing the inter-relationship (fulfilling equation 4.2) between the ME susceptibility (α_{me}) and ME voltage coefficient (α_{ME}) for a L-T PZT/Terfenol-D laminate: (a) the real components of the responses; and (b) the imaginary components.....73

Figure 4.3 Demonstration of the inherent limit of the upper magnitude of the ME susceptibility modulus ($|\alpha_{me}|$): (a) $|\alpha_{me}|$ and $\left(|K_{eff}| \bullet |\mu_{eff}| \right)^{1/2}$; and (b) the speed of an electromagnetic wave in the ME media.....75

Figure 4.4 the coordinate system used in calculating of the demagnetization for rectangle prism.....79

Figure 4.5 DC magnetic field dependence of the ME output voltage. All the laminates have the same dimensional PZT. (a)The length of the Metglas is various from

18 mm to 110 mm. (b) The thickness of the Metglas varies from 0.05mm to 0.25mm.....	80
Figure 4.6 DC magnetic field dependence of the ME output voltage of Terfenol-D/PZT. All the laminates have the same thickness and width. The length of the Metglas is various from 7 mm to 23 mm.	82
Figure 4.7 ME voltage coefficient of the (a) Metglas/PZT and (b) Terfenol-D/PZT at different position. Point 1 is the center of the laminate and point 4 is the edge of the laminate.....	83
Figure 4.8 Magnetostriction and piezomagnetic constant of the Terfenol-D/PZT laminate as a dependence of H_{DC} from 0Oe to 5000Oe. Insert graph shows a schematic graph of the Terfenol-D/PZT sandwich structure laminate.....	86
Figure 4.9 (a) Frequency dependence of the ME voltage coefficient at various H_{DC} from 300 Oe to 5000 Oe; and (b) resonance frequency and Q of the Terfenol-D/PZT laminate as a dependence of H_{DC} from 0Oe to 5000Oe.....	88
Figure 4.10 (a) Quasi-static ME voltage coefficient and enhanced resonant ME voltage coefficient of the Terfenol-D/PZT laminate as a function of H_{DC} from 0Oe to 5000Oe.....	90
Figure 5.1 Schematic view of the magneto-electric (a) bimorph and (b) push-pull laminate composite magnetic field sensors. A magnetic field is sensed by straining magnetostrictive Terfenol-D layers that are epoxied to piezoelectric $Pb(Zr_{1-x}Ti_x)O_3$ ones, which subsequently converts the stress into a voltage via piezoelectric effect. In these two designs, enhanced signal-to-noise ratio is achieved by the back-to-back configurations of the piezoelectric layers, which rejects thermal noise. In Part (c), I illustrate the rejection in the pyroelectric current achieved by using the bimorph construction, relative to a unimorph of the same geometry.....	97

Figure 5.2 Noise spectra, given in Tesla/Hz^{1/2} on the left-hand side and Coulombs/Hz^{1/2} on right-hand, for the bimorph ME laminate. These data were taken at 300K, using a high-input resistance op-amp. The sensitivity limit was about 2x10⁻¹¹ T/Hz^{1/2} (or 2x10⁻¹⁶C/Hz^{1/2}) at 1Hz. Corresponding data for the unimorph laminate have been shown in order to demonstrate the enhanced noise rejection of the thermal noise by differential detection.....99

Figure 5.3 Noise spectra, given in Tesla/Hz^{1/2}, for the push-pull ME laminate. These data were taken at 300K. The low frequency data was taken using a high-input resistance op-amp to collect charge, whereas the high frequency was taken using a voltage method. The sensitivity limit was about 2x10⁻¹¹ T/Hz^{1/2} (or 2x10⁻¹⁶C/Hz^{1/2}) at 1Hz, and about 2x10⁻¹⁵T/Hz^{1/2} at 78kHz.....100

Figure 5.4 Time-domain response to a minute magnetic field of H_{ac}=2.4x10⁻¹¹Tesla (RMS) for the push-pull laminate at 7.75x10⁴Hz.....102

Figure 5.5 The DC magnetic field dependence of the ME voltage coefficient and phase for a Metglas/PZT fiber push-pull laminate, measured at 1 kHz under an applied current of 10 mA.....105

Figure 5.6 Sensitivity of a 3-layer Metglas/PZT laminate to small variations in H_{dc}, taken under a constant H_{ac}=0.1Oe at f=18 kHz.....107

Figure 5.7 Photograph of the geomagnetic field sensor measurement setup.....109

Figure 5.8 Output voltage from the magnetoelectric sensor, when it is rotated: (a) in the Earth's plane; (b) along the North-South axis; and (c) along the East-West axis.....111

Figure 5.9 (a) Gyration equivalent circuit; (b) illustration of longitudinal-transverse or L-T mode of a magnetoelectric laminate composite consisting of longitudinally-poled Pb(Zr_xTi_{1-x})O₃ layer sandwiched between two longitudinally-

magnetized Terfenol-D layers, epoxied together with a thin insulating resin layer; and (c) schematic illustrating the experiment setup.....	114
Figure 5.10 Phase difference between open and short circuit conditions for a L-T mode PZT/Terfenol-D laminate as a function of frequency from 1 to 10^5 Hz, where I designates the PZT capacitance side of the gyrator, and 2 the inductance side of the coils.....	118
Figure 5.11 Impedance inverter property of the gyrator under different resistance loads. The inset shows the measurement circuit. Z and Z' are not coexisting. Measurement were done near a resonance frequency of 84kHz.....	120
Figure 5.12 Conceptual illustration of the magneto-electric energy harvester: (a) schmatic of the ME laminate configuration, (b) photo of the ME laminate prototype, and (c) equivalent circuit model for a bi-mechanism of energy harvesting..	123
Figure 5.13 Voltage induced by “stray” magnetic field across the prototype as a function of electrical load.....	126
Figure 5.14 Voltage induced by “stray” vibration the prototype as a function of time..	127
Figure 5.15 Experimental confirmation of the bi-mechanism for magnetic field and mechanical vibration energy harvesting: (a) under only a “stray” magnetic excitation of $H_{ac}=2Oe$ ($f=20Hz$), (b) under only a “stray” vibrational excitation of $a=50mg$ ($f=20Hz$), and (c) under both “stray” magnetic and vibrational excitations.....	128

I. Introduction

1.1 Magnetoelectric effect

The **magnetoelectric** (ME) effect is defined by the electric field (E) induced under application of a magnetic field (H); or vice versa, by the magnetic induction (B) induced under application of an electric field (E). The ME effect can be obtained from the formula of the free energy (F) as follows:¹

$$\begin{aligned} F(\vec{E}, \vec{H}) = & F_0 - P_i^S E_i - M_i^S H_i \\ & - \frac{1}{2} \varepsilon_0 \varepsilon_{ij} E_i E_j - \frac{1}{2} \mu_0 \mu_{ij} H_i H_j - \alpha_{ij} E_i H_j \quad ; \\ & - \frac{1}{2} \beta_{ijk} E_i H_j H_k - \frac{1}{2} \gamma_{ijk} H_i E_j E_k - \dots \end{aligned} \quad (1.1)$$

where μ and ε are permeability and permittivity respectively; the tensor α is the linear ME effect; the tensors β and γ are the higher order ME effects; and M and P are induced magnetization and polarization charges, respectively.

Differentiation of Eq (1.1) yields the dependence of P on E and H

$$\begin{aligned} P_i(\vec{E}, \vec{H}) = & -\frac{\partial F}{\partial E_i} = P_i^S + \varepsilon_0 \varepsilon_{ij} E_j + \alpha_{ij} H_j \\ & + \frac{1}{2} \beta_{ijk} H_j H_k + \frac{1}{2} \gamma_{ijk} H_i E_j - \dots \end{aligned} \quad ; \quad (1.2)$$

and the responding dependence of M on H and E

$$\begin{aligned} M_i(\vec{E}, \vec{H}) = & -\frac{\partial F}{\partial H_i} = M_i^S + \mu_0 \mu_{ij} H_j + \alpha_{ij} E_j \\ & + \frac{1}{2} \beta_{ijk} E_i H_j + \frac{1}{2} \gamma_{ijk} E_j E_k - \dots \end{aligned} \quad ; \quad (1.3)$$

Compared to the linear ME effect α , the higher order ME effects are smaller. So normally calculation and experiments focus on the linear ME effect, and omit the higher order ME effects.

Electronic and magnetic materials can be found everywhere in modern technology and industry. These ME materials could potentially be used for fabricating new types of sensors, actuators and data storage devices. Currently, device miniaturization requires multifunctional materials that have integrated electric and magnetic properties. In this case, a single device could potentially serve as a multifunctional one, reducing the volume of the system. Magnetoelectric materials are an important class of materials for such applications, and offer potential revolutionary device designs.

The ME effect was first observed in single crystals² of single phase materials nearly 50 years ago, and subsequently in polycrystalline single phase materials³. The largest value of α_{ME} for a single phase material is that for Cr_2O_3 crystals², where $\alpha_{ME} \approx 20\text{mV/cm-Oe}$. The ME effect of single phase materials, although scientifically interesting, has always shown only small values of α_{ME} and only at low temperatures. The basic underlying problem is that the electronic configurations which favor magnetization are antagonistic to those that favor polarization. Accordingly, single phase ME materials are most often anti-ferromagnetic, where there is only a very weak exchange between the spin and polar subsystems.

The obvious thing to do in such cases where compromises are necessary is to turn to composite systems as alternative materials. This has been done, beginning with

early investigations at Philips^{4,5}; but was not successfully achieved in terms of realizing significantly enhanced values of α_{ME} until recently⁶⁻¹³. Various composite structures have been investigated, including laminated and particulate ones. Although theoretical studies¹³ predicted a large ME effect of $\alpha_{ME} \geq 1\text{V/cm-Oe}$ for piezoelectric and magnetostrictive particulate composites, experimental investigations have shown much smaller values. The cause of the non-ideal performance in ceramic-ceramic particulate composites of magnetostrictive ferrite and piezoelectric PZT can be attributed to (i) diffusion of ions from one phase into another; (ii) connection of the ferrite particles, (iii) small magnitude of magnetostriction in ferrite, and (iv) the fact that the resistance of the magnetostrictive phase is much smaller than that of the piezoelectric one, resulting in poor poling of the piezoelectric phase and the inability of the dielectric layer to store a charge once induced by H.

1.2 Piezoelectric and magnetostrictive materials

1.2.1 Piezoelectricity and piezoelectric materials

Piezoelectricity in a material is the ability to generate an electric charge under applied mechanical stress or strain. The piezoelectric effect can be found in crystal structures that lack a symmetry center, which results in the existence of a polar axis. If the piezoelectricity is under an open-circuit condition, the applied stress induces an electric field across the material; this is known as the direct piezoelectric effect, as shown in Figure 1.1. In addition, there is a converse piezoelectric effect (i.e., a strain generated under an applied electric field), as shown in Figure 1.2. In piezoelectric materials, this means that stress/strain can be converted to an electrical charge, or vice

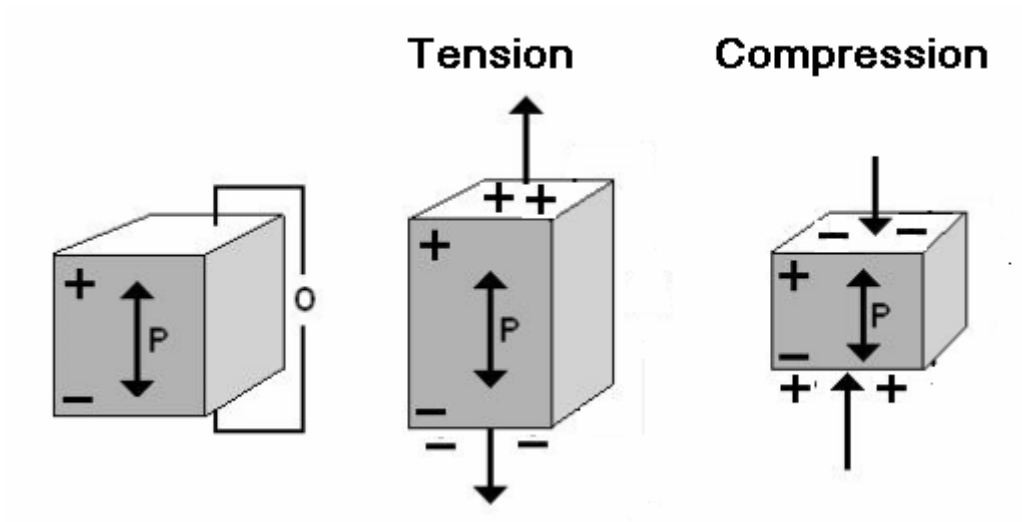


Figure 1.1 Direct piezoelectric effect

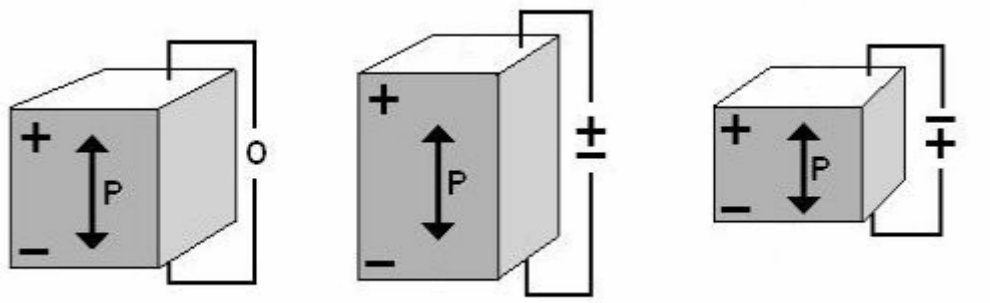


Figure 1.2 Converse piezoelectric effect

versa.

In a piezoelectric material, the coupling between electrical and elastic variables can be given as follows:

$$\begin{aligned}\sigma &= Cs - d^T E \\ D &= ds + \varepsilon E\end{aligned}\quad ; \quad (1.4)$$

where D is the charge density, s is the strain tensor, σ is the stress tensor, and d is the piezoelectric constant tensor.

The piezoelectric effect has found many useful technological applications such as the production and detection of sound, force sensors, actuators, transformers, generators and ultra-fine focusing (i.e. adaptive optical) assemblies. In addition, a number of scientific instrumental techniques are based on principals of the piezoelectric effect; for example, the scanning probe microscopies, such as the atomic force microscopy.

The first ME composites reported by Philips^{4,5} used BaTiO₃ as the piezoelectric phase, which had a transverse piezoelectric constant of $d_{31}=-90$ pC/N and an electromechanical coupling coefficient of $k_{33}=0.63$. Since 2000¹⁴, Pb(Zr,Ti)O₃ (PZT) ceramics have widely been used as the piezoelectric layers. This is because its piezoelectric constant ($d_{31}=-175$ pC/N) and electromechanical coupling coefficient ($k_{33}=0.72$) are notably larger than those of BaTiO₃. Recently, Pb(Zn_{1/3}Nb_{2/3})O₃-PbTiO₃ (PZN-PT) and Pb(Mg_{1/3}Nb_{2/3})O₃-PT (PMN-PT) single crystals have been used as the piezoelectric layers in ME laminates. Both of these materials have extreme electromechanical properties of $d_{33}=2000$ pC/N and $k_{33}=0.94$ ¹⁵. However, their Curie temperatures are lower, and they have lower

fracture toughnesses than PZT, this may limit their applications higher temperatures. Another material which has been incorporated into ME laminates is polyvinylidene difluoride or PVDF¹⁶. Polymeric material has advantages including soft elastic constants, high resistivity, and resistance to solvents. Table 1.1 summarizes the properties of these piezoelectric materials, that are relevant to predicting the ME properties.

1.2.2 Magnetostriction and magnetostrictive materials

Correspondingly, magnetostriction is a property where a material changes shape under an applied magnetic field, or changes magnetization under an applied mechanical stress. Magnetostriction is found in nearly all ferromagnetic materials; however, only a few ones have large magnetostriction.

The origin of magnetostriction is relatively complex at the atomic level, but at a macroscopic level, it is easy to understand. When a magnetic material has previously not been exposed to a magnetic field, the magnetic domains are randomly directed to each other along symmetry directions. Under application of magnetic field, these domain variants are repopulated, and domain walls move resulting in a shape change induced by H. This first mechanism is small compare to the second one, which is domain rotation under high magnetic field, as shown in Figure 1.3. Magnetostrictive materials are typically used under a preset dc magnetic bias, in order to achieve the highest sensitivity and/or shape change.

Table 1.1 Properties of piezoelectric materials

	BaTiO ₃	PZT-5	PZT-4	PZNPT	PMNPT	PMN-PZT	PVDF
d_{31} (pC/N)	-90	-175	-109	950	~700	1000	16.5
d_{33} (pC/N)	191	400	300	2200	1700	>2000	-33
ϵ	1700	1750	1350	7200	5000	6000	10
T_c (°C)	152	360	320	163	140	215	129
ρ (g/cm ³)	6	7.7	7.6	8.2	7.8	7.9	1.78
Q_m		80	500				4
k_{33}	0.63	0.72	0.68	0.94	0.9~0.94	0.92	0.19

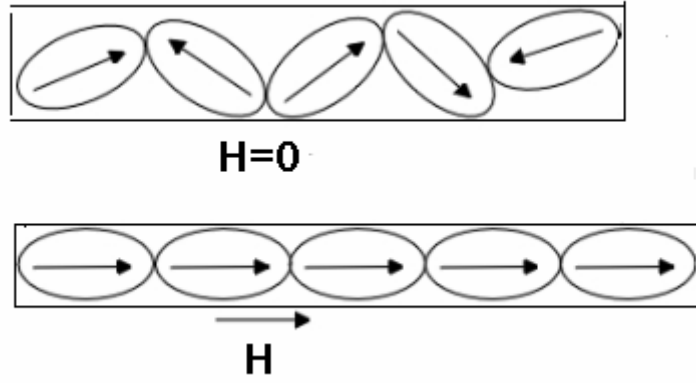


Figure 1.3 Domain rotate under applied magnetic field

Magnetostrictive materials also follow a reciprocal principal that is there are both direct and converse effects. The magnetization can be changed in response to applied stress. Like piezoelectric materials, magnetostrictive ones are widely used in actuators and transducers. Since such devices can be controlled by magnetic field, application of magnetostrictive materials operates in a non-contact mode.

Table 1.2 provides a summary of the properties of magnetostrictive materials that have previously been used in ME laminate composites. Ferrites have large resistances (relative to other magnetic materials), but small magnetostriction. They are widely used in microwave applications. Nickel ferrite is one of the best ferrites for ME laminates. Besides having a larger magnetostriction than any other ferrites, they also have good mechanical properties and are easily densified. The alloy Terfenol-D¹⁷ has the largest magnetostriction of any known material, more than 50x times than of nickel ferrite. But, unfortunately, being an alloy, it can not be co-processed with oxide ferroelectrics, as sintering would oxidize the iron and dramatically reduce the alloys superior magnetostriction. An alternative magnetostrictive alloy is Fe-Ga¹⁸. Its magnetostriction is less than Terfenol-D, but it is mechanically ductile whereas Terfenol-D is brittle. Finally, a most promising magnetostrictive alloy is Metglas¹⁹, which has an enormous relative magnetic permeability of $\mu_r > 10,000$: accordingly, its magnetization saturates at very low DC magnetic biases. Although its magnetostriction is far smaller than Terfenol-D, the maximum in its piezomagnetic coefficient is 4x larger than that of Terfenol-D.

Table 1.2 Properties of magnetostrictive materials

	NiFe ₂ O ₄	Terfenol-D	Fe-Ga	Metglas 2605
λ (ppm)	27	1600	200	40
μ	20	6~10	20	>40000
d_{33}	0.1	1	0.5	4
Qm		~10		1000
ρ (g/cm ³)	5.37	7.8	7.7	7.18
R(Ω -m)	1×10^6	5.8×10^{-7}	6×10^{-7}	1.3×10^{-6}
k_{33}		0.44		0.37

1.3 Magnetoelectric laminated composites

Since 2000, dramatically enhanced values of α_{ME} have been found in laminated composites²⁰⁻²⁵ consisting of magnetostrictive and piezoelectric layers epoxied together. Said laminated ME composites have ME voltage coefficients of up to 500x larger than any other ME materials: it has accordingly been designated as a giant ME effect. The mechanism behind the giant ME effect is easy to understand. As shown in Figure 1.4, when H is applied to the magnetostrictive layer, a strain is generated in the magnetostrictive layer. Then, this strain is transferred to the piezoelectric layer by elastic bonding to the magnetostrictive one, and finally an electric field is generated across the piezoelectric layer via piezoelectricity. Because of a large coupling between magnetic and electric properties, laminate composites with giant magnetoelectricity are potentially useful for applications in magnetic and electric current sensors, amongst other devices.

1.3.1 All Ceramic ME laminated composites

Srinivasan et al.⁸ have also reported studies of bi- and multi-layer composites of PZT and NiFe₂O₄ thick films fabricated by tape casting. Layer thicknesses in the range of 14 to 200 μ m were studied. In the case of a bi-layer structure, the ME voltage coefficient was found to be as high as $\alpha_{ME} = 460 \text{mV/cm-Oe}$: this is the giant magnetoelectricity first reported by Srinivasan and coworkers^{8,11}. In the case of multi-layers, even higher values of α_{ME} were found. Figure 1.5 shows the ME voltage coefficient as a function of dc magnetic bias (H_{dc}) for a bi-layer structure of

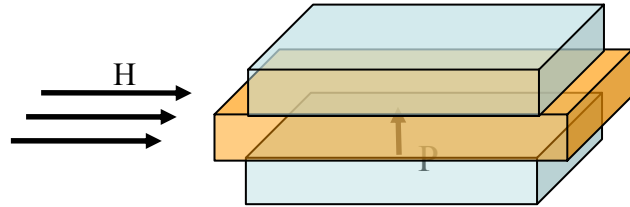


Figure 1.4. Schematic graph of magnetolectric laminated composites

NiFe₂O₄ and PZT. These data show that $\alpha_{ME}=0$ for $H_{dc}=0$: this is because the magnetostrictive phase has to be DC biased into a piezomagnetic condition. With increasing H_{dc} , the value of α_{ME} increases, reaching a maximum at the point of maximum slope in the M-H curve, subsequently decreasing with further increase of bias. These findings clearly illustrate the fact that a DC bias is required in order to observe the magnetoelectric effect in composites. For the PZT / NiFe₂O₄ bi-layer structures, the required DC bias was $H_{dc}=80$ Oe, as can be seen in Figure 1.5.

Figure 1.6 (a) shows a cross-sectional scanning electron microscopy (SEM) image taken from an all ceramic PZT/NiFe₂O₄ laminate fabricated by co-sintering¹². The dark layer is the NiFe₂O₄ one and the other two lighter layers are PZT ones. The interface of the PZT and NiFe₂O₄ layers (Figure 1.6 (b)) was not smooth, and thus it has inefficient stress transfer across the boundary and a low interfacial coupling factor. In the NiFe₂O₄ layer, this image also shows many pores near the surface, which decreased the mechanical coupling between layers.

The effective dielectric constant (ϵ_{33}^{eff}) of this composite has been calculated by a well known series mixture rule:

$$\epsilon_{33}^{eff} = \frac{\epsilon_{33}^p \epsilon_{33}^m}{\epsilon_{33}^p (1 - \nu) + \epsilon_{33}^m \nu} ; \quad (1.5)$$

where ν is the volume fraction of the magnetostrictive phase. The value of ϵ_{33} can be lowered by porosity, and can be accounted for in (2) by adding air as a third phase. In addition, the effective piezoelectric constant (d_{33}^{eff}) of the composite can be calculated by a similar mixing rule, given as

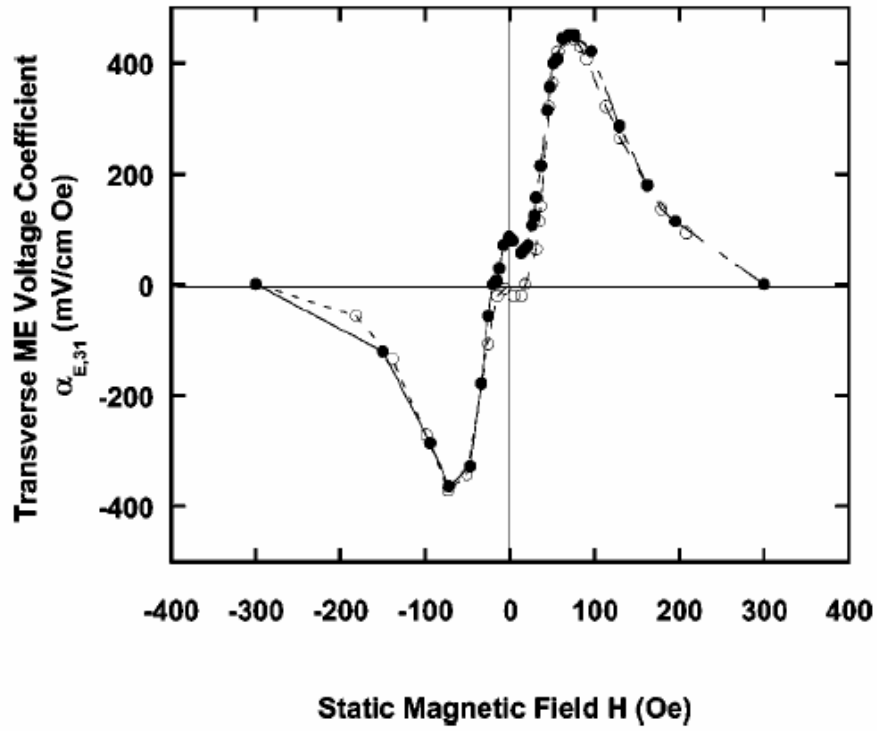


Figure 1.5 Transverse ME voltage coefficient at room temperature as a function of static magnetic field H for a two-layer structure consisting of 200-nm films of NFO and PZT.

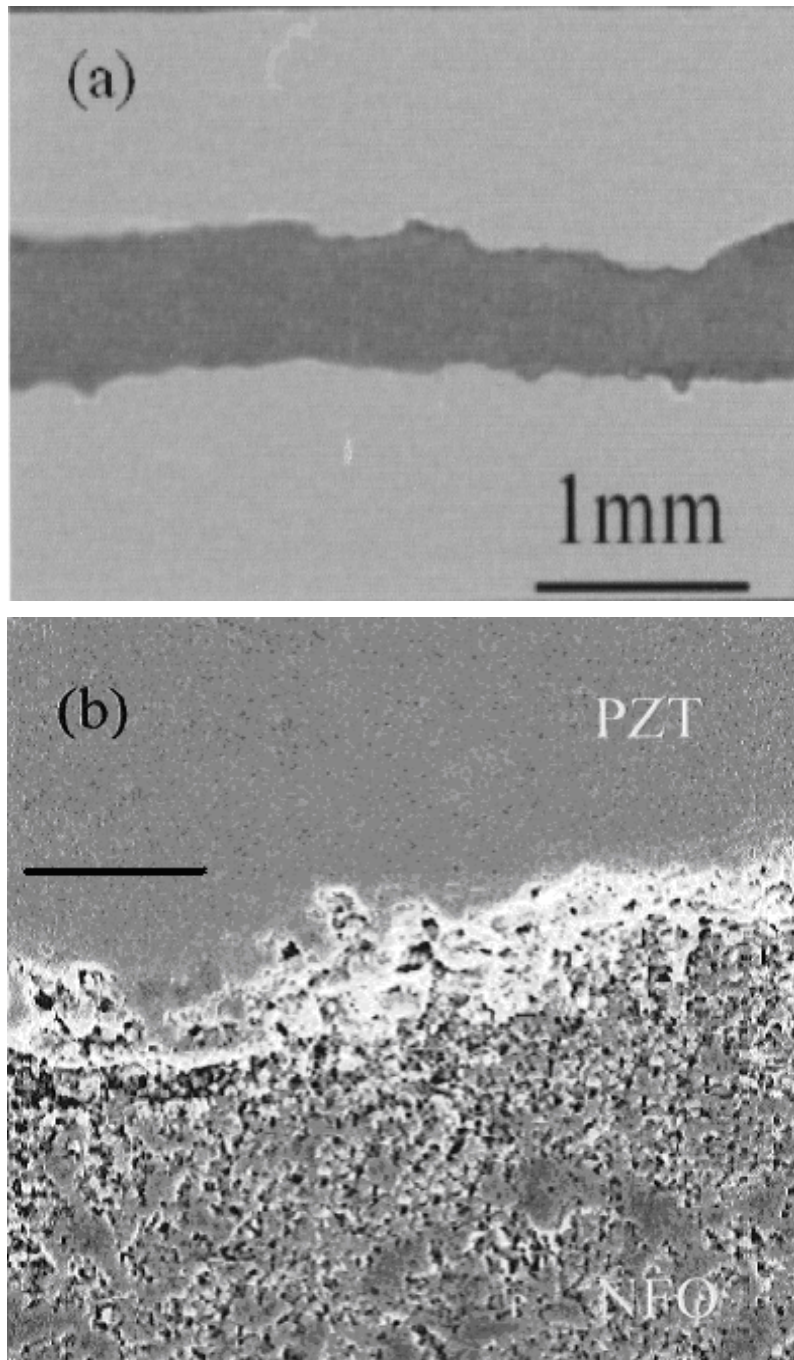


Figure 1.6 (a) An optical and (b) scanning electron micrograph of the fractured surface of the sandwiched PZT/NiF₂O₄/PZT ceramics.

$$d_{33}^{eff} = \frac{\nu d_{33}^p \epsilon_{33}^m}{\epsilon_{33}^p (1 - \nu) + \epsilon_{33}^m \nu}. \quad (1.6)$$

The ME voltage coefficient for the sintered PZT/NiFe₂O₄ laminate shown in Figure 1.6 has been reported to be $\alpha_{ME} = 160 \text{ mV/cm-Oe}$. Please note that this value is significantly smaller than the value predicted by Equation 1.14. This reduction in α_{ME} relative to the ideal value can be attributed to the residual porosity and poor mechanical coupling across the interface, as mentioned above.

1.3.2 Ceramic/alloy ME composites

Although ferrite/PZT laminates have giant ME voltage coefficients, the limited magnetostriction of the ferrite phase was a bottleneck to developing composites with further increased values of α_{ME} . Dong and co-workers²⁶ realized the potential usefulness of the giant magnetostrictive alloy Terfenol-D as an important solution to this bottleneck – enabling the achievement of further enhancements in α_{ME} . However, Terfenol-D and PZT are incompatible with regards to co-processing. Sintering of layers together to form a monolithic composite with an interface of good integrity is not possible: the high sintering temperature of PZT would oxidize Terfenol-D, which would reduce PZT in the process. The solution to this dilemma is simple, low cost, and does not require high temperature co-sintering: just use an epoxy layer between the PZT and Terfenol-D ones to bond them together. To achieve good magnetoelectric effects, it is essential to keep the epoxy layer as thin as possible; otherwise the viscoelastic nature of an epoxy will relax the mechanical coupling between the layers. An important benefit of the simple epoxy approach was that it

opened up possibilities of many more designs than that offered by traditional ceramic methods.

Investigations of the ME voltage coefficient of Terfenol-D/PZT laminates²⁵⁻²⁸ has shown that values as high as $\alpha_{ME}=4.6$ V/cm-Oe can be achieved, which is nearly an order of magnitude higher than the giant ME effect in ferrite / PZT laminates. Figure 1.7 (a) shows these highest values of α_{ME} as a function of H_{dc} , previously reported for Terfenol-D/PZT. These data clearly demonstrate the realization of ME coefficients much larger than the giant ones of ferrite/PZT. Further investigations revealed that a dramatic enhancement of α_{ME} near the electromechanical resonance (EMR) frequency of the piezoelectric phase of the laminate. These findings are illustrated in Figure 1.7 (b), and demonstrate that α_{ME} is enhanced by a factor of nearly 10x under resonance excitation at the EMR frequency.

Other investigations^{21,29} have shown that an alternative magnetostrictive Fe-Ga alloy (Galfenol) can be substituted for Terfenol-D. The Galfenol / PZT laminates were found to have lower ME properties than the corresponding Terfenol-D ones, with $\alpha_{ME} \approx 0.3$ V/cm-Oe in the low (quasi-static) frequency range.

1.3.3 Working mode of ME laminates

In addition to the numerous types of materials that have been incorporated into ME composites, there has been an equal number of investigations concerning composite configurations and the poling (magnetization) direction with respect to long axis of the composite layers. There are many different ways to put ME laminate composites together of various texture symmetries. Four basic modes of operation can

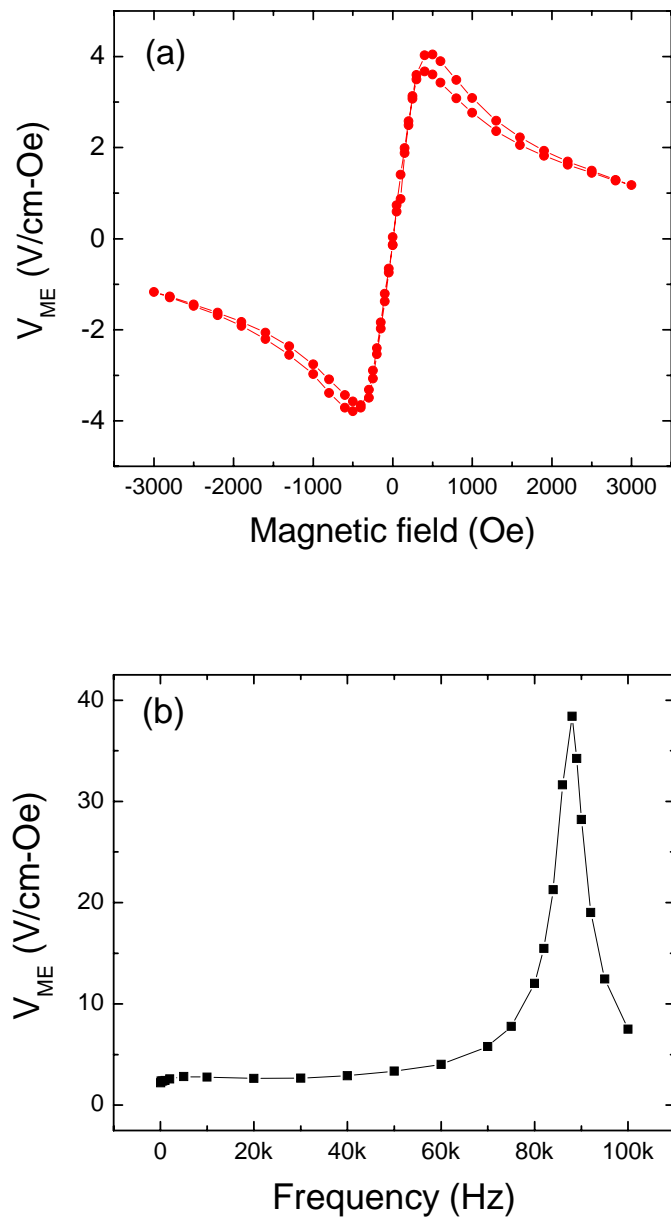


Figure 1.7 (a) Induced ME voltages as a function of DC magnetic field of Terfenol-D / PZT / Terfenol-D trilayers. The polarization direction of PZT and is along the longitudinal direction. (b) Frequency dependence of the ME voltage coefficient for $1 < f < 100$ kHz. These data were taken using a $H_{dc}=550$ Oe and $H_{ac}=1$ Oe.

be identified in a long axis laminate, and subsequently other more complex designs^{27,30}.

Figure 1.8 illustrates the four (4) basic types of modes that have been categorized^{31,32}. These are the longitudinally magnetized and longitudinally poled or (L-L) mode, the longitudinal magnetized and transversely poled or (L-T) mode, the transversely magnetized and longitudinally poled or (T-L) mode, and the transversely magnetized and transversely poled or (T-T) mode. In Table III, typical values of the ME voltage coefficient α_{ME} for these four basic types of operational modes were given. In this table, it can be seen that the (L-L) mode has a larger value of α_{ME} than the (L-T) one. This is because the longitudinal piezoelectric coefficients d_{33} of PZT, PMN-PT and PZN-PT are larger than the transverse one d_{31} . In addition, the value of α_{ME} was notably lower for the (T-T) mode. This undoubtedly is due to the effect of demagnetization fields on the magnetostrictive layers, which result in much larger required DC magnetic biases to reach the maximum value of the effective piezomagnetic coefficient.

Theoretically, the (L-L) mode²⁶ should have the largest ME voltage coefficient of all the four basic modes illustrated in Figure 1.8. However, in actuality, this was not initially found to be the case, simply because the capacitance of the piezoelectric layer in the laminate was very small. To circumvent this difficulty, the ability to build complexity into the laminate composite design was taken advantage of. In particular, a ‘push-pull’ mode was designed²⁵, which has as a trade-off between the output ME voltage and the output ME charge. The push-pull mode is illustrated in

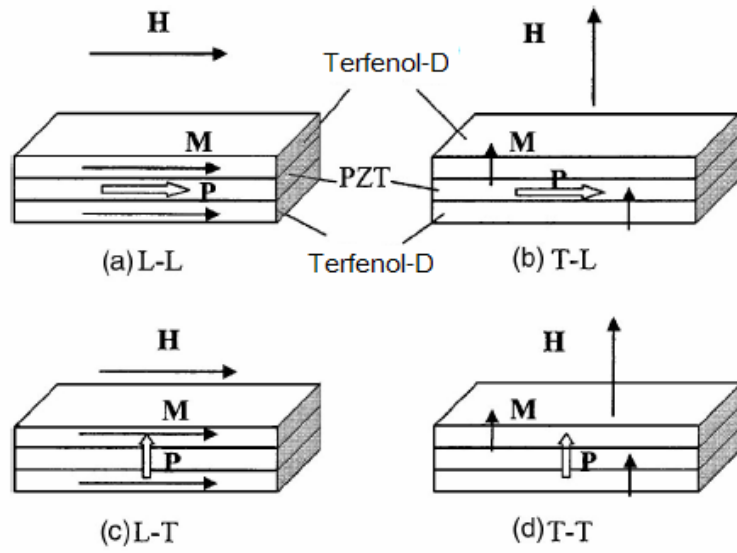


Figure 1.8 Schematic illustration of the various ME coupling modes (a) L-L; (b) T-L; (c) L-T; and (d) T-T

Figure 1.9. It consists of a tri-layer structure with 2 layers of Terfenol-D sandwiched between an inner layer of PZT or PMN-PT. It is similar to the basic (L-L) mode, except that the piezoelectric layer of the push-pull configuration is symmetrically poled about its center node in reverse directions along the longitudinal axis. Compared to a composite of the exact dimensions operated in the (L-L) mode, the push-pull mode has a capacitance that is 4x larger. This configuration allowed for the achievement of the promise of high magnetoelectricity in a (L-L) type mode. This trade-off is important for application such as magnetic sensor, allowing for the achievement of sensitivities to small ac magnetic field variations on the order of 10^{-10} Tesla/ $\sqrt{\text{Hz}}$ at a frequency of $f=1\text{Hz}$ ³³.

Finally, it is important to mention that ring mode ME laminates^{28,30,34,35} have also been fabricated and studied for AC electric current sensors³⁰. Tri-ring laminates have been constructed, consisting of two Terfenol-D rings and a single PZT one. Investigations were performed for a composite-ring operated in a (L-T) mode, as shown in Figure 1.10 (a); and in a four part push-pull ring mode³⁵ where the PZT ring was poled circumferentially using a four electrode pattern, as shown in Figure 10b. These ring laminates have proven useful for electric current sensing, in comparisons to reluctance coils, as their sensing capabilities were not affected by decreasing frequency.

It has been shown that the ME effect can be increased by a factor of up to 100x by resonance excitation, as mentioned above. For the four basic modes of Figure

Table 1.3 ME voltage coefficient of different mode *

	L-L	L-T	T-L	T-T
DC bias	500 Oe	500 Oe	2200 Oe	2200 Oe
ME voltage coefficient	2.4 V/cm-Oe	0.73 V/cm-Oe	0.78 V/cm-Oe	0.5 V/cm-Oe

* All laminates were made by 2 piece of Terfenol-D (14x6x1.2 mm³) and 1 piece of PZT (16x6x2 mm³)

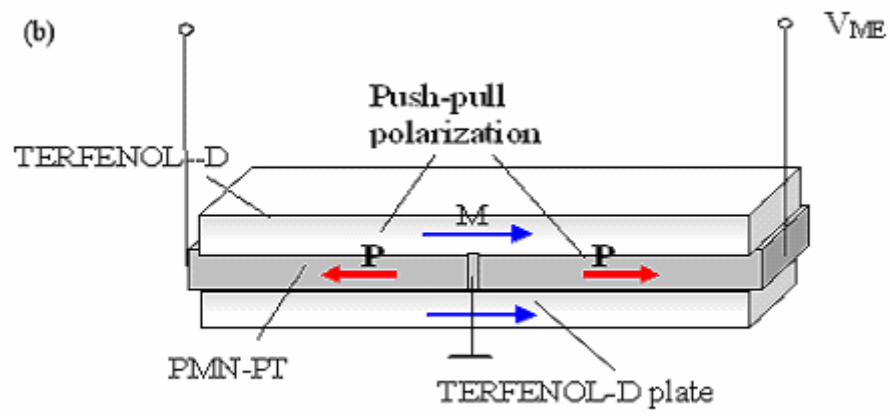


Figure 1.9 Schematic illustration of the various ME coupling mode push-pull mode.

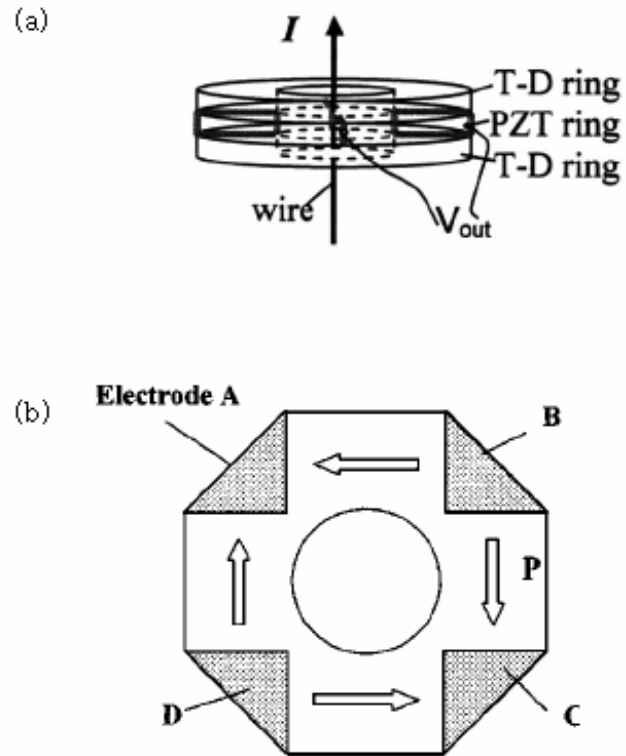


Figure 1.10 Schematic illustration of the various ME coupling ring modes (a) L-T; and (b) 4 parts push-pull.

8, the fundamental resonance frequency mainly depends on the length of the laminates (l)

$$f^L = \frac{1}{2l\sqrt{\rho s_{11}}}; \quad (1.7)$$

where f^L is the first longitudinal resonance frequency, ρ is the average density of the laminates, and s_{11} is the elastic compliance of the laminates. Investigations have shown that ME laminates can have sensitivities to minute magnetic field variations as low as 2 pTesla/ $\sqrt{\text{Hz}}$ ³³, when actively driven as an oscillator. This is potentially a very important aspect about ME laminates, with regards to inexpensive and extremely sensitive magnetometers. But, realization of these unique advantages is restricted to the EMR frequency range, because of geometry.

Obviously, f^L can be decreased by increasing l . But, this is an inefficient means by which to lower the frequency, as the composite could become prohibitively big and bulky. A simple solution has been proposed to shift the frequency of the resonance enhancement: this is by the use of a unimorph mode³⁶, illustrated in Fig. 1.11 (a). Unlike the symmetric structure of above mentioned basic laminate modes shown in Figure 8, the unimorph mode consists of only 2 layers laminated together: one piezoelectric layer and one magnetostrictive layer. The first resonance frequency of these unsymmetrical structures is a bending mode one, which was a much lower longitudinal resonance frequency than that of the basic modes, given as

$$f^B = \frac{\pi d}{2\sqrt{12}l^2\sqrt{\rho s_{11}}}\beta^2; \quad (1.8)$$

where f^B is the first bending resonance frequency, and d is the thickness of the laminates. Using this approach, resonance enhancements of the ME coefficient have been achieved in the frequency range of 100Hz, using cm-long laminates.

Finally, another approach has been used to try and realize resonance enhanced ME coefficients at reduced frequencies³⁷. Third-phase steel layers having high mechanical quality factors Q_m have been incorporated into two-layer unimorph structures, as illustrated in Fig. 1.11 (b). In this case, the resonance frequency was decreased to $f \sim 5.1$ kHz, while the maximum value of the ME resonance was enhanced at resonance by a factor of 2x relative to that of a unimorph. Steel increases the resonance frequency of the unimorph, but because of the high Q_m it also increases the amplitude of the resonance oscillation.

1.3.4 Quasi-static Calculations

Previously, Harshe^{38,39} et al proposed a mode of operation for ME laminated composites. They assumed an ideal coupling between the interfaces of each layer, and that the ME laminates operate at quasi-static frequencies. For the piezoelectric layer, the stress, strain, electric field and polarization relationship that they derived are:

$$S_i^p = s_{ij}^p T_j^p + d_{ii}^p E_i^p; \quad (1.9)$$

$$D_k^p = d_{kl}^p T_l^p + \epsilon_{kn}^p E_n^p; \quad (1.10)$$

where S , D , T are the strain, stress, and electric displacement tensors; s , d , ϵ are the compliance, piezoelectric and permittivity tensors respectively, where the

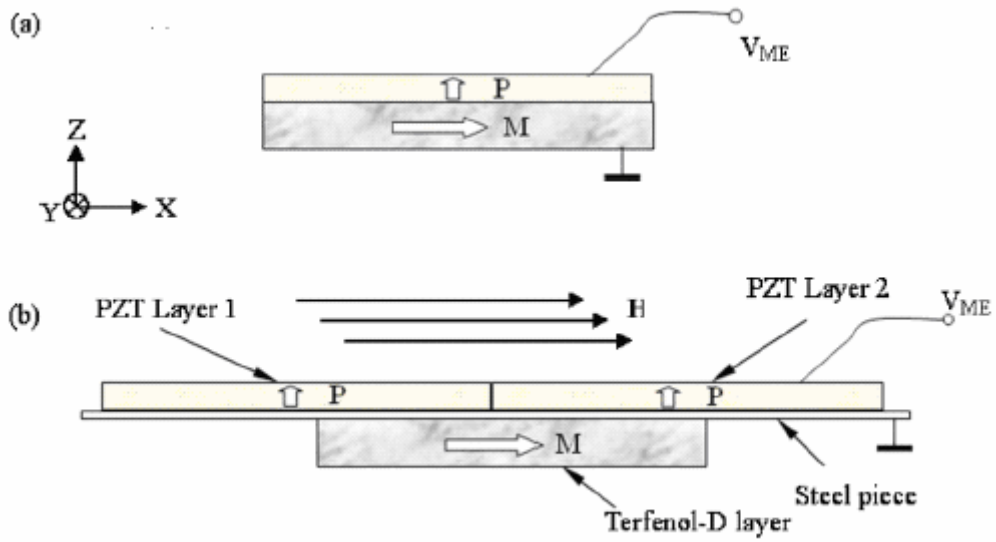


Figure 1.11 Schematic illustration of the various ME coupling mode (a) Unimorph mode; and (b) Three phase unimorph mode.

index p designates piezoelectric phase. Furthermore, for the magnetostrictive layer, an analogous relationship can be given as:

$$S_i^m = s_{ij}^m T_j^m + q_{il}^m H_l^m ; \quad (1.11)$$

$$B_k^m = q_{kl}^m T_l^m + \mu_{kn}^m H_n^m ; \quad (1.12)$$

where q and μ are the compliance and piezomagnetic tensors, and where the index m designates magnetostrictive phase.

The ME voltage coefficient can be calculated from Equations 1.9 to 1.12 by assuming (i) a perfect boundary condition; (ii) that the thickness and the polarization directions are along the 3 axis; (iii) the magnetic field is also along the 3 axis. In this case, the ME voltage coefficient is the longitudinal one, given as:

$$\alpha_{E,33} = \frac{|dE_3|}{|dH_3|} = \frac{2\nu(1-\nu)d_{31}^p q_{31}^m}{2(d_{31}^p)^2(1-\nu) + \epsilon_{33}^S[(\nu-1)(s_{11}^p + s_{12}^p) - k\nu(s_{11}^m + s_{12}^m)]} ; \quad (1.13)$$

where ν is the thickness ratio of the piezoelectric layer. However, if the magnetic field is applied along direction 1, the ME voltage coefficient is the transverse one, given as:

$$\alpha_{E,31} = \frac{|dE_3|}{|dH_3|} = \frac{\nu(1-\nu)d_{31}^p(q_{11}^m + q_{21}^m)}{2(d_{31}^p)^2(1-\nu) + \epsilon_{33}^S[(\nu-1)(s_{11}^p + s_{12}^p) - k\nu(s_{11}^m + s_{12}^m)]} ; \quad (1.14)$$

1.3.5 Frequency dependent response - an equivalent circuit method

An equivalent circuit approach has also been developed to describe the ME properties of laminate composites²⁷. This was done by model both the electromechanical and magnetoelastic coupling though an equation of motion.

Using this approach, the ME properties could be predicted as a function of frequency. For ME laminates based on piezoelectric and magnetostrictive materials, this equivalent circuit approach is a good method by which to estimate the ME performance for potential use in electronic applications.

The equivalent circuit approach can be summarized as follows. The piezoelectric and magnetostrictive mass units (Δm^p and Δm^m) in the laminates have the same displacement $u(z)$ and strain $\partial u / \partial z$ along axis z , given as

$$u_3^p = u_i^m; \quad (1.15)$$

$$S_3^p = S_i^m = \partial u / \partial z; \quad (1.16)$$

When $i=1$, the magnetic field is applied along the 1 axis, and when $i=3$ is applied along the thickness direction. The equation of motion for the laminates can be given as:

$$(\Delta m^p + \Delta m^m) \frac{\partial^2 u}{\partial t^2} = \Delta T_3^p A^p + \Delta T_i^m A^m; \quad (1.17)$$

where A is the cross section area, $\Delta m = \rho A \Delta z$, and ρ is the mass density. The static strain in Equations 1.9-1.12 can be then put into the above elastic motion of Equation 1.17. When the laminates are open-circuit and do not have an applied mechanical force, the equivalent circuit can be given as shown Figure 1.12. In this case, the ME voltage coefficient has been predicted to be:

$$V_{ME}^{LT} = \frac{|dE_1|}{|dH_3|} = \frac{\nu d_{33}^m d_{31}^p}{\nu \epsilon_{33}^p s_{11}^p + (1 - \nu) s_{33}^m [\epsilon_{33}^p + (d_{31}^p)^2 / s_{11}^p]}. \quad (1.18)$$

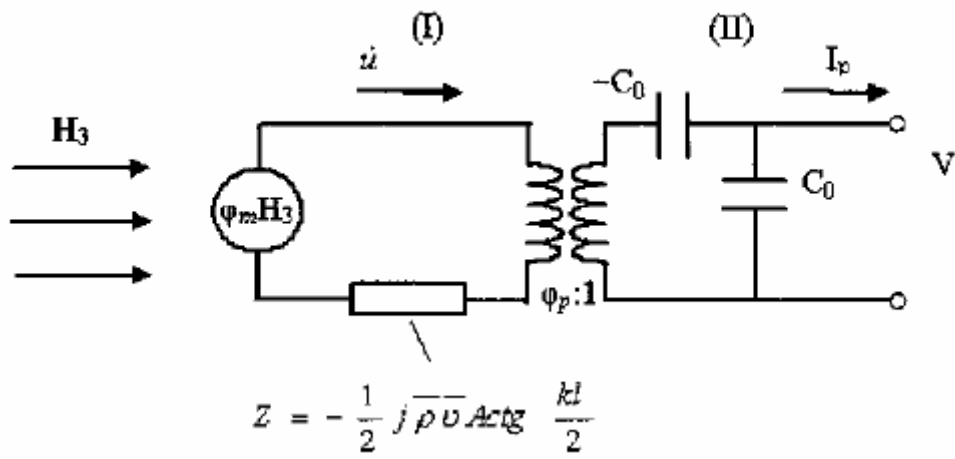


Figure 1.12 ME equivalent circuit under free-free boundary conditions

1.4 Section Summary

In summary, ME laminate composites are a recent development that has the potential to revolutionize the field of electro-ceramics. It has enabled the achievement of magnetoelectric voltage coefficients many orders of magnitude larger than previously reported values for single phase or particulate composites. The advancements in this field since the turn of the millennium has opened up many possibilities in new and unique applications of transformers^{25,28}, tunable microwave filters^{40,41} and microwave devices⁴².

Although ME effect has developed rapidly in the last 10 years, there remains many things to be done, including (i) further improvement of ME voltage coefficient; (ii) dramatically decreasing the DC bias or achieve optimum output ME voltage without DC bias; (iii) designing new configurations to increase the signal to noise ratio; (iv) investigating fundamental structure of laminate - property relationships; and (v) designing new devices based on the ME effect. These are the purposes of my Thesis.

II. Purpose of this thesis

The purpose of my dissertation work was to investigate the ME effect in laminate composites: from the fundamental properties to applications. Specifically, the road map of my thesis is as follows:

(1) ME materials and structures

Previous investigations of ME laminates¹ focused on large magnetostriction materials; however, such materials have low magnetic permeability. Thus, these laminates require large DC magnetic biases to achieve optimum ME voltage coefficients. Here, in my thesis, low magnetostriction materials, but ones that have large permeability Metglas foils have been used to stack with piezoelectric materials such as PVDF and PZT fibers. My investigations were focused on improving the ME voltage coefficient, decreasing required optimum DC biases and investigating the directional dependence of the ME voltage coefficient. [Please see Section 3.2]

Furthermore, the structure of ME laminates not only changes the ME voltage coefficient and required optimum DC bias, but also alters the signal to noise ratio (SNR). Not only optimizations of materials, but also configurations have been considered, that can aide in environmental noise reject. In my thesis, I have designed a symmetric bimorph mode to reject thermal fluctuation by differenting the noise from the signal, also I have found a differential mode capable of reduce vibration noise. [Please see Section 3.3]

(2) Fundamental ME parameter

Previously, the ME voltage coefficient has been widely used to benchmark ME effects of various materials to each other⁴³. However, V_{ME} is not a fundamental parameter. Here, a ME susceptibility has been introduced, including a calculation from the corresponding fundamental electrical and magnetic susceptibilities of the stricitive phases, i.e., the layers. An explanation of the importance of this parameter will be provided. [Please see Section 4.1]

The magnetic properties are affected by the shape of magnetic materials because of shape demagnetization effects. Previous investigations have omitted this fact. The geometric shape of a laminate does have an important affect on the ME properties, especially for those using large permeability Metglas. I have investigated the shape effect in ME laminates for (i) large permeability Metglas/PZT laminates, and (ii) low permeability Terfenol-D/PZT laminates. [Please see Section 4.2]

The ME effect is known to be enhanced at the mechanical resonance frequency. However, the resonance peak is sharp and fixed for ME laminates, limiting the bandwidth of applications that use resonant enhancement. Large magnetostriction can change the internal stress of a laminate and tune its resonance frequency, this broadens the ME applications under enhanced resonance drive. [Please see Section 4.3]

Magnetolectric devices and applications

The ME effect is an induced dielectric polarization under an applied magnetic field, and/or an induced magnetization under an external electric field. Thus

it can be used in magnetic sensor applications. Here, I demonstrate that ME laminates can be used as passive magnetic field sensors for detection of low frequency magnetic anomalies, and as DC field sensors if used in an active oscillator mode. I have given special attention to development of ME sensors with ultra-high sensitivity. [Please see Section 5.1]

Earth's magnetic field is of the magnitude of about 0.5 Oe. This is a good application range for my Metglas/piezoelectric ME sensors. Three dimensional ME sensors can measure both the intensity and inclination of the geomagnetic field. By comparing with a known database of the Earth magnetic field, these sensors could be used to identify position on the Earth: i.e., a potential global positioning system, in a GPS void environment. [Please see Section 5.2]

In 1948⁴⁴, Bernard Tellegen published seminal work on classic passive network elements, in which he theorized that an additional network element based on magneto-electric (ME) interaction should exist – which he designated the gyrator. An ideal gyrator would be unique with respect to the other known four network elements – capacitance, resistance, inductance, and transformer – in that it would not comply with reciprocity, but rather would be anti-reciprocal. In the course of my thesis, I have shown the realization of this 5th discrete network component – the Tellegen gyrator. [Please see Section 5.3]

Finally, ME laminates induce voltage under both magnetic field and mechanical vibrations. This means that ME laminates offer the capability to transform both magnetic and mechanical energies to electrical power for the device applications.

In the course of my investigations, I have developed a bi-mechanism for energy harvesting that can synchronously collect both stray magnetic and acoustic energies, via magnetoelectric and piezoelectric effects. [Please see Section 5.4]

III. Magnetoelectric laminated composites and structures

3.1 Introduction

During the past fifty years, although the ME voltage coefficient has been dramatically enhanced from 20 mV/cm-Oe (single crystal Cr₂O₃) to 4 V/cm-Oe (laminated Terfenol-D/PZT composites), there still remain some challenges in improving the coefficient to near its theoretical limit, and in the applications of the ME effect. Specifically, we can ask:

i) Does any material have a larger ME voltage coefficient than Terfenol-D/PZT laminates? We know that piezoelectric/magnetostrictive laminates have large ME voltage coefficients. Terfenol-D is one of the materials that has the highest magnetostriction. PZT is a commercially available piezoelectric material with good properties and low cost. We need to ask if we can find new magnetostrictive or piezoelectric materials, which after stacked together into laminates, have larger ME voltage coefficient than that of Terfenol-D/PZT laminates?

ii) Can we eliminate or dramatically decrease the DC magnetic bias? A limitation of previously reported ME laminates is a low permeability in the magnetostrictive layers. This limitation, in conjunction with the demagnetization field, has required relatively high DC magnetic biases of $H_{dc,opt} \approx 4000\text{Oe}$ applied by permanent magnets in order to achieve a maximum

effective piezo-magnetic coefficient. Lowering of this required H_{dc} by use of an alternative magnetostrictive phase is an important goal, which would enable laminate miniaturization for applications in magnetic sensing³³ and transduction^{45,46}.

iii) Can we develop laminate configurations that enable environmental noise rejection, while not affecting the signal to magnetic fields? The challenge is whether we can incorporate into the composite structure additional important functions that can be used to noise rejection. Piezoelectric layers will introduce noise from the pyroelectric effect that will couple to temperature fluctuations, which can generate charges that are one of main noise sources. In addition, the piezoelectric layers by nature will couple to vibrations in the environment, resulting in a generated charge. This is another important noise source to be rejected from the ME magnetic signal by using ME laminates.

3.2 New Metglas based ME laminates

From a theoretical perspective, the really important parameter for the magnetic phase in ME laminates is the piezomagnetic coefficient, not the total magnetostriction. The piezomagnetic coefficient is determined by both magnetostriction and permeability. There is no known material with larger magnetostriction than Terfenol-D. Thus, to improve the performance of the magnetic layers, we can only hope to identify a material with giant permeability, which still has a magnetostriction sufficient to increase the ME voltage coefficient of ME laminates.

In this section of my thesis, I have investigated the ME properties of Metglas based laminates.

3.2.1 Metglas/PVDF

Iron-based Metglas¹⁹ 2605 SA1 or CO have compositions of $\text{Fe}_{81}\text{B}_{14}\text{Si}_3\text{C}_2$ or $\text{Fe}_{66}\text{Co}_{15}\text{Si}_1\text{B}_{14}$, both with magnetostrictions of 27~45 ppm. The thickness of Metglas 2605 SA1 and CO layers was 25 and 23.5 μm , respectively. The use of a thin-foil form offers the additional advantage of reducing Eddy current losses at high frequencies. These thin layers were obtained from Metglas Inc (Conway, SC). Without annealing, Metglas has a high DC permeability >40,000 for a $\text{Fe}_{81}\text{B}_{14}\text{Si}_3\text{C}_2$ alloy, and >120,000 for a $\text{Fe}_{66}\text{Co}_{15}\text{Si}_1\text{B}_{14}$ alloy: after annealing, their permeability are increased, however their magnetoelastic properties are decreased. The piezoelectric layers were PVDF thin-films of thickness 28 μm . The metglas layer and PVDF layers were glued together using an epoxy.

Figure 3.1(a) shows a photo of a Metglas/PVDF laminate: unlike previous ME laminates, this Metglas/PVDF one was very thin, flexible, and capable of being bent (as shown in the figure).

Figures 3.1(b) and (c) show Metglas/PVDF laminate configurations: (b) is a unimorph consisting of single layers of Metglas 2605 CO and PVDF that were epoxied together; whereas (c) is a sandwich structure, made of two layers of Metglas 2605 SA1 and a single PVDF layer. In both configurations, the Metglas layer(s) were longitudinally magnetized, whereas the piezoelectric ones were transversely poled.

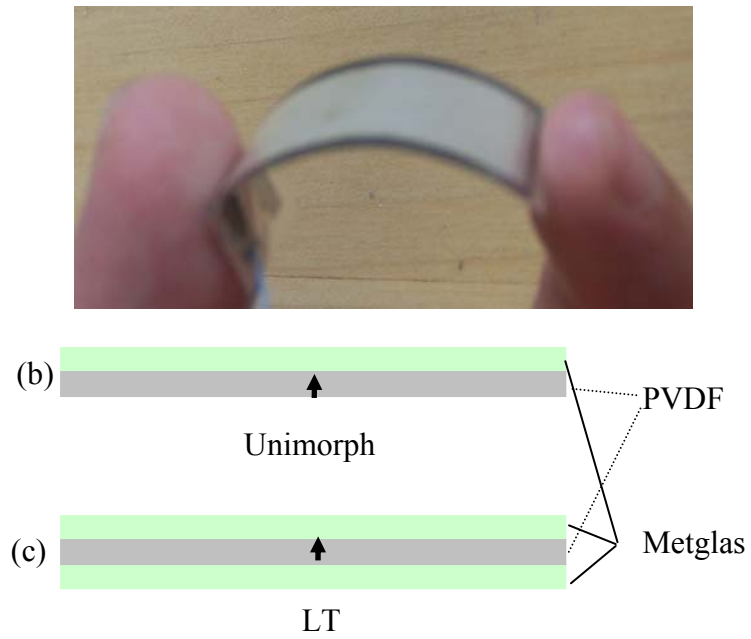


Figure 3.1 (a) Photograph of a Metglas/PVDF unimorph laminate; and the structure of (b) the unimorph configuration, and (c) the 3-layer L-T sandwich configuration. In both configurations, the Metglas layer(s) were longitudinally magnetized, whereas the piezoelectric ones were transversely poled.

During the ME measurement, DC (H_{dc}) and AC (H_{ac}) magnetic fields were applied along the length of the laminates. An electromagnet was used to provide H_{dc} , and a Helmholtz coil was used to generate $H_{ac}=1\text{Oe}$. A lock-in amplifier (SR850) generated a controllable input current to the Helmholtz coil; and subsequently to measure the output voltage and phase from the PVDF film.

Figure 3.2(a) shows the dependence of V_{ME} on H_{dc} for the 3-layer Metglas/PVDF laminate, measured at 1kHz. The maximum value of V_{ME} was 7.2V/cm-Oe under $H_{dc}=8\text{Oe}$: this is 3x greater than the largest value previously reported for 3-layer Terfenol-D/PMNPT L-T laminates³¹. However, it is important to note that H_{dc} was only 8 Oe, which is $\sim 1/50^{\text{th}}$ of that needed for the maximum ME effect in Terfenol-D/PMNPT laminates. According to the magneto-electric equivalent circuit method^{11,20}, the ME voltage coefficient V_{ME} for L-T laminates can be derived as²¹:

$$V_{ME}^{LT} = \frac{|dE_1|}{|dH_3|} = \frac{nd_{33,m}d_{31,p}}{n\epsilon_{33}^S s_{11}^E + (1-n)s_{33}^H (\epsilon_{33}^S + d_{31,p}^2 / s_{11}^E)}; \quad (3.1)$$

where n is the magnetic phase thickness ratio; s_{11}^E and s_{33}^H are the elastic compliances of the piezoelectric and magnetostrictive layers; ϵ_{33}^S is the dielectric constant of the piezoelectric material at constant strain; and $d_{33,m}$ and $d_{31,p}$ are the longitudinal piezomagnetic and transverse piezoelectric coefficients.

Although the magnetostriction of Metglas SA1 was only 42 ppm (Figure 3.2(b)), which is far smaller than the giant magnetostriction of Terfenol-D, the maximum value of its effective piezomagnetic coefficient ($d_{33,m} = 4 \times 10^{-6}/\text{Oe}$, see right-hand axis of Fig.3.2(b)) is 3-4 \times larger than that of Terfenol-D ($d_{33,m} =$

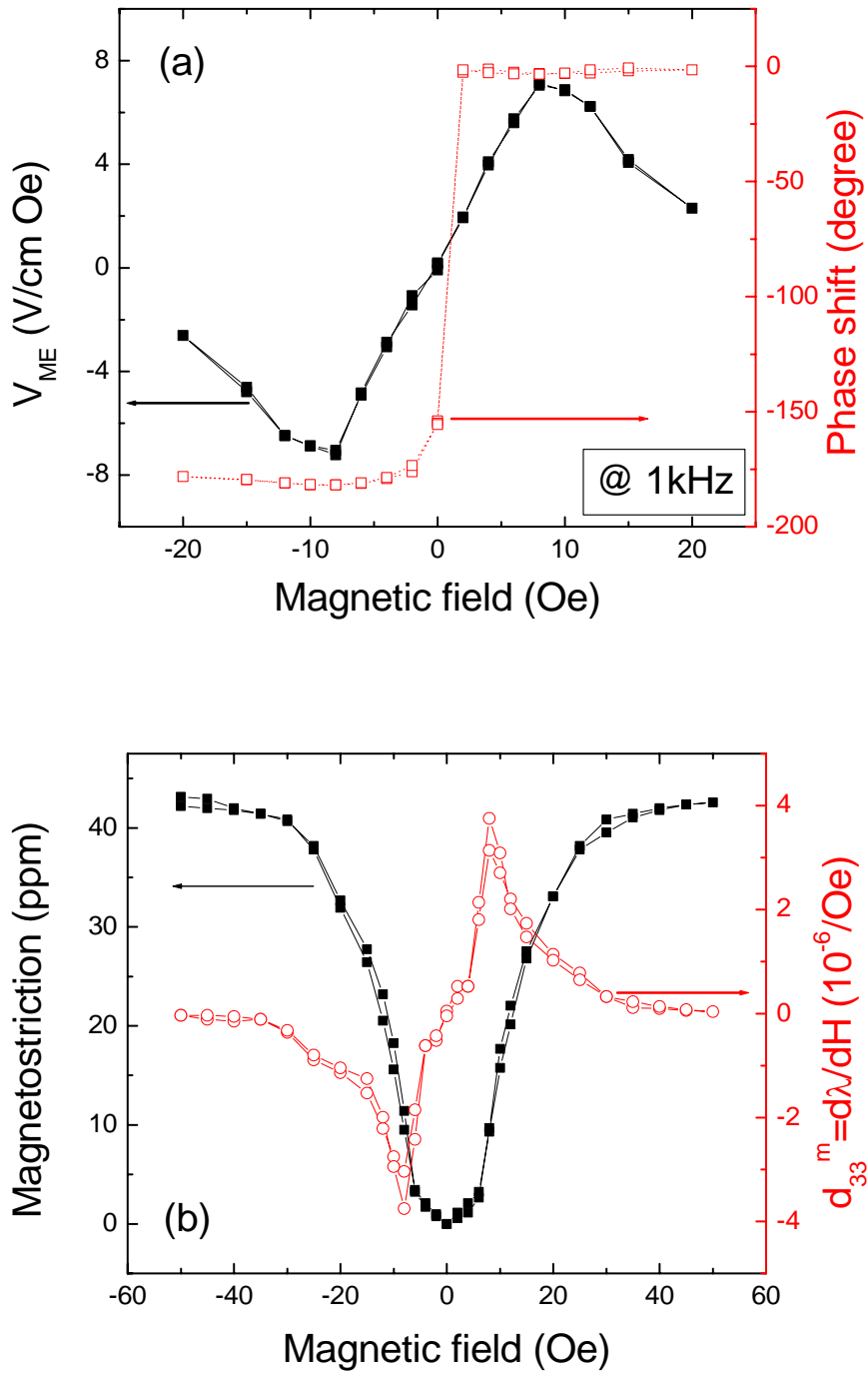


Figure 3.2. (a) DC magnetic field dependence of the ME voltage coefficient and phase for a Metglas/PVDF 3-layer laminate, measured at 1 kHz and $H_{ac} = 1$ Oe; (b) magnetostriction (closed square) and piezomagnetic coefficient (open dot) for a Metglas (2605 SA1) layer in the L-T mode.

$1.2 \times 10^{-6} \text{Oe}^{25}$, due to the small saturation field. This difference reflects the much higher magnetic permeability of Metglas: a high μ_r results in a low saturation field, and thus a large value of $d\lambda/dH$ at low H_{dc} . In addition, high- μ Metglas layers also concentrate magnetic flux.

These results demonstrate the potential of FeBSiC as a superior dc-biased piezomagnetic layer for ME laminate composites, one that can also operate under much reduced H_{dc} . This extremely low DC bias requirement is an important advantage of Metglas/PVDF laminates over other previously reported types, offering potential in practical applications. In addition, a large phase shift from 0° to 180° was found under small dc bias changes on the order of one Oe, as shown on the right-hand axis of Fig.3.2(a), further offering ability to read the sign of a small moment or magnetic field direction spin.

The 3-layer sandwich laminate of Figure 3.1(b) has a symmetric structure. Under a H_{ac} applied along the length axis, the Metglas layers will elongate and shrink along that direction. This will force the thin PVDF layers to undergo an AC longitudinal strain, inducing a dielectric polarization change in its thickness or transverse direction. As can be seen in Figure 3.3, V_{ME} for the 3-layer sandwich laminate was flat with frequency over the bandwidth of the sub-resonant range; experiencing a dramatic resonance-enhancement at the first longitudinal mode $f=50\text{kHz}$, with a peak value of $V_{ME}=238 \text{ V/cm-Oe}$.

However, the two-layer unimorph laminate of Figure3.1(c) has an unsymmetrical structure. Figure 3.3 also shows V_{ME} as a function of frequency for this

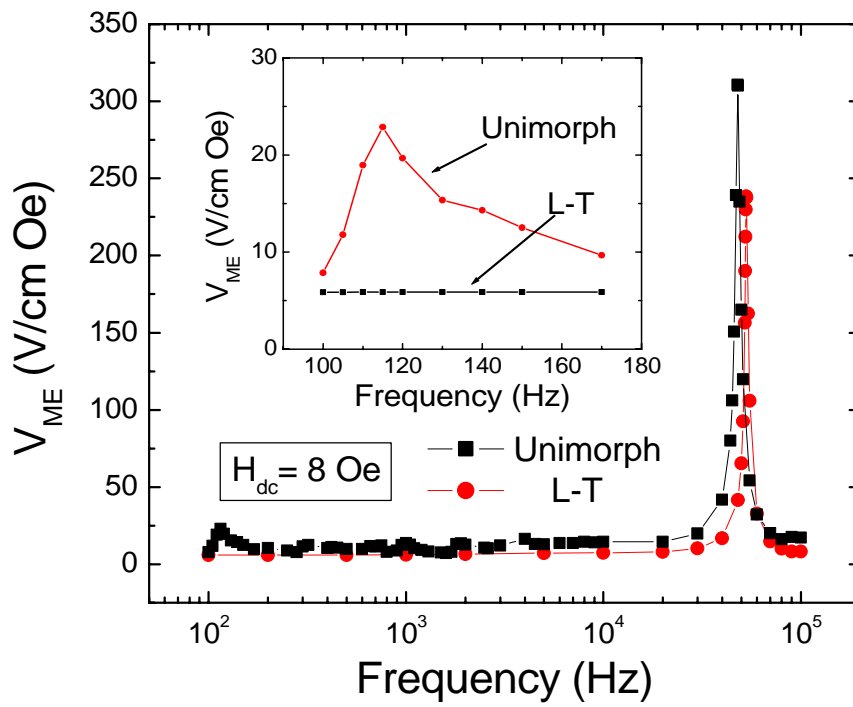


Figure 3.3 Frequency dependence ($10^2 < f < 10^5$ Hz) of the ME voltage coefficient of both 3-layer Metgals(SA1)/PVDF and unimorph Metglas(CO)/PVDF laminates measured under $H_{dc}=8$ Oe and $H_{ac}=1$ Oe. The inset shows the ME voltage coefficient of both laminate types at low frequencies, illustrating a bending-mode enhancement in the unimorph at 110 Hz.

unimorph with $H_{ac}=10e$ applied along the length of the sample. In addition to a principle longitudinal mode resonance near 50kHz, a very low bending-mode resonance frequency was found. The inset of Fig. 3.3 shows a low frequency ($\sim 110\text{Hz}$) resonance with a maximum V_{ME} of 25V/cm-Oe (resonant-bending-enhancement of $\sim 5x$). Such low-frequency enhancement in V_{ME} was not observed for the 3-layer structure: although, both laminate types were found to have a strong ME enhancement (3-layer, 238V/cm-Oe: unimorph, 310V/cm-Oe) near 50kHz at the longitudinal resonance frequency.

3.2.2 Metglas/PZT fiber

Although PVDF has a large output voltage, its output charge is quite small since it has very small permittivity. To achieve high power, large output charges from the piezoelectric phase are necessary. Here, PZT ceramic was used to substitute PVDF, and to continue to obtain flexibility, very thin PZT fiber layers were used. A ($L-L$) ME composite consisting of a 1-D phase connectivity of piezoelectric PZT-fiber thin layers laminated between two 2-D phase connectivity of high-permeability magnetostrictive Metglas 2605 SA1 foils was used, forming a magneto-electric laminate with a ($2-1$) phase connectivity.

Figure 3.4 illustrates this new ($L-L$) configuration, which consists of a piezo-fiber layer laminated between two high-permeability Metglas 2605SA1 alloy ones. The piezo-fibers were PZT-5A ceramic ones that were 100 μm in thickness, 350 μm in width, and 30mm in length. A 1-D piezoelectric active fiber/epoxy composite (AFC) thin layer was then made, following a construction used in

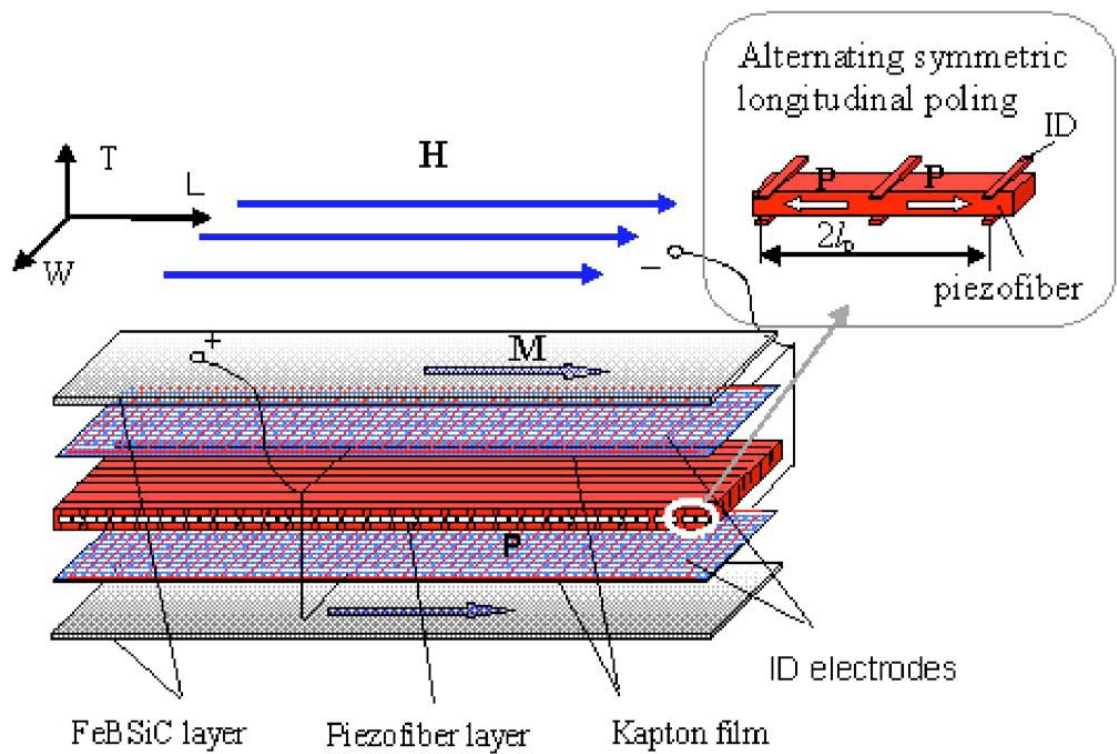


Figure 3.4. Illustration of the FeBSiC/piezofiber (L-L) laminate configuration. It consists of a (1-3) piezoelectric active fiber/epoxy composited (AFC) thin layer where the fibers are oriented along the longitudinal axis, which is laminated between two FeBSiC layers. Insulating Kapton films with inter-digitated (ID) electrodes were placed between layers. Each piezo-fiber had numerous alternating symmetric longitudinally-poled ('push-pull' units) that were each $2l_p=1\text{mm}$ in length, as shown in the inset.

actuators^{47,48}. The piezo-fibers were oriented along the longitudinal axis of the laminate. Thin polymer (Kapton) insulating films with inter-digitated (ID) electrodes were placed between PZT-fiber and FeBSiC layers, which were then assembled into a laminated composite using an epoxy resin. Each piezo-fiber had numerous alternating symmetric longitudinally-poled ‘push-pull’ units with a length of $2l_p=1\text{mm}$, as shown in the inset of Figure 3.4. This multiple ‘push-pull’ (L-L) configuration not only optimizes stress transfer²⁵, but also enhances the dielectric capacitance of the laminate. A second longer laminate was also constructed by laminating a 1-D piezo-fiber layer (30mm in length) between two long FeBSiC layers (100mm in length). Following Newnham’s composite nomenclature⁴⁹, these ME laminates have a 2-1 connectivity of magnetic-piezoelectric phases.

The voltage induced across the ID electrodes of the piezofiber layer was measured as a function of (i) H_{dc} in response to a constant ac ($f=1\text{kHz}$) magnetic drive of $H_{ac}=1\text{Oe}$, both applied along the length of the laminate; and (ii) f under constant $H_{ac}=1\text{Oe}$ and $H_{dc}=4\text{Oe}$. An electromagnet was used to apply H_{dc} ; a pair of Helmholtz coils was used to generate a small H_{ac} ; and the induced voltage was measured by a lock-in amplifier. First, in Figure 3.5(a), $\alpha_{ME}^{(L-L)}$ as a function of H_{dc} is shown. Data are given for both short ($l=30\text{mm}$) and long ($l=100\text{mm}$) laminates, demonstrating that (i) ME coupling in Metglas/PZT fiber laminates is much higher than that in Terfenol-D/monolithic-piezoelectric laminates; and (ii) $\alpha_{ME}^{(L-L)} \sim l$ due to magnetic flux concentration effects, which result in stronger magnetic induction in the ME laminates. These data reveal maximum $\alpha_{ME}^{(L-L)}$ values of 18 (short) and 22V/cm-Oe (long) under H_{dc} of 8 and 40Oe, respectively: correspondingly $\alpha_{me}^{(L-L)} =$

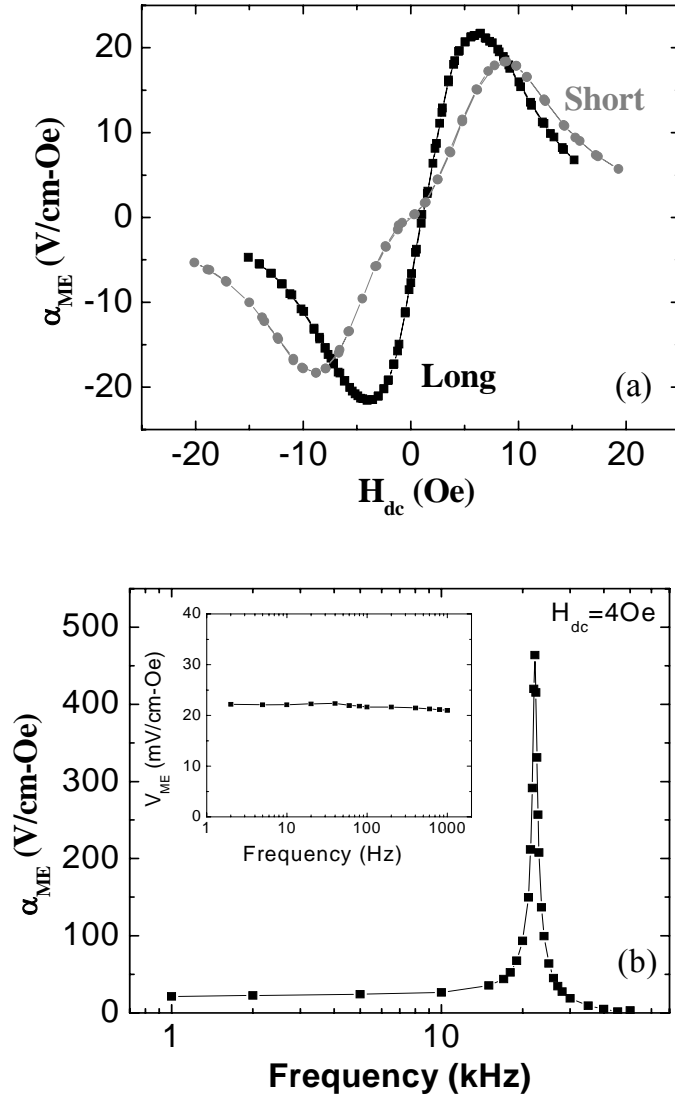


Figure 3.5. Magnetoelectric characterizations of FeBSiC/piezofiber laminates: (a) the ($L-L$) ME voltage coefficient $\alpha_{ME}^{(L-L)}$ as a function of H_{dc} for both short (30mm) and long (100mm) laminates; (b) $\alpha_{ME}^{(L-L)}$ as a function of frequency illustrating a strong enhancement at the electromechanical resonance frequency, where the inset shows a flat response over the quasi-static frequency range;

3.2×10^{-7} and 4×10^{-7} s/m or C/m²-Oe. These maximum values are much higher than recently reported *giant* ones ($\alpha_{ME}^{(L-T)} \sim 0.5-2.2$ V/cm-Oe¹⁻⁴, $\alpha_{ME}^{(L-L)} \sim 0.1$ V/cm-Oe⁶; $H_{dc}=300$ Oe), and require much lower biases ($<60\times$). These values of $\alpha_{ME}^{(L-L)}$ approach the theoretical limiting ones for the case of near-ideal ME coupling given by (1). These very high effects occur due to (i) optimum stress transfer in the (L-L) (2-1) configuration, (ii) the large $d_{33,m}$ and magnetic flux concentration effect of high-permeability FeBSiC alloy layer, and (iii) the high $g_{33,p}$ of the 1-D piezofiber layer.

Next, in Figure 3.5(b), $\alpha_{ME}^{(L-L)}$ ($l=100$ mm) as a function of frequency under a constant bias of $H_{dc}=4$ Oe is shown. The inset demonstrates that very high values are maintained down to quasi-static frequencies. The figure itself reveals a strong resonance enhancement of $\alpha_{ME}^{(L-L)}$ to ~ 500 V/cm-Oe at $f_r \approx 22$ kHz; or, correspondingly $\alpha_{me}^{(L-L)} = 10^{-5}$ s/m.

In Figure 3.6, $\alpha_{ME} - H_{dc}$ is shown for H_{ac} applied along the length ($\alpha_{ME}^{(L-L)}$), width ($\alpha_{ME}^{(T1-L)}$), and thickness ($\alpha_{ME}^{(T2-L)}$) of the laminate. The data show that $\alpha_{ME}^{(L-L)}$ is dramatically larger than either $\alpha_{ME}^{(T1-L)}$ or $\alpha_{ME}^{(T2-L)}$, with a large anisotropy factor of $100 < K = \alpha_{ME}^{(L-L)} / \alpha_{ME}^{(T-L)} < 1000$: which can be attributed to the unidirectional natures of the (i) length-strain sensitivity of 1-D piezo-fibers; and (ii) demagnetization factor N of Metglas ribbon

3.3 New ME structure designs

In this section, I will discuss the noise generated by thermal fluctuations and vibrations in the environment. I will address how to reject these noise sources from the signal charges.

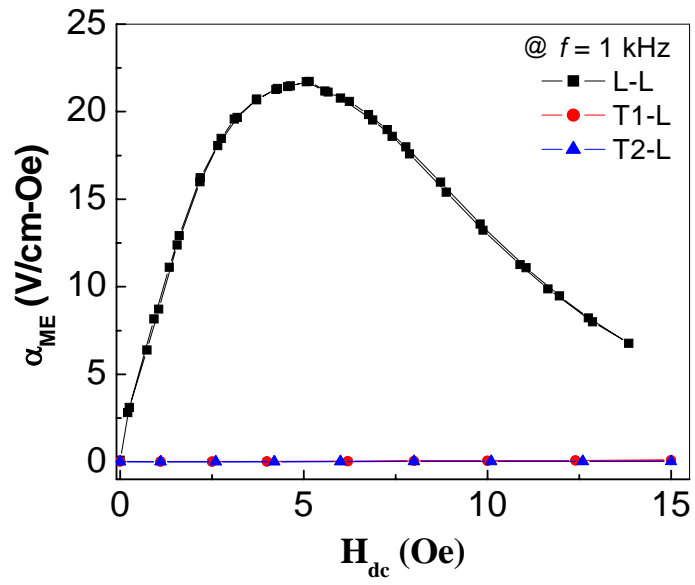


Figure 3.6 anisotropy of α_{ME} for H_{ac} applied along the length ($\alpha_{ME}^{(L-L)}$), width ($\alpha_{ME}^{(T1-L)}$) and thickness ($\alpha_{ME}^{(T2-L)}$) of the laminate.

3.3.1 Symmetric bimorph design

Giant ME effects in laminates have been investigated for highly sensitive, low frequency magnetic field sensors^{33,50}. However, as a magnetic sensor, the minimization in intrinsic⁵¹ and extrinsic noises is critical to achieving high sensitivity. In the case of ME sensors, the dominate noise sources are (i) thermal noise, introduced via pyroelectric currents; and (ii) vibration or acoustic noises, introduced via the piezoelectric effect. Accordingly, small temperature fluctuations (or environment air flow and vibrations) will act as noise sources in the piezoelectric layer. Unfortunately, the 4 basic types of modes, and unimorph structure, previously reported do not have the capability to reject thermal noise. Here, I focus on thermal noise cancellation: a different ME laminate structure – the symmetric bimorph configuration operating in bending mode – is proposed, which has the ability to reject thermal noise from the detected magnetic signals.

Figure 3.7 shows the symmetric configuration of the bimorph laminate. It consists of two PZT layers and two Terfenol-D layers, bonded together by a hard epoxy. The PZT layers were poled in the thickness direction, where the polarization directions of the two layers were reversed with respect to each other. Both Terfenol-D layers were magnetized along their longitudinal directions; however, unlike prior modes, the magnetization directions in the two Terfenol-D layers were reversed by using two U shaped DC magnetic biases. The dimensions of each Terfenol-D layer were $14 \times 6 \times 1.2 \text{ mm}^3$ and the dimensions of each PZT layer were $16 \times 6 \times 1 \text{ mm}^3$. To compare the ME voltage coefficient of this symmetric bimorph mode to that of the LT one, a Terfenol-D/PZT 4 layer LT laminate of the same dimensions was constructed, where the polarization directions of both PZT layers were the same.

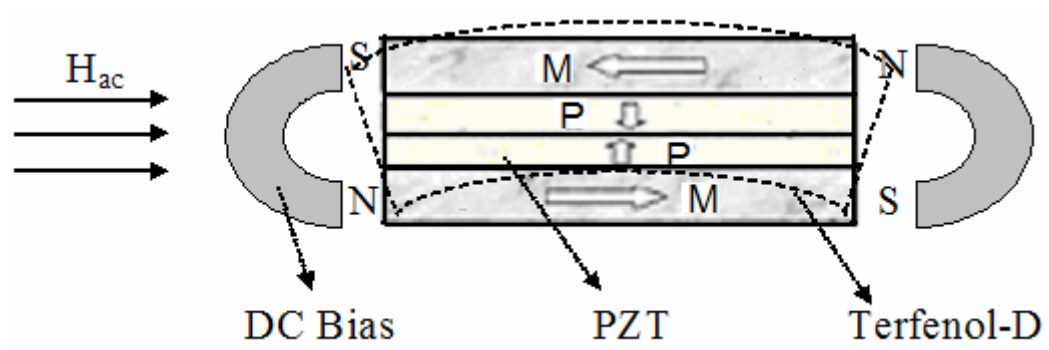


Figure 3.7 Schematic of the symmetric bimorph mode laminate with U shape DC magnetic biases.

When an AC magnetic field (H_{ac}) is applied along the longitudinal direction, the magnetization (M) in one Terfenol-D will decrease, whereas that in the other will increase: this will result in a decrease of the magnetostriction in one layer and an increase in the other. Thus, this symmetric bimorph laminate operates in a “pure” bending mode as a magnetic sensor, where the top and bottom PZT layers have induced charges of opposite signs. Thus, the differential output of these two PZT layers will be doubled, with respect to a single layer. Furthermore, when the temperature is changed, each layer in this symmetric structure will elongate or shrink together in a longitudinal mode. In this case, the top and bottom PZT layers will have induced thermal charges of the same sign: and consequently, the differential output of the thermal induced charge from the ME laminate will be essentially null. Theoretically, this ME symmetric bimorph should produce a high ME voltage, while at the same time rejecting thermal noise.

First, the ME voltage coefficients of both the symmetric bimorph and a LT mode laminate were measured. Figure 3.8 shows the measured frequency dependence of their ME voltage coefficients. In the quasi-static frequency range, the ME voltage coefficient of the symmetry bimorph and the LT mode were nearly equal (~ 1.2 V/cm-Oe). However, under resonance drive conditions, the ME coefficients of these two types of laminates were much different. The first resonance frequency of the symmetric bimorph was low (~ 34 kHz), whereas that of the LT mode was much higher (~ 83 kHz). In addition, a large ME voltage coefficient of 72 V/cm-Oe was

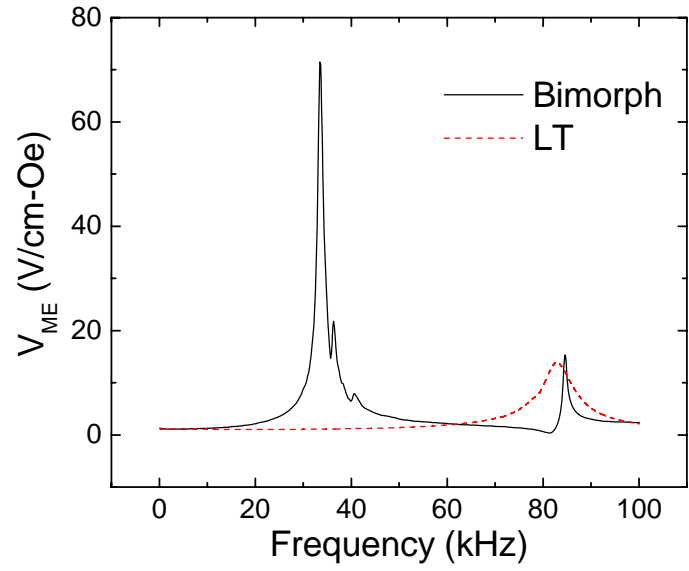


Figure 3.8. Frequency dependence ($10^2 < f < 10^5$ Hz) of the ME voltage coefficient for the symmetric bimorph and LT modes. These laminates have the same dimensions and were constructed from Terfenol-D and PZT layers of the same size.

found at the first bending mode resonance of the symmetric bimorph, which was much higher than that of the LT mode.

The lower resonance frequency of the symmetric bimorph is due to it being a bending mode. The bending mode resonance frequency of a laminate can be given as:

$$f_n^B = \frac{\pi d}{2\sqrt{12}l^2} \frac{(n+1/2)^2}{\sqrt{\bar{\rho}\bar{s}_{33}}}, n=1, 2, 3, \dots; \quad (2)$$

where f_n^B is the nth order bending resonance frequency, d the total thickness of the laminate, l the length, $\bar{\rho}$ the average density ($\bar{\rho} = v_T \rho_T + v_P \rho_P$), \bar{s}_{33} the equivalent elastic compliance of the laminate ($\bar{s}_{33} = s_{33,T} s_{33,P} / (v_P s_{33,T} + v_T s_{33,P})$), v the volume fraction of Terfenol-D or PZT, and the subscripts T and P designate Terfenol-D and PZT respectively. Whereas, the nth order longitudinal mode resonance frequency (f_n^L) is given by:

$$f_n^L = \frac{n}{2l} \frac{1}{\sqrt{\bar{\rho}\bar{s}_{33}}}, n=1,2,3, \dots \quad (3)$$

By using equation (3.2) and (3.3), The 1st order bending and longitudinal mode frequencies were calculated. The theoretical predictions were in agreement with the experimentally observed first order resonance frequencies for the symmetric bimorph and LT modes, which were 34kHz and 83kHz respectively.

Next, the effect of a thermal noise source on the ability of both the symmetric bimorph and LT laminates to sense small magnetic field changes were compared in the time domain. The thermal noise source was generated by a thermoelectric plate which was controlled by a DC current amplifier. Figure 3.9 shows the time dependence of the ME voltage when subjected to a small H_{ac} of 1.2×10^{-7} Tesla at 1Hz.

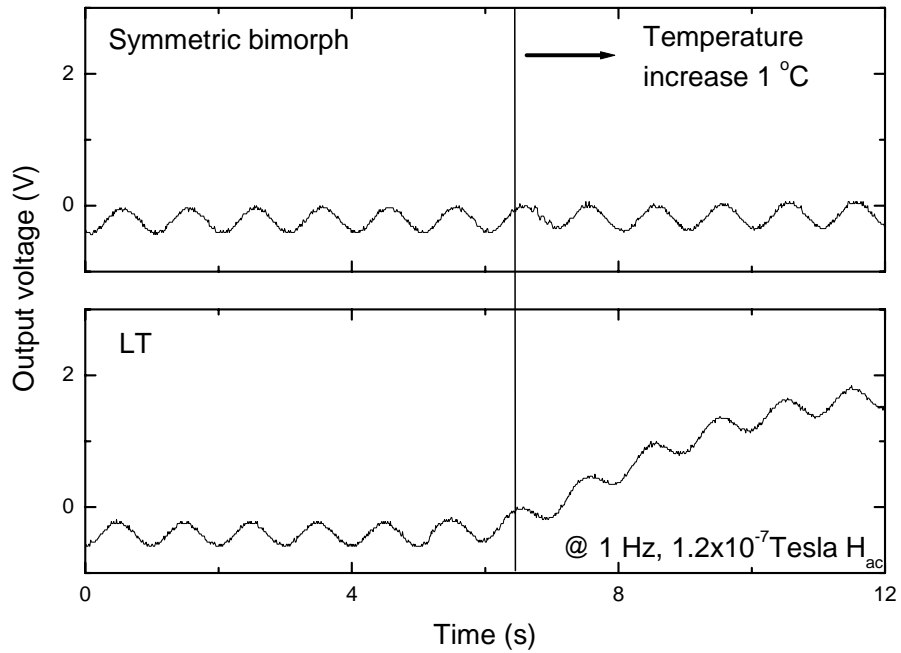


Figure 3.9 Time dependence of the voltage induced by an ac magnetic field of $H_{ac}=1.2 \times 10^{-7}$ Tesla ($f=1$ Hz) for (a) this symmetric bimorph, and (b) a LT mode laminate. At time $t=6.5$ s, temperature increased 1°C by thermoelectric plate.

Data are shown for both types of laminates. When the temperature was kept constant, the symmetric bimorph and LT modes had similar output voltages, which had sinusoidal wave forms, corresponding to that of H_{ac} . However, when the temperature was modulated by 1 °C, the voltage signal of the LT mode laminate was offset to higher voltages, resulting in the accumulation of charge across the PZT layer via the pyroelectric effect. For the symmetric bimorph, the same temperature flux did not result in any noticeable changes of the output voltage in the time domain. These results demonstrate the ability of the symmetric bimorph mode to reject a thermal noise source from a signal, due to its internal structure.

3.3.2 Differential mode

Vibration noise is an important noise source that must be considered for ME sensor applications. This is because piezoelectric materials are sensitive to vibrations. However, there are no second physical way by which to substitute piezoelectric materials in the ME laminates. Using the thermal stabilization designs of section 3.3.1, configurations were obtained that yield charges of the same sign and magnitude as the pyroelectric noise, while at the same time obtaining charges of opposite sign from the ME signal. The signals can be subtracted to eliminate pyroelectric noise, and a “pure” signal can be obtained. In other words, this method can increase the signal-to-noise ratio by rejecting thermal noise.

Figure 3.10 illustrates a schematic of a corresponding differential vibration design that was developed in the course of my study. The top and bottom layers are

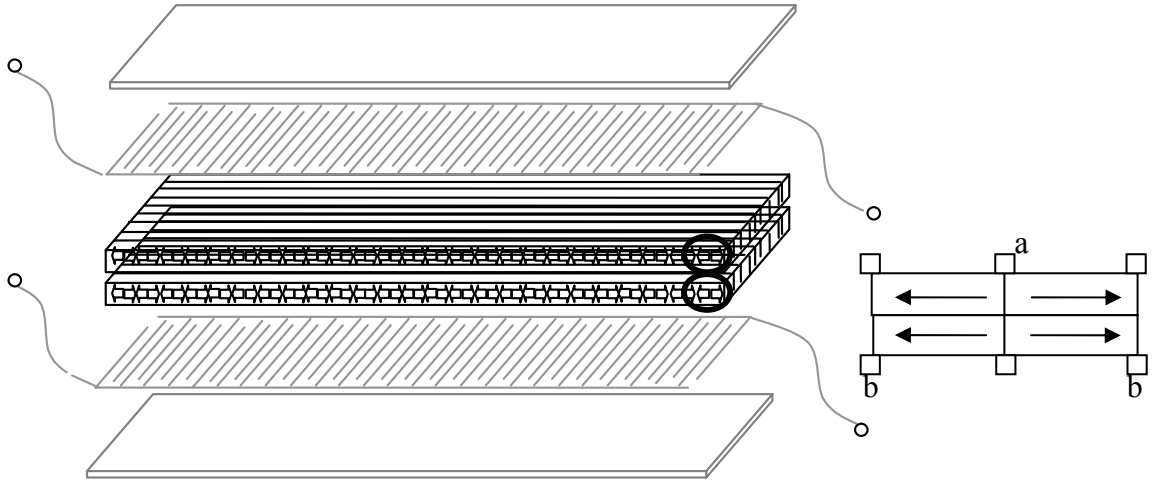


Figure 3.10 The schematic graph of the vibration differential design. The insert 2 layers are PZT fiber layer. The inset figure shows structure of each section. The small square is the electrodes. The arrow is the poling direction of the PZT fiber.

Metglas. The inside layers are two layers of PZT fibers that have the same thickness and volume. The electrodes are shown as the insert of Figure 3.10. The middle electrodes on the top of the PZT are of sign “a” and the other two are ground; whereas, the middle electrodes on the bottom of PZT are ground, and the other two are of sign “b”. When a magnetic field is applied along the length direction, the top and bottom PZT layers will have the same elongation, as a result “a” and “b” will be of different signs of charge. However, when a vibration noise is applied, the top PZT will elongate and the bottom one will shrink. Thus, “a” and “b” will be of the same sign. Upon taking the difference of “a” and “b”, (i.e., a-b) the ME signal will be increased by a factor of 2x times compared to the PZT fiber layer, while at the same time the vibration noise will be decreased to a small value.

First, the vibration noise cancellation capabilities of the differential mode are demonstrated in Figure 3.11. The center of the sample was placed on the top of a fixed point on a desktop. The vibration was applied by dropping a hammer from the same height each time, onto fixed position on the desktop. The signal 1 in Figure 3.11 was generated by the top PZT layer in the laminate and signal 2 was generated by the bottom PZT layer. The impact resulted in a huge surge in voltage at first, follow by a rapid damping. From Figure 3.11, it can be seen that signal 1 and signal 2 had nearly the same peak to peak values. In addition, the phases of signals 1 and 2 are similar. After subtracting signals 1 and 2, shown as the green line in Figure 3.11, the output voltage was decreased to $1/10^{\text{th}}$ of the original signal than both PZT layers. This demonstrates the capability of this ME composite design to reject vibration noise.

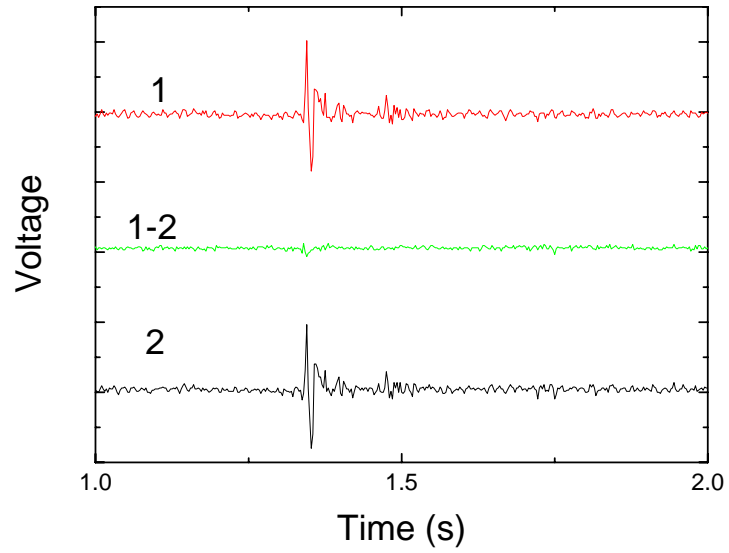


Figure 3.11 Demonstration of vibration noise cancellation by differential mode. Signal 1 and 2 are the voltages generated by vibration of top and bottom PZT layer respectively, the line in the center is the differential result of signal 1 and 2

Next, the output voltages of the two PZT layers were measured that were generated by application of magnetic field. Figure 3.12 shows that the magnetic field induced voltage was 180 degrees phase shifted with respect to each other. After subtraction, the induced voltage was increased by a factor of 2x times, relative to that of a single PZT layer. By using this differential design, the voltage/charge induced by magnetic field was increased by 2x, while at the same time, the voltage/charge generated by stray vibrations was reduced by a factor of ~10x. These results demonstrate a significant increase in the signal to noise ratio and in the sensitivity of ME laminates.

3.4 Section summary

In summary, giant permeability Metglas was incorporated into ME laminates. The piezomagnetic coefficient of the Metglas is larger than that of widely used magnetostrictive materials, such as Terfenol-D or nickel ferrite. The experimental results show that Metglas based ME laminates have giant ME voltage coefficients and small required DC magnetic biases. I have shown

- (i) that Metglas/PVDF laminates are thin, flexible, inexpensive, and only require a very small magnetic bias of $H_{dc}=8\text{Oe}$ ($1/50^{\text{th}}$ that of other ME laminates) to achieve the maximum ME coefficient. These ME laminates have giant ME voltage coefficients and excellent sensitivity to small variations in both AC and DC magnetic fields.

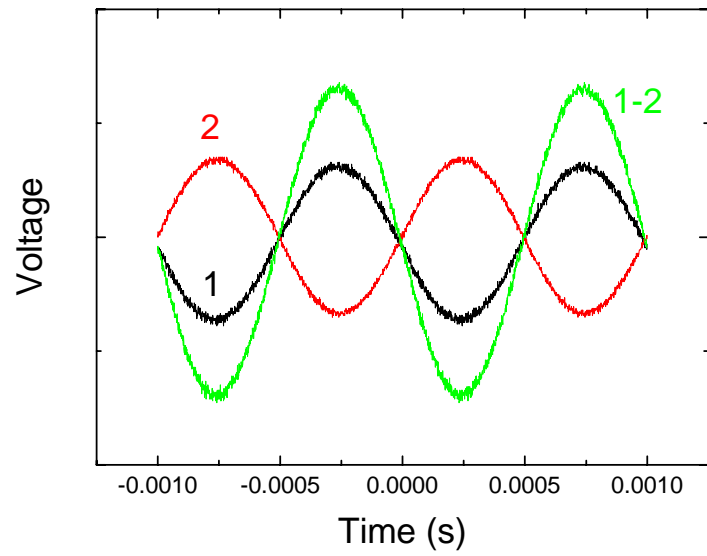


Figure 3.12 Voltages of the top and bottom PZT layer in the differential mode by applied magnetic field. The green line shows the differential result of the voltage 1 and voltage 2.

- (ii) that Metglas/PZT fiber laminates can be fabricated that unleash a near-ideal magnetoelectricity latent in (*L-L*) laminates. These laminates consist of a (1-3) piezoelectric PZT-fiber layer sandwiched between two high-permeability magnetostrictive Metglas foils. The experimental results show that they have colossal ME coefficients of $\alpha_{ME}^{(L-L)} > 20\text{V/cm-Oe}$ under small biases of 5 Oe. These values were strongly enhanced further to $\alpha_{ME}^{(L-L)} = 500\text{V/cm-Oe}$ by driving them under the electromechanical resonance conditions. The response was highly anisotropic, offering unidirectional sensitivity.

After that, I investigated the noise cancellation capabilities of ME laminate structures. The mechanisms behind the cancellation of thermal and vibration noises were studied, in addition to corresponding structure designs. I have shown:

- (i) that a new symmetric bimorph ME laminate has the unique capability to reject thermal noise from a magnetic signal. It works in a bending mode, rather than a longitudinal one, although it has a symmetric structure. At the 1st bending resonance, ME voltage coefficients as large as 70 V/cm-Oe can be achieved. This is much higher than that of the LT mode. This new symmetric ME bimorph offers potential application as a magnetic sensor, due to its large ME properties and noise rejection capabilities.
- (ii) that a differential mode of the ME laminate can reject vibration noise from a magnetic signal. It contains 2 layers of PZT sandwiched between the magnetic layers. Vibration induces bending modes in the PZT layers, generating charges

of the same sign from both top and bottom layers. Whereas a magnetic field induces a longitudinal mode, at the same time generating charges of different sign from the two PZT layers. After subtraction, the vibration noise was dramatically decreased, whereas the induced magnetic signal was increased.

IV. Fundamental ME properties

In the last chapter, the ME voltage coefficient was shown to be most important with regards to evaluating the ME effect. However, theoretically, it is not a fundamental materials parameter. Here, I will introduce the ME susceptibility: the fundamental ME parameter, which can be calculated from the piezoelectric and piezomagnetic coefficients.

Prior investigations of ME laminates has focused on material couples and geometrical structures. Changing piezoelectric or magnetostrictive materials, and/or geometrical shape or configuration of laminates, was the principal methods used to enhance the ME voltage coefficient and to decrease the required optimum DC bias. In this chapter, I will present an investigation of various characteristics of ME laminates at have been omitted by prior studies, which are quite important to design and applications, including: (i) how laminate shape affects the ME effect; (ii) how magnetic field may tune the resonance frequency of ME laminates, and enhanced the ME voltage coefficient; and (iii) how magnetic field direction can be measured by two-dimensional ME sensors.

4.1 ME susceptibility

Nearly all prior investigations have reported the ME coefficient as a voltage (V_{ME}) induced by a unit applied ac magnetic field (H_{ac}), given as $\alpha_{ME} = \frac{\Delta V_{ME}}{\Delta t \cdot H_{ac}}$

[V/Oe-cm], where α_{ME} is the ME voltage coefficient and Δt is the sample thickness. However, this coefficient is not the fundamental ME parameter; rather, it is the voltage induced across an insulating ME material by H_{ac} . Early investigations properly identified the fundamental parameter as the ME susceptibility (α_{me}), given as $\alpha_{me} = \Delta P / \Delta H_{ac}$ [in s/m], where P is the polarization. In the case that the external electric field is $E=0$, another formula $\alpha_{me} = \Delta D / \Delta H_{ac}$ [in s/m] can be obtained for the ME susceptibility, where D is the dielectric displacement. Early room temperature ME measurements of Cr_2O_3 crystals reported a value of $\alpha_{me} = 2.67 \times 10^{-12}$ s/m, which remains to this day the highest value for any single phase ME material. However, subsequent measurements have ignored the study of α_{me} , rather focused on α_{ME} . This is unfortunate, as α_{me} is the fundamental ME parameter (analogous to dielectric constant and magnetic permeability), whose understanding is essential to design of new devices such as gyrators⁵² and E-field tunable microwave dielectric resonators^{40,41}. Here, investigations of the ME susceptibility for various ME composites will be reported, which will reveal that the fundamental parameter α_{me} is on the order of 10^{-7} s/m, which is $\sim 10^5$ x larger than that of Cr_2O_3 crystals.

The ME susceptibility must be a complex quantity, similar to the effective dielectric permittivity (K_{eff}) and effective magnetic permeability (μ_{eff}) – even though it has never been treated as such. Accordingly, the basic properties of the complex ME susceptibility (α_{me}^*) are as follows: (i) it is described as

$$\alpha_{me}^* = \alpha'_{me} - i\alpha''_{me} = |\alpha_{me}| e^{-i\phi} \quad , \quad (4.1)$$

where α'_{me} and α''_{me} are the real and imaginary components of the response, and ϕ is the phase angle; (ii) it is connected in a general case to the ME voltage coefficient as

$$\alpha_{me}^* = |\alpha_{ME}^*| \bullet |K_{eff}^*| e^{-i\phi} = \alpha'_{me} - i\alpha''_{me}, \quad (4.2)$$

where $\alpha_{ME}^* = |\alpha_{ME}| e^{-i\phi_1}$, $K_{eff}^* = |K_{eff}| e^{-i\phi_2}$, and $\phi = \phi_1 + \phi_2$; and (iii) there is an inherent limit of the upper magnitude of the modulus given as

$$|\alpha_{me}| \leq \left(|K_{eff}| \bullet |\mu_{eff}| \right)^{1/2}, \quad (4.3)$$

which is fixed by the laws of electromagnetism due to the restriction that $|\alpha| \bullet |\nu| \leq 1$ where ν is the speed of the electromagnetic wave in the ME media.

Both modulus and phase of α_{me}^* for a number of laminate composites of different configurations were measured: (i) a longitudinally-poled piezoelectric layer laminated between longitudinally-magnetized magnetostrictive ones, or L-L mode; and (ii) a transversely-poled piezoelectric layer laminated between two longitudinally-magnetized ones, or L-T mode. Laminates of different materials couples were studied, including (i) piezoelectric $\text{Pb}(\text{Mg}_{1/3}\text{Nb}_{2/3})\text{O}_3$ - PbTiO_3 (PMN-PT) and magnetostrictive Terfenol-D; (ii) piezoelectric $\text{Pb}(\text{Zr}_x\text{Ti}_{1-x})\text{O}_3$ (PZT) and Terfenol-D; and (iii) PZT and magnetostrictive NiFe_2O_4 (NFO). A summary of materials couples used in the hybrid and laminate configurations is given in Table 4.1, along side the modulus of α_{me}^* at 1kHz. During the ME measurement, DC (H_{dc}) and AC (H_{ac}) magnetic fields were applied along the length of the laminates. An electromagnet was used to provide H_{dc} , and a Helmholtz coil was used to generate $H_{ac}=1\text{Oe}$. A lock-in amplifier (SR850) generated a controllable input current to the

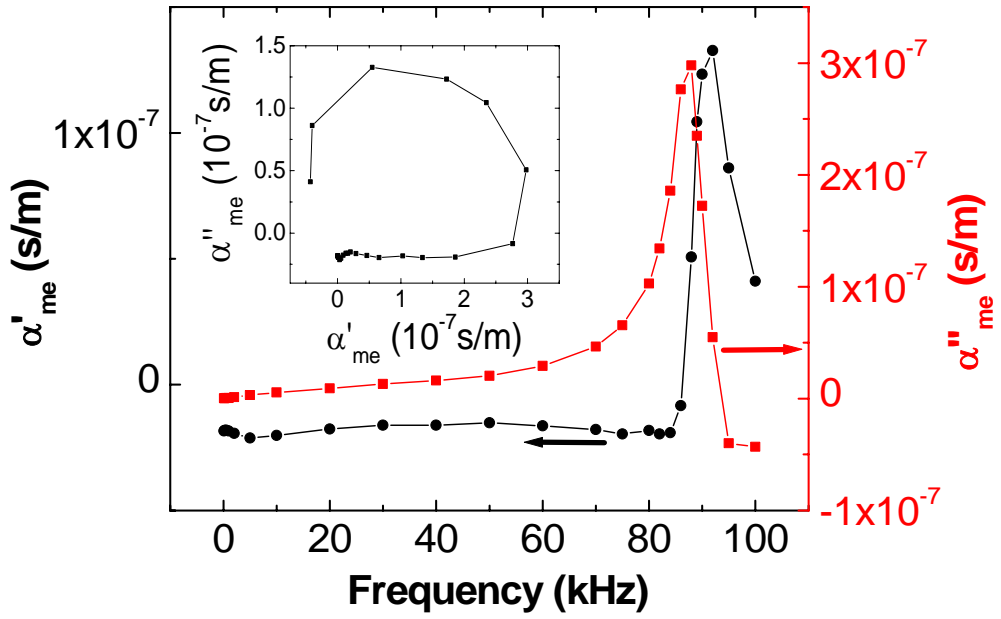
Table 4.1 Modules of the ME susceptibility for various ME laminate composites, and different mode configurations.

Composite type	Mode (thickness)	m_e (s/m)
<i>(a) PMN-PT / Terfeno l-D</i>	LL (1 mm)	8.7×10^{-8}
	LT (0.6 mm)	5.2×10^{-8}
<i>(b) PZT / Terfenol-D</i>	LL (2 mm)	4.2×10^{-8}
	LT (2 mm)	1.5×10^{-8}
<i>(c) PZT / NFO</i>	LT (1.2 mm)	1.1×10^{-9}

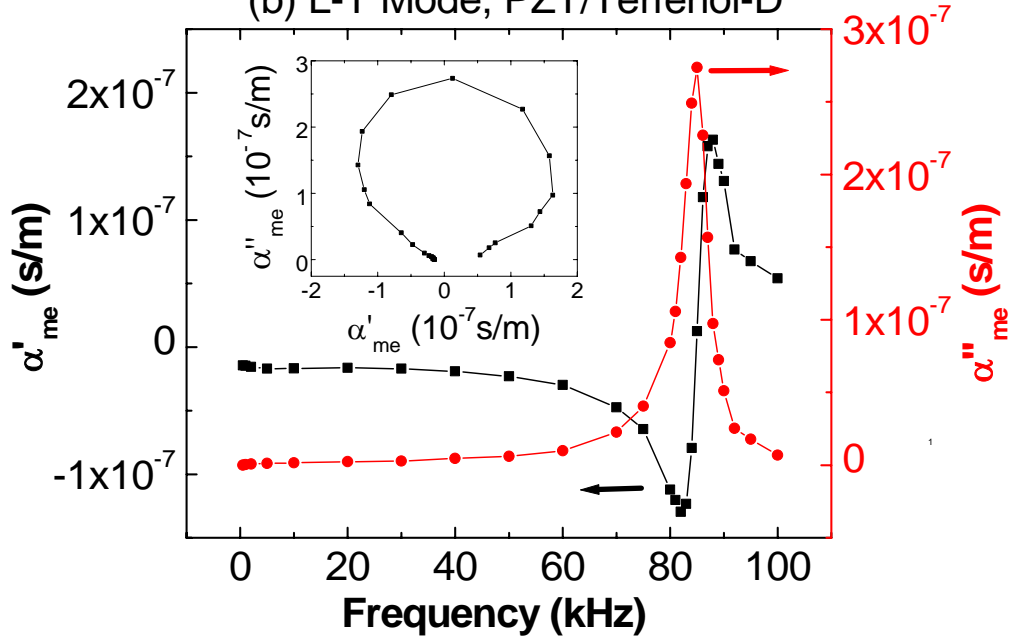
Helmholtz coil, and subsequently to measure the output voltage and phase from the piezoelectric layer. The complex ME susceptibility was then calculated using measurements made by a lock-in method, via the ME output charge and the phase shift between this output charge and input reference current. Due to a phase delay introduced by the input charge amplifier to the lock-in, the phase shift between the H-induced voltage across the PZT and the reference current was different than that of the induced charge and reference. This was mitigated by placing large capacitors in series with the charge amplifier.

Figure 4.1 shows the complex ME susceptibility as a function of frequency over the bandwidth of $10 < f < 10^5$ Hz for three layer laminates operated in (a) the L-L mode, consisting of Terfenol-D/PZT/Terfenol-D; and (b) the L-T mode consisting of Terfenol-D/PZT/Terfenol-D. In both figures, the real component α'_{me} of the ME susceptibility is given on the left-hand axis, and the imaginary one α''_{me} on the right-hand axis. The value of the α_{me}^* modulus was found to be dramatically enhanced near the electro-mechanical resonance (EMR) frequency, similar to prior investigations of α_{ME} , reaching values as high as 3×10^{-7} s/m in both modes. At lower frequencies of $f \approx 10^3$ Hz, the modulus α_{me}^* was found to be on the order of 10^{-8} s/m (see Table I). The imaginary component of the ME susceptibility was also found to demonstrate a strong enhancement at the EMR. Part (c) of this figure shows the complex ME susceptibility as a function of frequency for NFO/PZT/NFO three layer laminates operated in the L-T mode. The frequency range investigated ($10 < f < 10^5$ Hz) was insufficient to drive the laminate through its natural resonance. However, the

(a) L-L Mode, PZT/Terfenol-D



(b) L-T Mode, PZT/Terfenol-D



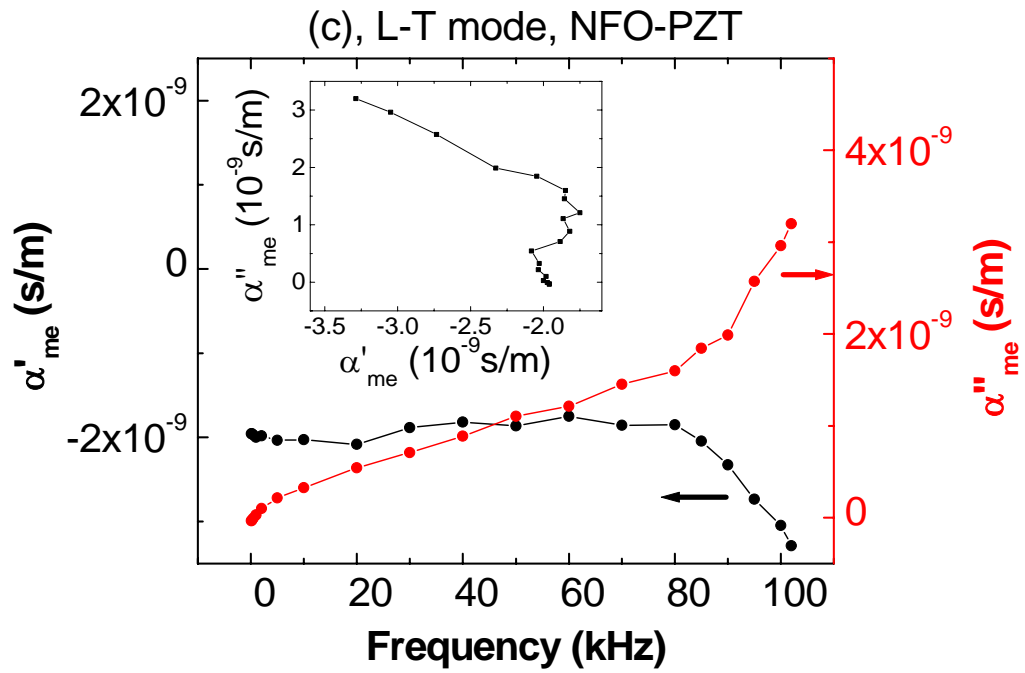


Figure 4.1 The real (left-hand side) and imaginary (right-hand side) components of the ME susceptibility as a function of frequency for (a) a L-L mode configuration consisting of PZT layers laminated together with Terfenol-D ones; (b) a L-T configuration consisting of PZT layers laminated together with Terfenol-D ones; and (c) a L-T configuration consisting of PZT layers laminated together with NiFe_2O_4 ones. The insets show Cole-Cole or Argand-type plots of the real and imaginary components. These measurements were performed under an ac magnetic field of $H_{ac}=1\text{Oe}$, and dc magnetic bias of $H_{dc}=500\text{Oe}$.

results in the figure clearly show similar frequency dispersion of α''_{me} and α'_{me} as that given in Figure 4.1.

The insets of Figure 4.1 show plots of α''_{me} vs. α'_{me} : known as Cole-Cole plots or Argand diagrams in dielectric or magnetic dispersion analysis, respectively. The plots of α''_{me} vs. α'_{me} nearly make a complete circle, when all the data pairs for the various frequencies are included over the bandwidth about the EMR. Semi-circles in such plots are typical of a complete relaxing out of a contribution to a storage modulus, and the loss of an underlying susceptibility mechanism. For the ME laminates, this is the loss of the elastic interaction between magnetostrictive and piezoelectric layers, as at frequencies greater than the EMR the laminates become elastically clamped. The full circle simply reflects an 180° phase shift in α''_{me} on going through the EMR, creating two semi-circles.

These results clearly demonstrate that the high ME susceptibility of ME laminates is due to elastic interactions between strictions of the individual layers, and that dispersion is a natural consequence of the loss of the underlying ME mechanism as the inertial mass clamps out the samples ability to vibrate with increasing frequency. The findings firmly establish (i) that the ME susceptibility is a complex quantity; (ii) that follows conventional types of dispersion relationships; and (iii) which has enormous storage compliance of $3 \times 10^{-7} \text{ s/m}$ at the EMR, nearly five (5) orders of magnitude higher than that of Cr_2O_3 which has the highest value of any known single phase material.

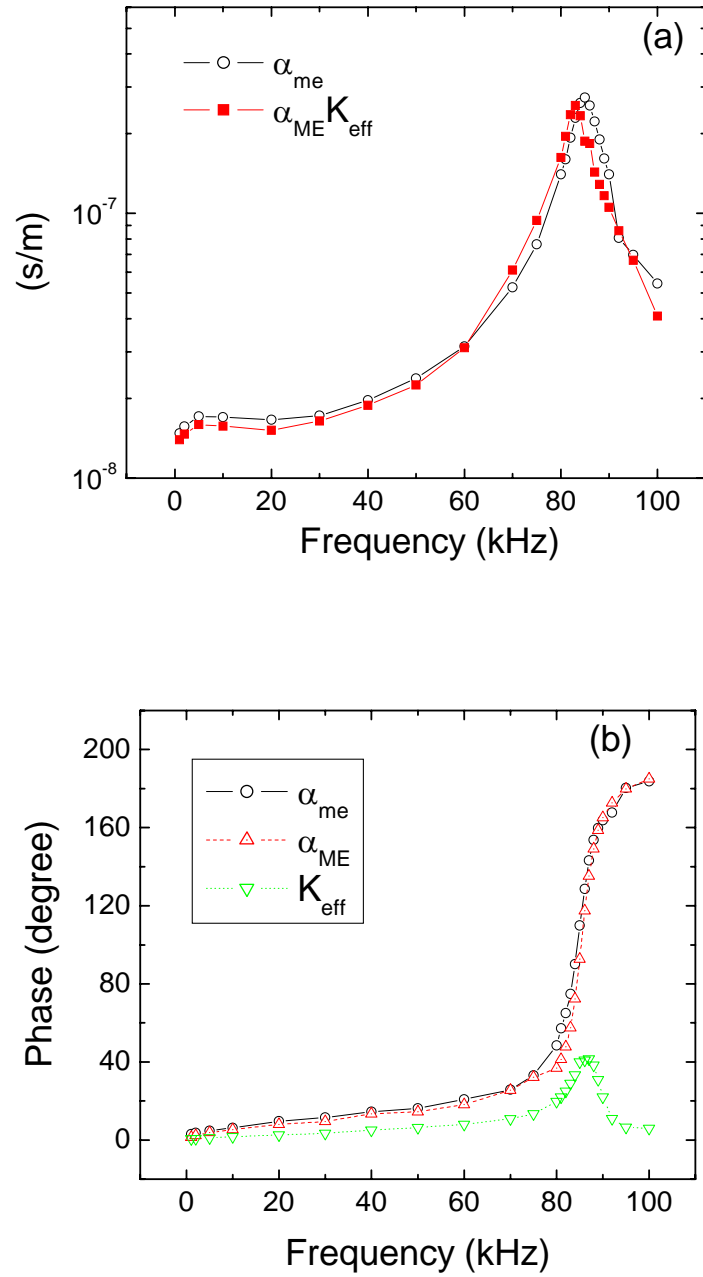


Figure 4.2 Demonstration showing the inter-relationship (fulfilling equation 4.2) between the ME susceptibility (α_{me}) and ME voltage coefficient (α_{ME}) for a L-T PZT/Terfenol-D laminate: (a) the real components of the responses; and (b) the imaginary components.

Figure 4.2(a) shows that the modulus of the ME susceptibility is connected to the modulus of the ME voltage coefficient. This data was taken for the L-T mode of a PZT/Tefenol-D laminate. In this figure, it can be seen that α_{me} and $\alpha_{ME} \cdot \epsilon_{eff}$ are equivalent over the entire bandwidth range of $10 < f < 10^5$ Hz. Next, Figure 4.2(b) shows that the corresponding phase angle of the ME susceptibility for this same laminate is related to that of the ME voltage coefficient. Together, these results show that the modulus and phase angle of the ME susceptibility are related to those of the ME voltage coefficient, as given by equation (1b).

Finally, Figure 4.3(a) shows the frequency dependence of the α_{me}^* modulus plotted next to that of $\left(K_{eff} \bullet |\mu_{eff}| \right)^{1/2}$. Inspection of this figure will reveal that equation (1c) is fulfilled over the entire bandwidth, i.e., $|\alpha_{me}| \leq \left(K_{eff} \bullet |\mu_{eff}| \right)^{1/2}$. It can be then used to calculate the speed of electromagnetic radiation in the ME laminate using the fact that $|\alpha| \bullet |\nu| \leq 1$. The results for this calculation are shown in Figure 4.3(b), which gives ν as a function of the H_{ac} applied to the laminate. In this figure, it can be seen (i) that the speed of electromagnetic radiation in a ME laminate under resonant drive is a mere 3×10^6 m/s, 1% of that of an electromagnetic wave in vacuum; (ii) that the modulus of $\alpha_{me}^* \approx \nu$ only in the vicinity of the EMR, and at sub-resonant frequencies the modulus of $\alpha_{me}^* \ll \nu$; (iii) that ν is nearly independent of the frequency of H_{ac} for that less than the EMR; and (iv) with increasing frequency and relaxing out of the elastic contribution to the ME susceptibility, that the value of ν increases. These results also bring to focus the difficulty of achieving large values of

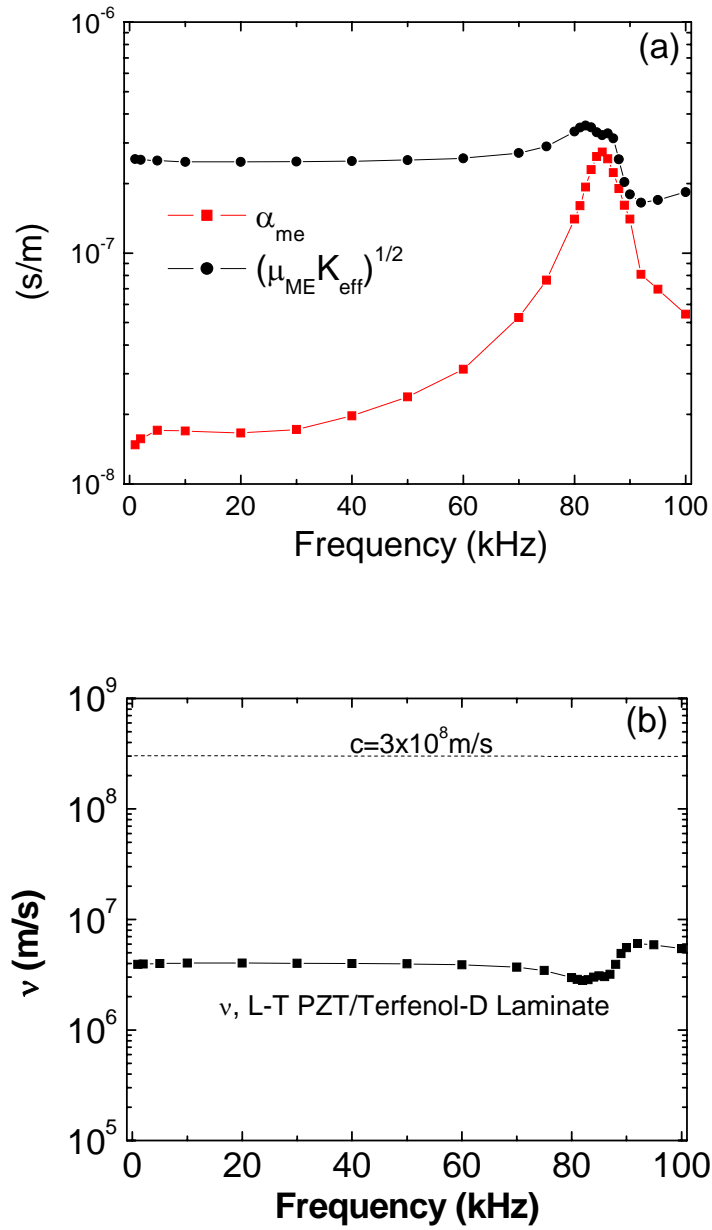


Figure 4.3 Demonstration of the inherent limit of the upper magnitude of the ME susceptibility modulus ($|\alpha_{me}|$): (a) $|\alpha_{me}|$ and $\left((K_{eff} \bullet \mu_{eff}) \right)^{1/2}$; and (b) the speed of an electromagnetic wave, v , in the ME media.

α_{me} , as it requires a dramatic slowing down of ν : an instability in the modulus of α_{me}^* would require the trapping of electromagnetic radiation. Clearly, the ME susceptibility is a fundamental parameter that relates the coupling between polarization and magnetization, via the media's interaction with an electromagnetic wave.

4.2 Demagnetization (shape) and magnetization distribution (position) effects

Most previous investigations of ME laminates focused on selecting piezoelectric or magnetostrictive materials, and optimizing the laminate structure. Theoretical calculations in design were always based on two assumptions: (i) that there is no shape demagnetization effect in the magnetic phase; and (ii) that the internal magnetization in the magnetic layer is homogeneous. However, shape demagnetization effects⁵³ can change the internal magnetization, and affect the piezomagnetic coefficient of the magnetic layer; and consequently, altering the ME effect of laminated composites. Also, the internal magnetization distribution may vary from the edge to the center of a laminate even under a constant magnetic bias. The magnetostriction at different positions may vary, and accordingly the ME effect may also be notably different at various positions of the laminate. Here, in this section, I have investigated how the shape and the position of a magnetic layer affects the ME coupling. Two typical magnetostrictive materials were selected, one is the giant

permeability material Metglas and the other is low permeability, giant magnetostrictive material Terfenol-D.

Magnetic materials have an internal field that normally opposes the magnetization. This field is called the demagnetization field or H_d . The demagnetization field is affected by the shape and the permeability of magnetic materials. The demagnetizing field in a uniformly magnetized ellipsoid can be given as:

$$H_d = -NM ; \quad (4.4)$$

where N is the demagnetization coefficient tensor. For a rectangular shaped (as showed in Figure 4.4) magnetic materials, the demagnetization coefficient can be given as:

$$\begin{aligned} \pi N_z = & \frac{b^2 - c^2}{2bc} \ln\left(\frac{\sqrt{a^2 + b^2 + c^2} - a}{\sqrt{a^2 + b^2 + c^2} + a}\right) + \frac{a^2 - c^2}{2ac} \ln\left(\frac{\sqrt{a^2 + b^2 + c^2} - b}{\sqrt{a^2 + b^2 + c^2} + b}\right) \\ & + \frac{b}{2c} \ln\left(\frac{\sqrt{a^2 + b^2} - a}{\sqrt{a^2 + b^2} + a}\right) + \frac{a}{2c} \ln\left(\frac{\sqrt{a^2 + b^2} + b}{\sqrt{a^2 + b^2} - b}\right) + \frac{c}{2a} \ln\left(\frac{\sqrt{b^2 + c^2} - b}{\sqrt{b^2 + c^2} + b}\right) \\ & + \frac{c}{2b} \ln\left(\frac{\sqrt{a^2 + c^2} - a}{\sqrt{a^2 + c^2} + a}\right) + 2 \arctan\left(\frac{ab}{c\sqrt{a^2 + b^2 + c^2}}\right) + \frac{a^3 + b^3 - 2c^3}{3abc} ; \quad (4.5) \\ & + \frac{a^2 + b^2 - 2c^2}{3abc} \sqrt{a^2 + b^2 + c^2} + \frac{c}{ab} (\sqrt{a^2 + b^2} + \sqrt{b^2 + c^2}) \\ & - \frac{(a^2 + b^2)^{3/2} + (b^2 + c^2)^{3/2} + (a^2 + c^2)^{3/2}}{3abc} \end{aligned}$$

The other two demagnetization factors can be calculated by replacing c-a-b-c or twice c-a-b-c.

As a consequence of the demagnetization field, the shape of a material will affect its magnetization properties. This shape effect will also influence the DC magnetic field dependence of the magnetostriction curve, and the effective linear

piezomagnetic constants. Here, how shape affects giant permeability Metglas/PZT laminates, and then low permeability Terfenol-D/PZT ones, was shown.

Figure 4.5a shows the ME voltage induced by an applied DC bias. The composite is Metglas/PZT operated in the LT mode. The dimensions of the PZT layer was $18 \times 6 \times 0.3 \text{ mm}^3$. The thickness and width of the Metglas layer were 25 μm and 6mm. The length of the Metglas was varied from 18mm to 110mm. These data clearly show with increasing length of the Metglas that the output ME voltage increases from 90mV to 260mV, and that the DC bias decreases from 30Oe to 2 Oe. These data illustrate a new approach to increasing the ME voltage coefficient and to decreasing the required DC bias, which is based on the demagnetization effect.

Figure 4.5b shows the DC magnetic field dependence of the ME effect of this Metglas/PZT for various thicknesses of Metglas. The thickness of the PZT was 0.25mm and the thickness of each Metglas layer was 0.025mm. The ME voltage coefficient increased with increasing thickness of the Metglas, until the thickness of the Metglas was 0.15mm. After that point, the ME voltage coefficient decreased with increasing thickness of the Metglas. At the same time, the required optimum DC bias increased quickly with increasing thickness of the Metglas.

There are two mechanisms for increasing the thickness ratio r of the magnetic layer. One is that the magnetic phase can have a larger induced magnetostrictive strain by which it can subsequently deform the piezoelectric phase, as discussed in Section 1.3.4. Accordingly, the ME voltage coefficient will increase with increasing thickness

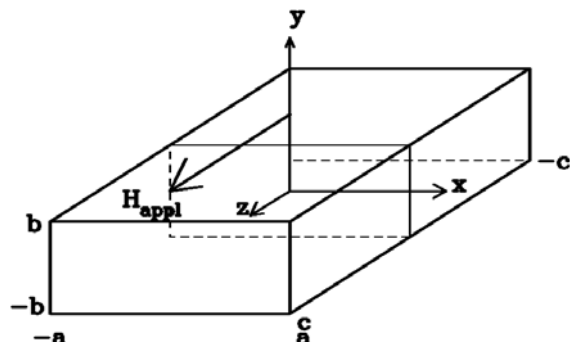


Figure 4.4 the coordinate system used in calculating of the demagnetization for rectangle prism.

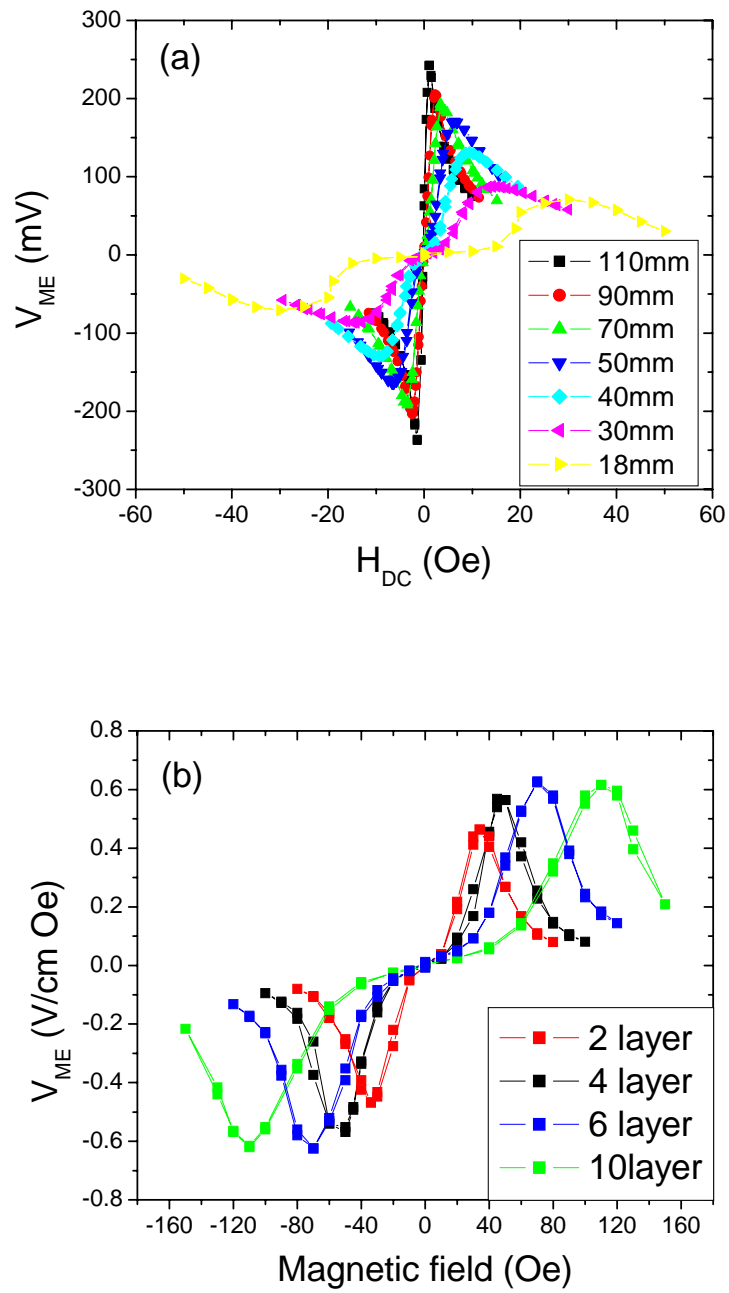


Figure 4.5 DC magnetic field dependence of the ME output voltage. All the laminates have the same dimensional PZT. (a) The length of the Metglas is various from 18 mm to 110 mm. (b) The thickness of the Metglas varies from 0.05mm to 0.25mm

of Metglas. The other one is a shape effect. With increasing thickness of Metglas, it saturates at higher magnetic fields. This results in a decrease in its effective piezomagnetic coefficient at optimum bias. Thus, the ME effect decreases with increasing thickness of Metglas. When the thickness of Metglas is below 0.15mm, the first mechanism dominates; whereas at higher thicknesses, the second one does

A shape effect was also found in low permeability Terfenol-D/PZT laminates, as shown in Figure 4.6. With increasing thickness of Terfenol-D from 7mm to 23 mm, the ME voltage coefficient increased from 80 mV/Oe to 90 mV/Oe. At the same time, the required optimum DC bias decreased from 800 Oe to 400 Oe. Compared to high permeability Metglas, the ME voltage coefficient of Terfenol-D only increased slightly with increasing length, while the required optimum DC bias changed by the same ratio. These results show that a long, thin and narrow shape is essential in order to obtain a large ME voltage coefficient and a small required optimum DC bias.

The magnetization distribution inside the magnetic layer is non-uniform. This will result in the magnetostriction being different at various positions within the magnetostrictive layer. Figure 4.7 shows the ME voltage coefficient at various locations along the length of a ME laminate. For large permeability Metglas/PZT, the ME voltage coefficient decreased rapidly from the center of the laminate to the edge, as shown in Figure 4.7a. In general, the magnetic field is concentrated along the length of the Metglas towards the center of the composite, simply because the giant permeability lens the flux lines. Correspondingly, the change of the induced

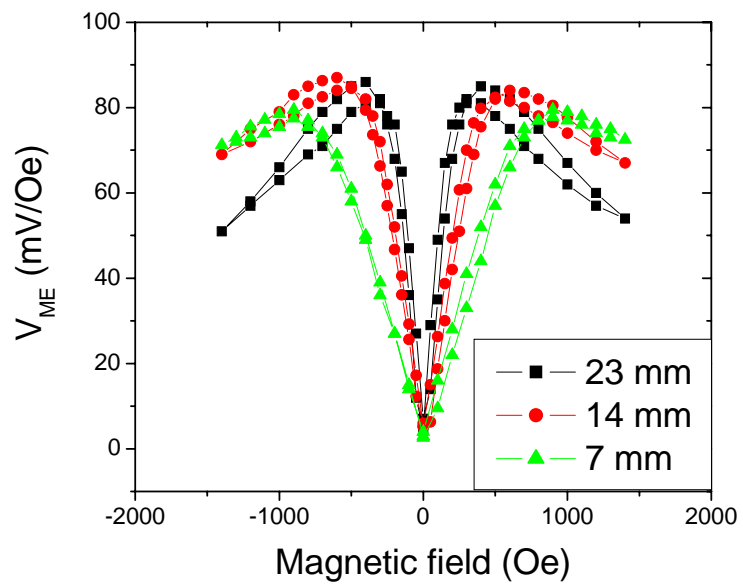


Figure 4.6 DC magnetic field dependence of the ME output voltage of Terfenol-D/PZT. All the laminates have the same thickness and width. The length of the Metglas is various from 7 mm to 23 mm.

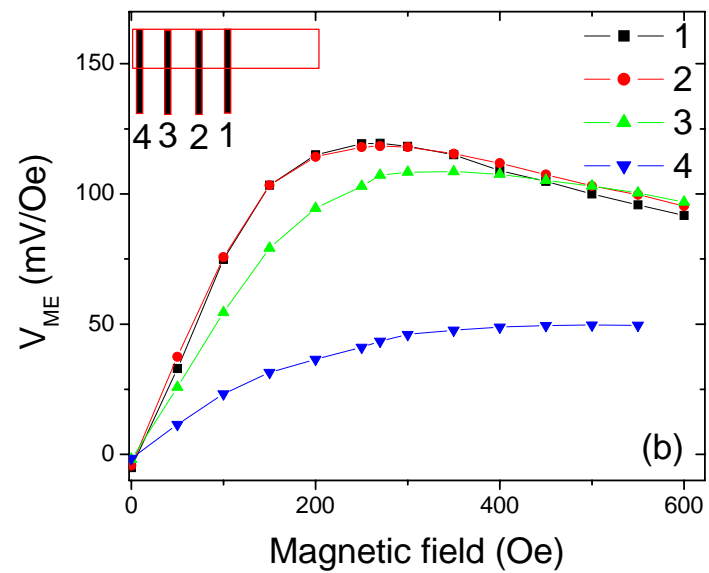
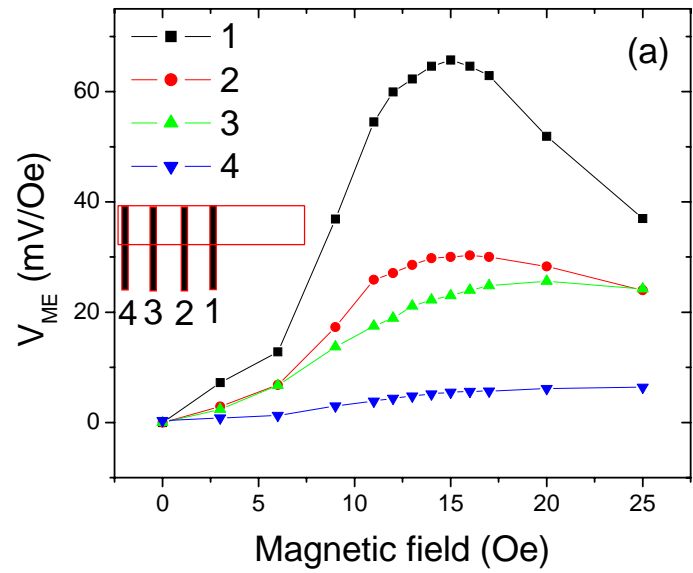


Figure 4.7 ME voltage coefficient of the (a) Metglas/PZT and (b) Terfenol-D/PZT at different position. Point 1 is the center of the laminate and point 4 is the edge of the laminate.

magnetostrictive strain is largest in the center of the Metglas layer, resulting in a larger ME voltage coefficient in the center of the laminate. However, for low permeability Terfenol-D/PZT (Figure 4.7b), this non-uniformity was not nearly as obvious. Only at the edge of the laminates was the ME voltage coefficient notably smaller than at the other points. For Metglas/PZT laminates, the length of the Metglas layer should be longer than that of the PZT. Whereas, for Terfenol-D/PZT laminates, the length of the Terfenol-D layer should be similar in size to the one for PZT as the magnetization inside the low permeability Terfenol-D is more uniform.

4.3 Magnetic field tunability of resonance frequency: enhanced effective bandwidth

The magnetoelectric (ME) effect has been widely investigated in piezoelectric/magnetostrictive composites, where a giant ME effect has been found in laminate composites: such as Terfenol-D/PZT and Metglas/PZT laminates^{23,24,54}. New and unique applications (such as magnetic sensors^{30,33}, transformers²⁸, gyrators⁵²) have been reported for ME composites. A number of these applications are based on an electromechanical resonant (EMR) enhancement of the ME effect, where the ME voltage coefficient is increased by a factor of 10-1000x times that at quasi-static frequencies. Energy conversion efficiency is high only near the EMR frequency.

However, the resonance peak is sharp and fixed for ME laminates, limiting the bandwidth of the applications that use the resonant enhancement. Any small aberrancy at the resonance point will result in a dramatic decrease in the ME voltage.

The simplest method by which to widen the resonance frequency is to select a low Q material; however, this will result in a notable decrease in the peak amplitude value. Alternatively, a series of laminates with different lengths could be used to broaden the bandwidth of an operational device⁵⁵, but the effective peak would not be smooth. Also, in this case, at any specific frequency, only one of the laminates in the series might work at its resonance condition: all the others would not make a significant contribution to the total output voltage at any particular frequency. In the microwave frequency range, ME composite resonators and phase shifters are known to have a dual electric and magnetic field tunable ferromagnetic resonance frequency (FMR)^{40,41}. The FMR is shifted due to a change in the piezoelectric deformation or the magnetostatic spin wave. In effect, this results in a broadening of the bandwidth of microwave devices based on ME composites.

Here, in this section, the effective bandwidth of the EMR enhancement of the ME coefficient will be shown to be notably broaden by magnetic field tuning. These studies show that Terfenol-D/PZT laminates are well suited for such tunable resonance devices because of the large magnetostriction (up to 1600 ppm) of Terfenol-D, which is 40x times larger than that of Metglas or nickel ferrite. The large magnetostriction of Terfenol-D is necessary in order to impose a large strain on the PZT; thus, enabling a dramatical shift of the resonance frequency under applied magnetic field.

The ME laminates used in this investigation were a tri-layer sandwich structure, as shown in the insert of Figure 4.8. The top and bottom layers were

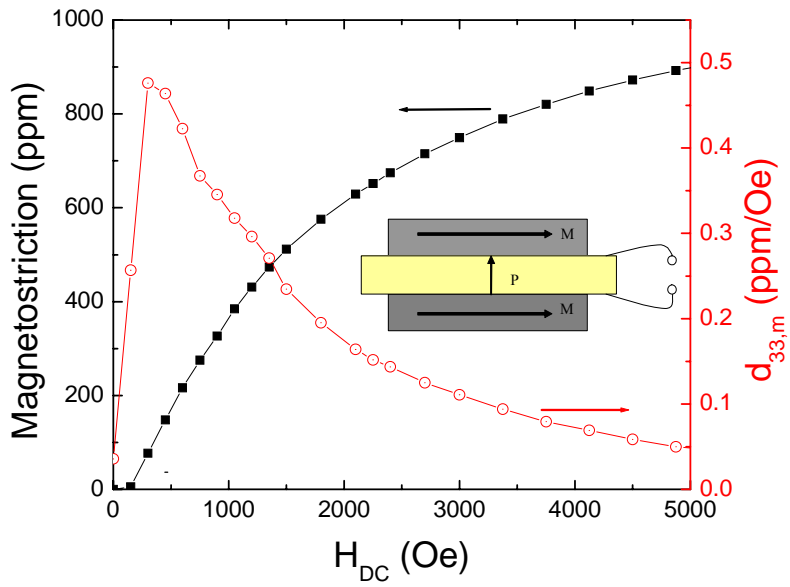


Figure 4.8 Magnetostriction and piezomagnetic constant of the Terfenol-D/PZT laminate as a dependence of H_{DC} from 0Oe to 5000Oe. Insert graph shows a schematic graph of the Terfenol-D/PZT sandwich structure laminate.

Terfenol-D ($28 \times 6 \times 1.2 \text{ mm}^3$) and the inner layer was PZT ($30 \times 6 \times 1 \text{ mm}^3$). The PZT layer was poled along its thickness direction. During measurements, both DC (H_{DC}) and AC (H_{AC}) magnetic fields were applied along the longitudinal direction of the laminate. The working mode was the so called longitudinal magnetization – transverse polarization or L-T mode.

First, the magnetostriction of Terfenol-D/PZT laminates was measured under mechanical free conditions. Figure 4.8 shows the measured strain as a function of applied magnetic field. Note that the magnetostriction of Terfenol-D tends towards saturation (900 ppm) at a field near $H_{DC}=5000\text{Oe}$, at which point its effective linear piezomagnetic constant $d_{33,m}$ tends to a minimum. In addition, under a large applied magnetic field, the elastic stiffness of Terfenol-D will be affected, resulting in a shift of the resonance frequency. To achieve a large strain of 800 ppm by applying an electric field to PZT, a field of $E=20\text{kV/cm}$ would be needed. This would require a large voltage to be applied to the bulk laminates. If the ME laminates operate in the LL or push-pull mode, voltages as high as 10 kV maybe required. Clearly, electric tunable designs are not very feasible for bulk composites.

Next, the resonance enhancement of the laminate under different magnetic biases was measured. Figure 4.9a shows the frequency dependence of the ME voltage coefficient under various H_{DC} . The resonance frequency can be seen to be notably increased with increasing DC bias. These results demonstrate a pronounced shifting of the resonance frequency from $f_0=40\text{kHz}$ for $H_{DC}=0\text{Oe}$ to $f_0=55\text{kHz}$ for $H_{DC}=5000\text{Oe}$. Furthermore, the peak resonance enhancement of V_{ME} was increased with increasing

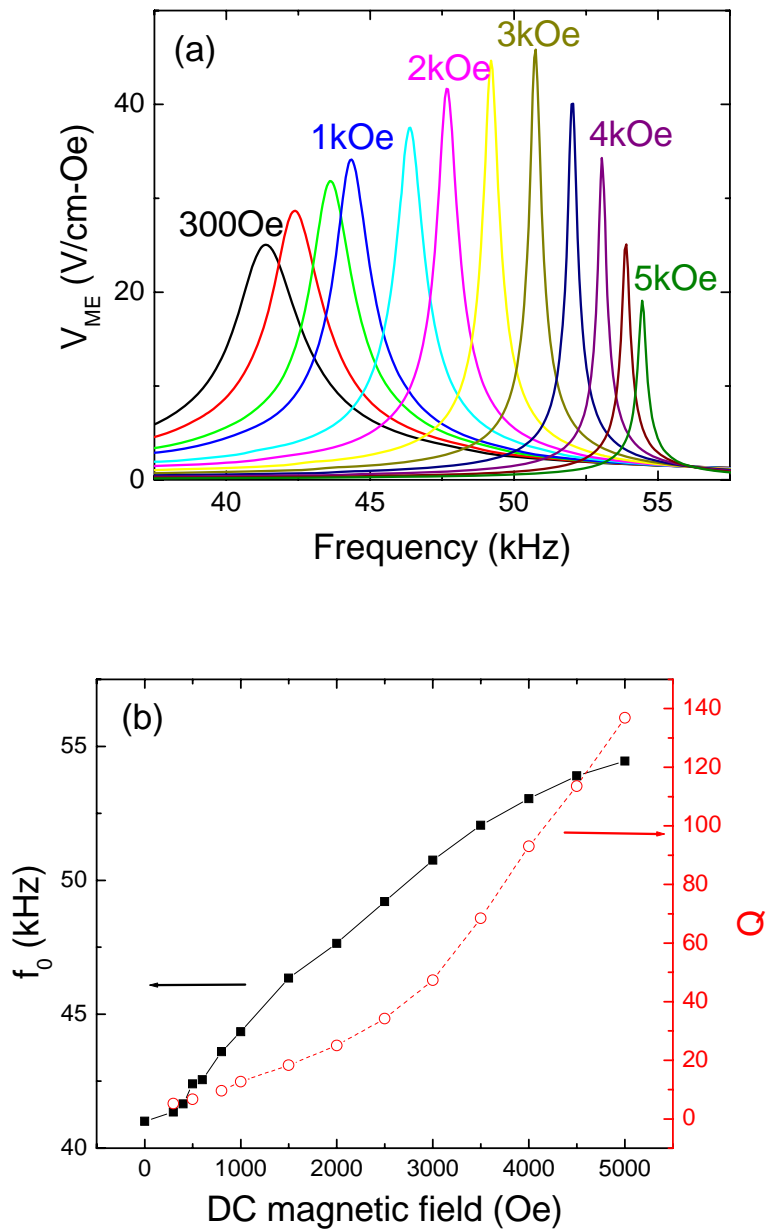


Figure 4.9 (a) Frequency dependence of the ME voltage coefficient at various H_{DC} from 300 Oe to 5000 Oe; and (b) resonance frequency and Q of the Terfenol-D/PZT laminate as a dependence of H_{DC} from 0Oe to 5000Oe.

bias for $H_{DC} \leq 3000\text{Oe}$. The maximum resonance enhanced value of V_{ME} was $\sim 46\text{V/cm-Oe}$ under a $H_{DC}=3000\text{Oe}$: above which point, further increases of H_{DC} resulted in a decrease of V_{ME} . This trend is different from that for the quasi-static ME voltage coefficient which is shown in Figure 4.8. The optimum bias condition is $H_{DC}=300\text{Oe}$ for the quasi-static case, which has a value 10x times smaller than that at the EMR.

In Figure 4.9b, the resonance frequency f_0 and mechanical quality factor Q as a function of H_{DC} are shown. The value of f_0 increased with increasing DC bias due to an increased elastic stiffness induced by magnetostriction. For $H_{DC} < 300\text{Oe}$, f_0 was only slightly changed with increasing bias, and the resonance ME voltage coefficient was small. In this figure, it can also be seen that f_0 increased much more dramatically in the range of $1000\text{Oe} \leq H_{DC} \leq 4000\text{Oe}$; whereas when $H_{DC} > 4000\text{Oe}$, f_0 increased only gradually with further increasing bias, as the magnetostriction of Terfenol-D tended towards saturation. Correspondingly, it can be seen that Q notably increases with increasing bias: indicating that the loss mechanism may be controlled by the magnetostrictive phase, where the Q value increases with H_{DC} .

It is relevant to note that the observed trends in the peak value of the resonance enhanced value of V_{ME} as a function of H_{DC} are notably different than that at quasi-static frequencies. For comparisons, Figure 4.10 shows the value of V_{ME} for the laminate at a sub-resonant frequency of 1kHz. In this figure, it can be seen that V_{ME} reached a maximum value of $\sim 2\text{V/cm-Oe}$ under $H_{DC}=500\text{Oe}$. At higher bias

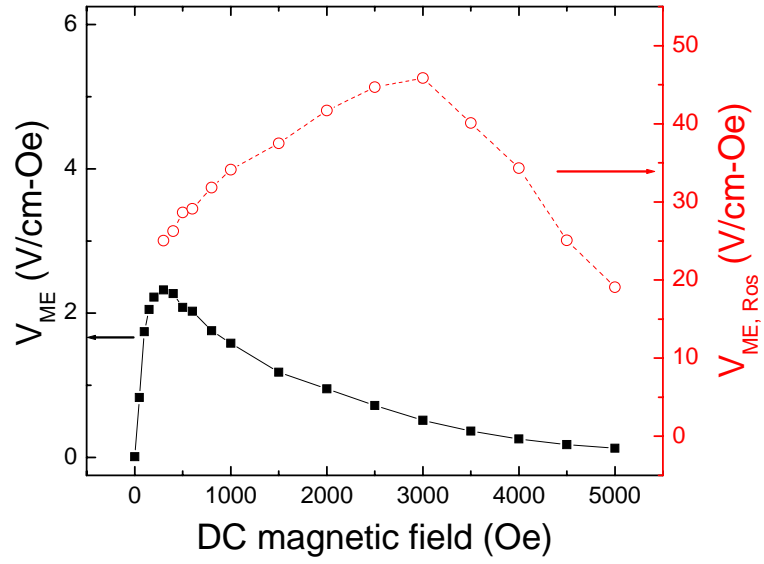


Figure 4.10 (a) Quasi-static ME voltage coefficient and enhanced resonant ME voltage coefficient of the Terfenol-D/PZT laminate as a function of H_{DC} from 0Oe to 5000Oe.

levels, the value of V_{ME} can be seen to continuously decrease with increasing bias for $500 < H_{DC} < 5000 \text{Oe}$, approaching a value of 0.2V/cm-Oe under $H_{DC} = 5000 \text{Oe}$. Comparison of this quasi-static V_{ME} data with that taken at the EMR will demonstrate significantly different trends with increasing H_{DC} .

For the LT mode, the quasi-static ME voltage coefficient can be calculated by

$$V_{ME}^{LT} = \frac{nd_{33,m}d_{31,p}}{n\epsilon_{33}^S s_{11}^E + (1-n)s_{33}^H (\epsilon_{33}^S + d_{31,p}^2 / s_{11}^E)}; \quad (4.6)$$

where n is the magnetic phase thickness ratio; s_{11}^E and s_{33}^H are the elastic compliances of the piezoelectric and magnetostrictive layers; ϵ_{33}^S is the dielectric constant of the piezoelectric material at constant strain; and $d_{31,p}$ is transverse piezoelectric coefficient. Under various DC magnetic biases, all parameters except $d_{33,m}$ will remain the same. The trend of the piezomagnetic coefficient with H_{DC} , as shown in Figure 4.8, is similar to that of the quasi-static ME voltage coefficient.

Finally, the frequency dependence of the ME voltage coefficient under various H_{DC} was shown in Figure 4.10. For $H_{DC} = 0$, the resonance ME voltage coefficient was only 5V/cm-Oe : this is because Terfenol-D has only a small remnant magnetization. The maximum resonance ME voltage coefficient was 45.85V/cm-Oe under $H_{DC} = 3000 \text{Oe}$. For $H_{DC} > 3000 \text{Oe}$, the resonance ME voltage coefficient was dramatically decreased with increasing H_{DC} . This trend is different from that of the quasi-static ME voltage coefficient, shown in Figure 4.10. The optimum DC bias was only 3000Oe at the EMR, which was 10x times larger than that at the quasi-static frequency.

The resonant ME voltage coefficient at the EMR can be estimated by

$$V_{ME}^{Res} = \frac{8Qnd_{33,m}d_{31,p}}{\pi^2[n\epsilon_{33}^S s_{11}^E + (1-n)s_{33}^H(\epsilon_{33}^S)]}. \quad (4.7)$$

For $H_{DC} < 3000$ Oe, the resonant of enhanced ME coefficient increases with increasing bias because Q increases faster than d_{33} decreases. Although d_{33} decreased from 0.5 ppm/Oe to 0.1 ppm/Oe for $300 < H_{DC} < 3000$ Oe, Q increased from 5.2 to 47.3. However, for $H_{DC} > 3000$ Oe, the magnetostriction of Terfenol-D approaches saturation and the piezomagnetic coefficient becomes very small. Thus, the resonant enhanced voltage coefficient decrease with further increasing H_{DC} .

4.4 Section summary

In summary, three basic magnetoelectric properties have been investigated in this Chapter. These properties were either important to understanding the magnetoelectric coupling between the piezoelectric/magnetostrictive laminate, or to helping the design of ME devices and applications. The results of this chapter can be summarized, as follows:

- (i) The ME susceptibility is a fundamental parameter: one relating the coupling of magnetization and polarization, via a media's interaction with electromagnetic radiation. It is a complex quantity. The velocity of electromagnetic radiation is dramatically slowed down on propagating in a media with a high α_{me} , such as a ME laminate.
- (ii) The shape of the magnetic layer has a larger impact on giant permeability materials. A long, thin and narrow shape will increase the ME voltage coefficient and decrease the required optimum DC bias. For low permeability

magnetic layers, although shape does not affect the ME voltage coefficient of ME laminates, it does change notably the required optimum DC bias. For large permeability magnetostrictive/piezoelectric laminates, the length of the magnetic layer should be longer than that of piezoelectric one since the internal magnetization is non-uniform.

- (iii) The resonance frequency of Terfenol-D/PZT laminates can be continuously tuned by magnetic field over a wide range from 41 kHz to 55 kHz. This large tunability is due to the large magnetostriction of Terfenol-D. It results in a dramatic increase in the bandwidth over which devices might take advantage of the resonance enhanced ME coefficient.

V. Magnetoelectric devices and applications

In the prior chapters, an enhanced ME effect and properties in piezoelectric/magnetostrictive laminates was presented. Here, several applications are introduced based on this enhanced ME effect: including magnetic sensors, gyrators and energy harvesters.

5.1 Ultra-sensitive magnetic field sensors

New sensors are need for the detection of low-frequency minute magnetic field (H) variations in applications ranging from non-invasive neurological interfaces for quadriplegics, to magnetoencephalogy⁵⁶ and magnetic anomaly detectors⁵⁷. These applications require sensitivity to minute (10^{-12} Tesla), low frequency (10^{-2} to 10^3 Hz) magnetic field variations in a time-domain mode without signal averaging. In addition, in order to be deployable, new magnetic field sensor technologies need to operate at 300K, be passive, and quite small. No known sensor can met all of these stringent requirements.

The best magnetic field sensors are superconducting quantum interference devices (or SQUIDS)^{58,59}. The highest sensitivities (at 1Hz) of low-temperature ($T < 4K$) and high-temperature ($T < 77K$) SQUIDS are about 10^{-15} Tesla/Hz^{1/2}⁶⁰ and 5×10^{-14} Tesla/Hz^{1/2}⁶¹, respectively. These sensitivities are achievable only in the best shielded rooms, under cryogenic operating conditions, and using a sensing current of 15mA. Another important type of magnetic field sensor is the giant

magneto-resistance (or GMR) spin valve⁶². At 300K, the best sensitivity is $\sim 4 \times 10^{-10}$ Tesla/Hz^{1/2} (1Hz) for I=1mA. Thermal or shot-noise is the limitation. At 4.2K, the sensitivity is increased to $\sim 4 \times 10^{-11}$ Tesla/Hz^{1/2}. Recently, enhanced 1/f-noise rejection has been achieved by hybridizing a GMR sensor with a superconducting flux-to-field transformer⁶³. The best sensitivity reported was $\sim 10^{-12}$ Tesla/Hz^{1/2} at 77K and $\sim 3 \times 10^{-13}$ Tesla/Hz^{1/2} at 4.2K, using sensing currents of 5mA and 15mA respectively. Recently, a chip-size atomic magnetometer has been reported⁶⁴ that is low-power consuming and has sensitivity as low as 5×10^{-11} T /Hz^{1/2} at 10 Hz.

5.1.1 Passive AC magnetic sensor

The ME effect offers an alternative *passive* approach to magnetic field sensing at room temperature. It involves the direct conversion of an input magnetic field H to an electric voltage V. An input H-field strains magnetostrictive layers that are elastically coupled to piezoelectric ones, which subsequently transduces the applied stress to a voltage via piezoelectricity. Using signal averaging to assist in noise rejection, it has been shown feasible to detect magnetic field variations as low as $\sim 10^{-11}$ Tesla at a drive frequency of $f=10^3$ Hz. However, in applications, noise rejection by signal averaging also limits detection of anomalies. In particular, pyroelectric currents from the $\text{Pb}(\text{Zr}_{1-x}\text{Ti}_x)\text{O}_3$ (PZT) layer can be quite significant at low frequencies, on the order of $\sim 100 \mu\text{C}/\text{m}^2\text{-K}$. For example, a temperature fluctuation of $\Delta T=0.1^\circ\text{C}$ in a PZT layer of dimensions $1 \times 0.2 \text{cm}^2$ would generate a noise-equivalent

charge of $\sim 10^{-11}C$. Clearly, low-frequency thermal fluctuations present serious equivalent-noise limitations to ME sensors.

However, in this chapter, the low frequency thermal-noise limitations have been mitigated by developing identical piezoelectric layers which are (i) mechanically disconnected; (ii) thermally connected (i.e., packaged together); and (iii) electrically connected in reverse. Figure 5.1 illustrates the laminate configurations which have been developed to achieve these requirements. They are (a) a two-element piezoelectric bimorph, and (b) a push-pull laminate configuration. The samples were made of Terfenol-D and PZT layers, which were attached to each other using a hard epoxy. The bimorph laminate consisted of two PZT plates ($13 \times 6 \times 0.5 \text{mm}^3$) and one Terfenol-D plate ($13 \times 6 \times 1 \text{mm}^3$), and the push-pull laminated consisted of one PZT plate ($16 \times 6 \times 2 \text{mm}^3$) and two Terfenol-D plates ($14 \times 6 \times 1.2 \text{mm}^3$). For these two configurations, thermal noise acts on small neighboring elements similarly; consequently, any temperature changes generate an equal and compensating charge in the mechanically disconnected layer, resulting in enhanced noise rejection.

The ability of the bimorph to reject pyroelectric noise is illustrated in Fig. 1c, which shows the pyroelectric current as a function of temperature for (i) a bimorph, consisting of two PZT layers; and (ii) a corresponding unimorph of the same geometry, but consisting of a single PZT layer. It can be seen that the bimorph configuration reduces the pyroelectric current by a factor of $\gg 10x$. Accordingly, for both configurations, we established (i) that the ME voltage coefficient is frequency

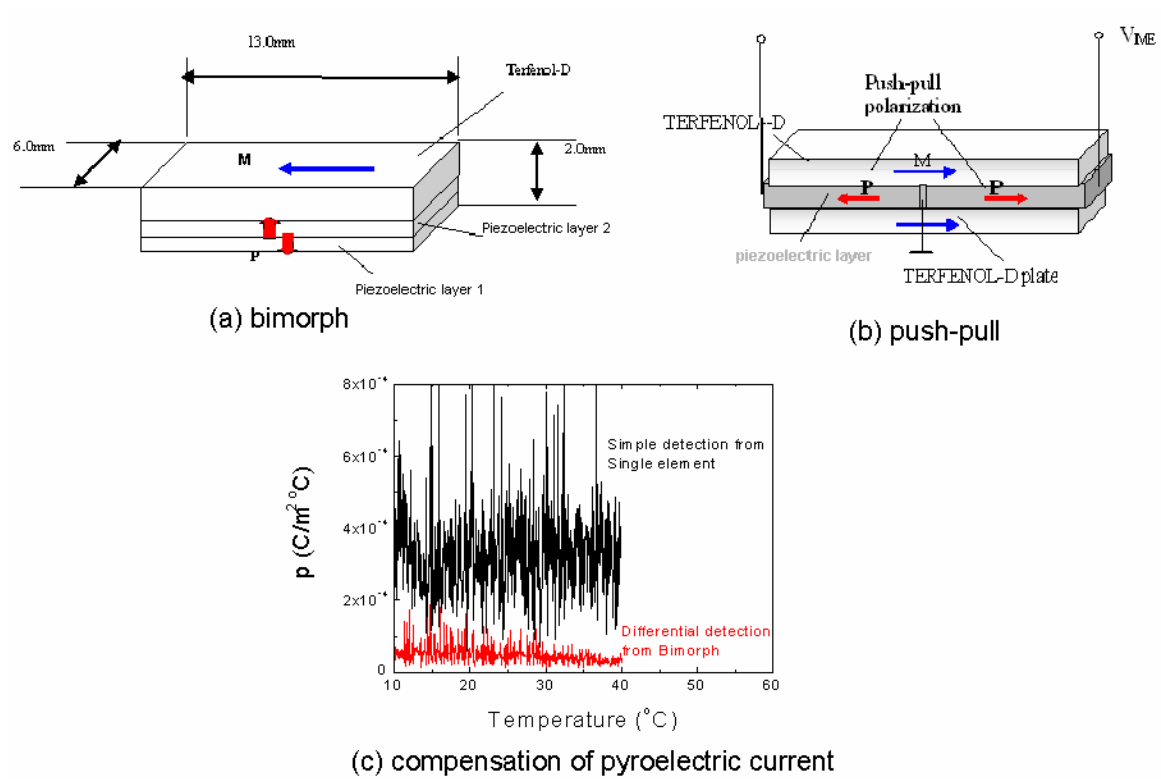


Figure 5.1 Schematic view of the magneto-electric (a) bimorph and (b) push-pull laminate composite magnetic field sensors. A magnetic field is sensed by straining magnetostrictive Terfenol-D layers that are epoxied to piezoelectric $\text{Pb}(\text{Zr}_{1-x}\text{Ti}_x)\text{O}_3$ ones, which subsequently converts the stress into a voltage via piezoelectric effect. In these two designs, enhanced signal-to-noise ratio is achieved by the back-to-back configurations of the piezoelectric layers, which rejects thermal noise. In Part (c), I illustrate the rejection in the pyroelectric current achieved by using the bimorph construction, relative to a unimorph of the same geometry.

independent over $10^{-2} < f < 10^3$ Hz; (ii) that the induced ME voltage is linear with respect to H_{ac} ; and (iii) that the time domain response of the laminate to a H_{ac} Can be captured. These measurements were done using an op-amp with a high input resistance to collect the charge from the laminates induced by H_{ac} . During measurement, a DC magnetic bias of 400 Oe was applied along the length of the laminate using permanent magnets.

First, noise spectra for the bimorph construction are presented, as given in Figure 5.2. These measurements were performed at room temperature, in a magnetically shielded environment made of μ metal that had a noise rejection capability of $\sim 10^5$, and by using a simple high-input resistance op-amp operated in a time-domain capture mode. Data are only shown for the low frequency range of $f < 10$ Hz, due to the low inertial resonance frequency of a bimorph. In this figure, the sensitivity limit to minute magnetic field variations can be seen to be about 2×10^{-11} T/Hz^{1/2} (RMS) at 1 Hz, where the noise floor has $1/f$ dependence. The noise-equivalent charge was $\sim 10^{-16}$ C (1 Hz). In this figure, the corresponding data for a unimorph ME laminate were also provided, which had a sensitivity limit of about 10^{-9} T/Hz^{1/2} (RMS) at 1 Hz and a noise-equivalent charge of $\sim 10^{-14}$ C. Comparisons of the results for the bimorph and unimorph clearly demonstrate the importance of lowering the pyroelectric noise-floor of the PZT layer.

Next, in Figure 5.3, the noise spectra for the push-pull laminate are presented. Data are shown over a frequency range of $0.1 < f < 10^5$ Hz. The low frequency data were taken using a high-resistance input op-amp, whereas the high frequency

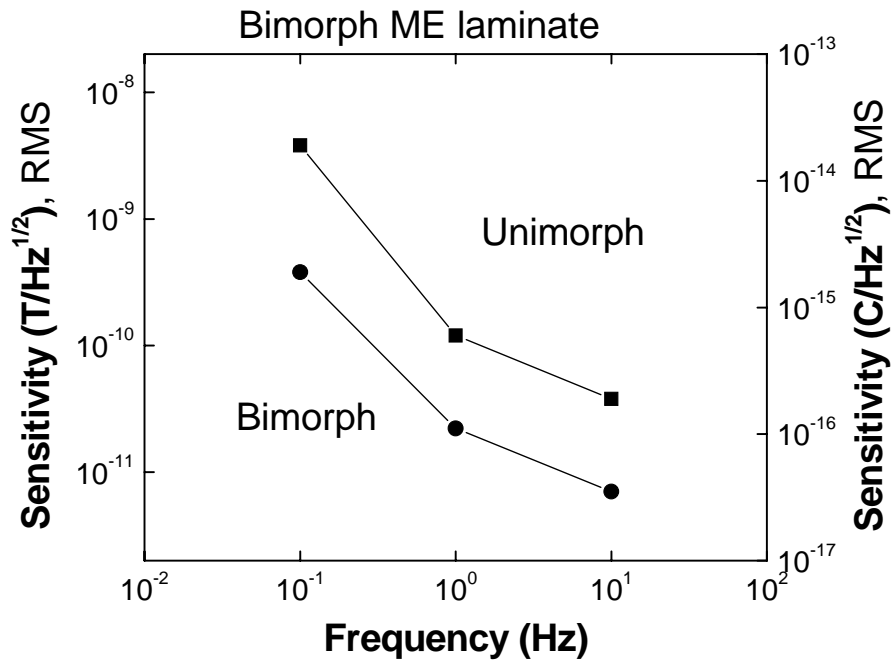


Figure 5.2 Noise spectra, given in Tesla/Hz^{1/2} on the left-hand side and Coulombs/Hz^{1/2} on right-hand, for the bimorph ME laminate. These data were taken at 300K, using a high-input resistance op-amp. The sensitivity limit was about 2x10⁻¹¹ T/Hz^{1/2} (or 2x10⁻¹⁶C/Hz^{1/2}) at 1Hz. Corresponding data for the unimorph laminate have been shown in order to demonstrate the enhanced noise rejection of the thermal noise by differential detection.

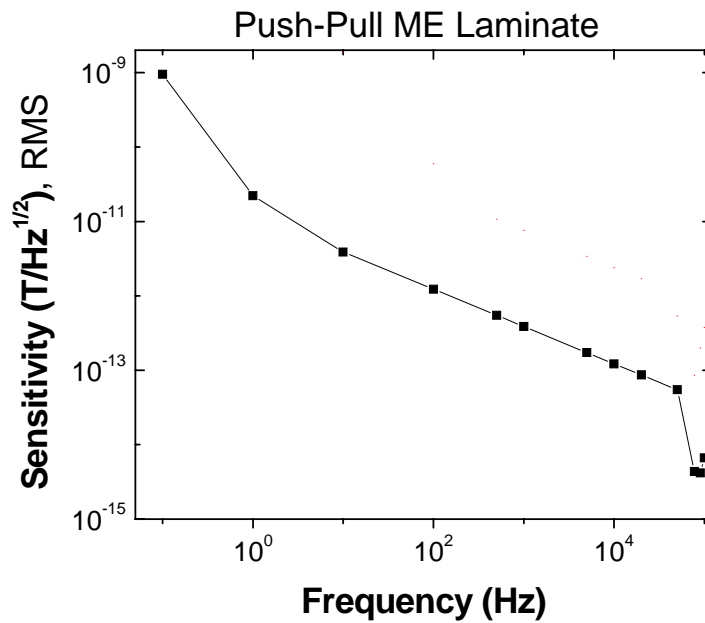


Figure 5.3 Noise spectra, given in Tesla/Hz^{1/2}, for the push-pull ME laminate. These data were taken at 300K. The low frequency data was taken using a high-input resistance op-amp to collect charge, whereas the high frequency was taken using a voltage method. The sensitivity limit was about 2x10⁻¹¹ T/Hz^{1/2} (or 2x10⁻¹⁶C/Hz^{1/2}) at 1Hz, and about 2x10⁻¹⁵T/Hz^{1/2} at 78kHz.

data were taken by a voltage method. At 1Hz, the sensitivity limit to minute magnetic field variations was about $3 \times 10^{-11} \text{T/Hz}^{1/2}$ (RMS), and its noise-equivalent charge on the order of 10^{-15}C . With increasing frequency, the noise floor was dramatically lowered, reaching about $2 \times 10^{-15} \text{T/Hz}$ (RMS) at the resonance frequency of the laminate ($\sim 10^5 \text{Hz}$).

Finally, in Figure 5.4, the high sensitivity of a time-domain response to a magnetic input signal of $H_{ac} = 2.4 \times 10^{-11} \text{Tesla}$ (RMS) is illustrated. The results show the voltage response of the push-pull laminate under resonance drive ($7.75 \times 10^4 \text{Hz}$), where the drive is shown beneath the response. At this minute field, the ME response had an extremely clean waveform. These results clearly demonstrate extreme sensitivity limits of between pico- and femto-Tesla over a broad frequency range, which can be captured in the time-domain. The popcorn noise results from the frequency response limitations of the high-input resistance op-amp operating in a time-domain mode.

The findings of this section can be summarized as follows. New ME laminate composite configurations have been developed which reject pyroelectric noise. This results in a dramatic lowering of the noise floor. In so doing, a sensitivity limit to minute magnetic field variations of about $2 \times 10^{-11} \text{Tesa/Hz}^{1/2}$ (@1Hz) was achieved when operated at 300K. This sensitivity limit is an order of magnitude better than the best previously reported for a GMR spin valve operated at 300K and 1mA, which is about $4 \times 10^{-10} \text{Tesla/Hz}^{1/2}$ (@1Hz)⁶². Thus, bimorph and push-pull ME laminates do not have as high a sensitivity as that of a hybrid GMR-superconducting

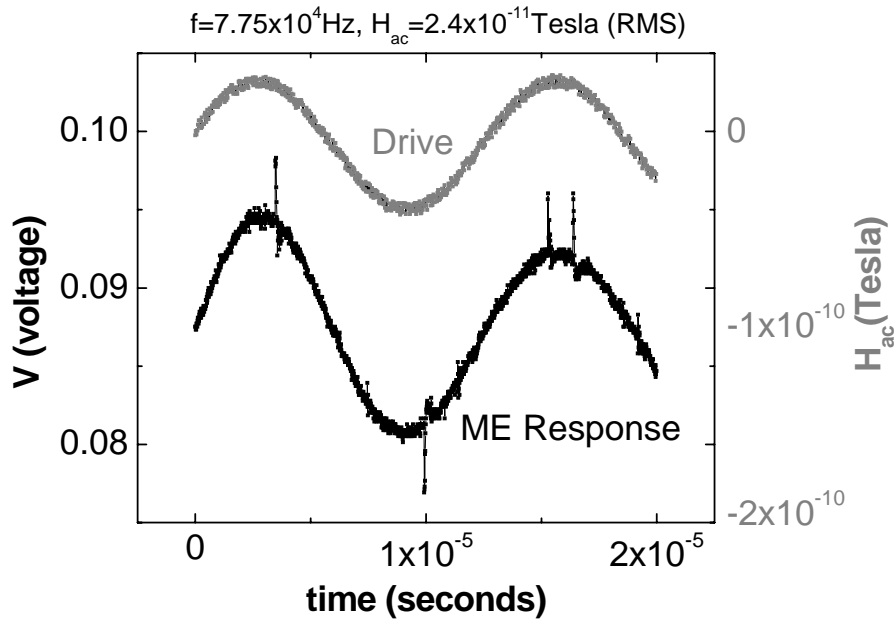


Figure 5.4 Time-domain response to a minute magnetic field of $H_{ac}=2.4 \times 10^{-11}$ Tesla (RMS) for the push-pull laminate at 7.75×10^4 Hz.

sensor operated at 77K and 5mA⁶³, which is 10^{-12} Tesla/Hz^{1/2} (@1Hz). However, bimorph and push-pull ME sensors (i) are entirely passive; (ii) operate at room temperature, rather than under cryogenic conditions, making it suitable for long-term deployment in non-invasive neurological/biological applications and magnetic anomaly detection; (iii) are small, robust, and simple to operate; in addition to being (iv) extremely sensitive and responsive to minute magnetic signals over a broad bandwidth.

Ultimately, it is recognized that further significant enhancements in the sensitivity limits of ME laminates are feasible. First, in the case of the push-pull laminate, the extreme enhancement ($\sim 10^{-15}$ Tesla/Hz^{1/2}) under resonant drive is nearly equivalent to that offered by a SQUID sensor operated at 4K and 15mA⁵⁹⁻⁶¹. Second, more sophisticated design configurations of unimorph, bimorph, and other miniature structures are possible to more fully compensate noise contributions to the total charge, via tuning of various electrical parameters within and between layers.

5.1.2 Active DC magnetic sensor

Besides being used in designs for passive AC magnetic sensors, ME laminates can also be used for DC magnetic field detection. This is made possible due to the fact that the ME effect is a strong function of H_{dc}. Thus, by using a constant H_{ac} drive, ME laminates have the potential to be used for small H_{dc} signal detection.

The active DC ME sensor developed was a Metglas/PZT-fiber laminate with a 100 circles coil wrapped tightly around it. The PZT fibers were 200 μ m in thickness and were laminated between four layers of Metglas by use of a thin layer epoxy; the

thickness of each Metglas layer was 25 μm ; and the total dimensions of the laminates were 100x6x0.48mm³. The working principal of the ME sensor is that an input magnetic field changes the length of the Metglas via magnetostriction; and because the PZT fibers are elastically bound to the Metglas layers through an epoxy interfacial layer, the PZT fibers also change their length, and generate an output voltage via piezoelectricity. Detection of the magnetic field was performed by applying a 1kHz AC magnetic field (H_{AC}) via a 10mA AC current input to the coil, and by measuring the DC voltage and its phase induced in the PZT-fibers by a lock-in amplifier (SR-850).

Figure 5.5 shows the dependence of the induced ME voltage (V_{ME}) on H_{DC} . Over the range of $-1.5 < H_{DC} < 1.5\text{Oe}$, V_{ME} was linearly proportional to H_{DC} and equal to 300mV under a $H_{DC}=1\text{Oe}$: which was $>10^3$ x times that of a corresponding Terfenol-D/PZT DC magnetic field sensor operated at 1kHz. Another important finding was that unlike Terfenol-D/PZT magnetic sensors, V_{ME} for Metglas/PZT-fiber sensors was not dependent on H_{DC} history (i.e., no hysteretic phenomena): rather, V_{ME} only depended on momentary changes of H_{DC} in the environment. This is very important to stable and repeatable detection of DC magnetic fields and their variations. In addition, when the sign of H_{DC} was changed, a dramatic 180° phase shift was found. This shift could be used to distinguish the direction along which changes in H_{DC} occur with respect to the length (long axis) of the sensor. This is an important advantage compared to fluxgate. Previously, it was reported that V_{ME} from a Metglas/PZT-fiber laminates was strongly anisotropic, offering good sensitivity to magnetic

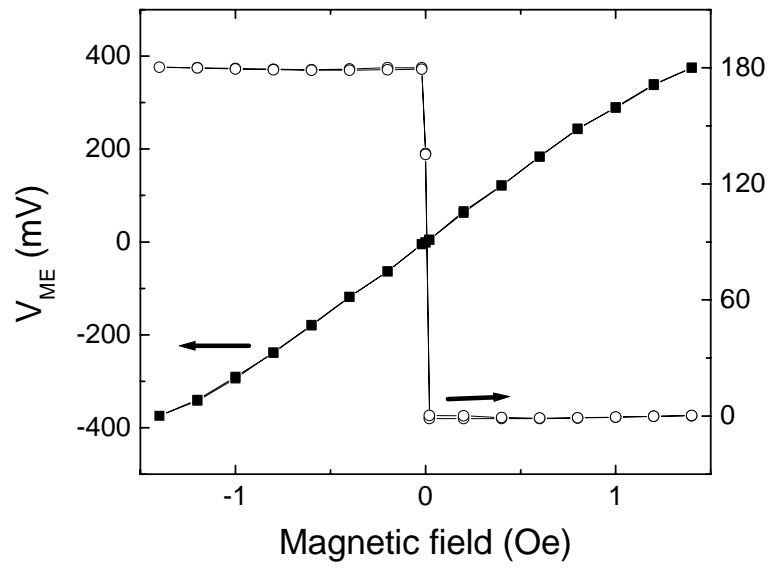


Figure 5.5 The DC magnetic field dependence of the ME voltage coefficient and phase for a Metglas/PZT fiber push-pull laminate, measured at 1 kHz under an applied current of 10 mA.

field variations only along its length direction. In the other two perpendicular directions, only very weak signals were found with changes in H_{DC} . These unique properties of Metglas/PZT-fiber ME sensors are due to the ultrahigh relative permeability (μ_r) of Metglas: which is $>10^3$ x larger than that of Terfenol-D or nickel ferrite. Correspondingly, the high μ_r of Metglas results in an ultra-small demagnetization field, enabling a high effective piezomagnetic coefficient at low biases.

Next, the sensitivity of the Metglas/PZT laminates to small variations DC magnetic fields was determined. Figure 5.6 shows the voltage induced by step-like changes in magnetic bias of $\Delta H_{dc}=8nT$, measured in a time-domain capture mode. These measurements were performed in magnetically-shielded environment under a resonant frequency (18kHz) drive of $H_{ac}=1Oe$: no H_{dc} was applied by permanent magnets. Inspection of the data will reveal rapid and stable responses in the voltage induced across the piezo-polymer layers in response to ΔH_{dc} . This also establishes that step-like changes in ΔH_{dc} as small as 2nT can be discriminated from the background noise.

5.2 Geomagnetic sensor

Migratory animals are capable of sensing variations in geomagnetic fields as a source of guidance information during long-distance migration^{65,66}. It is well known that geomagnetic fields are on the order of 0.4-0.6Oe and have different inclinations

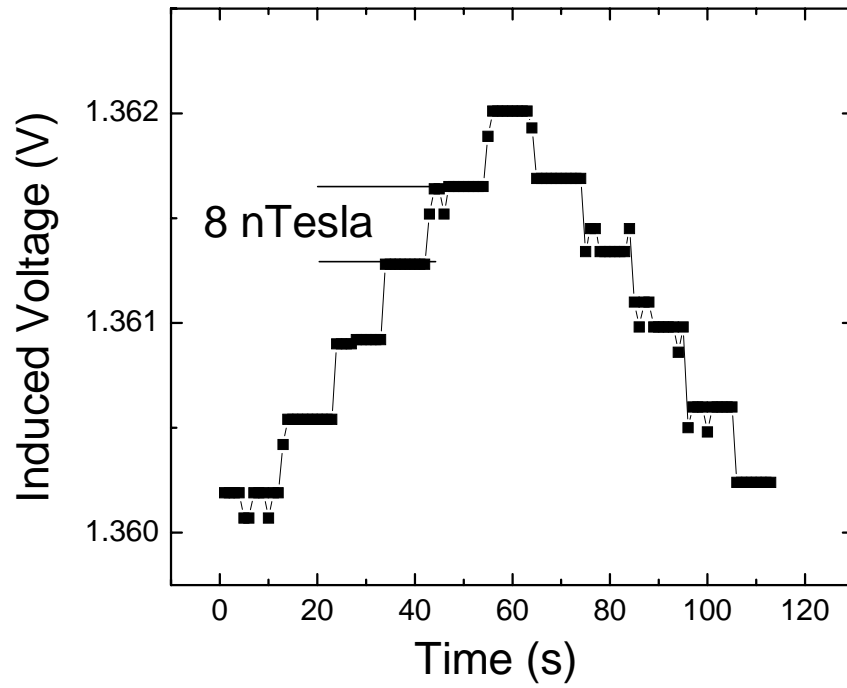


Figure 5.6 Sensitivity of a 3-layer Metglas/PZT laminate to small variations in H_{dc} , taken under a constant $H_{ac}=0.10\text{Oe}$ at $f=18\text{ kHz}$;

at different locations. The Earth's mean field and its inclinations at many points over much of the Earth's surface, including spatial variations and temporal evolutions have been tabulated by the United States Geological Survey. Accordingly, geomagnetic field sensors could be used in guidance and positional location.

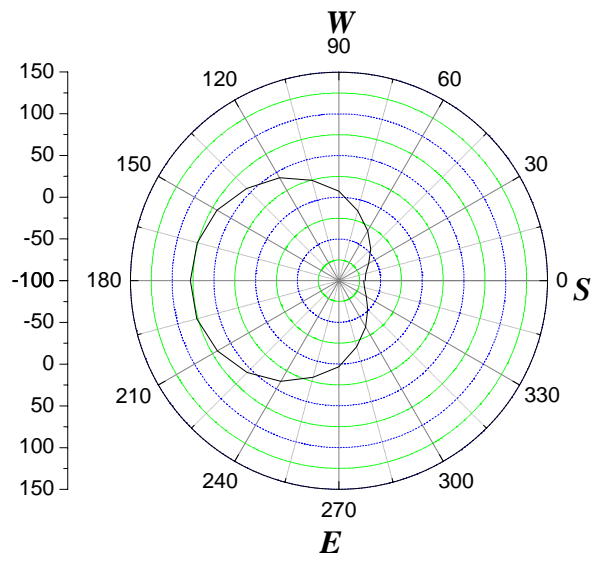
Above, in the last sections, new types of passive AC^{33,67} and active DC⁶⁷ magnetic field sensors were demonstrated based on the giant magnetoelectric (ME) effect which were simple devices operated at room temperature. Here, it will be shown by using a set of Metglass/PZT-fiber ME sensors that one can precisely detect both geomagnetic fields and their inclinations along various axes of a globe.

Figure 5.7 illustrates the experimental setup for measuring the Earth's magnetic field. The globe was mounted on a three-axis circle, enabling rotation in all directions. The ME sensor was placed inside of the globe on an aluminum holder. A lock-in amplifier was used to generate a 1kHz AC current, which was used as an input to the coil wrapped around the sensor, and which was also used as a reference signal for detection. During measurements, the globe was first rotated about the up-down axis inside of the Earth's plane; subsequently, it was rotated about the north-south axis, and then about the east-west one. Each time it was rotated by an angle of 5°. Please note, that the designations of North and South direction are not that of the Earth's direction, but rather that of the magnetic North and South ones.

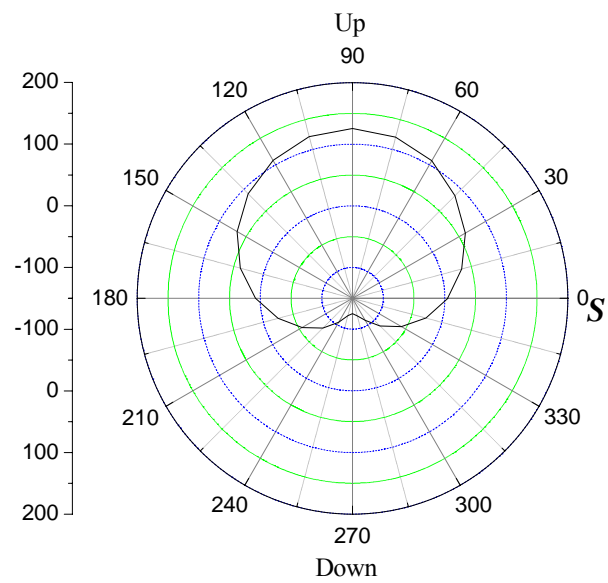
Figure 5.8(a) shows the angular dependence of V_{ME} when the sensor is rotated in the Earth's plane. As expected, when the sensor was oriented along east and west directions in this plane, its output was essentially 0mV; whereas, when it was oriented



Figure 5.7 Photograph of the geomagnetic field sensor measurement setup.



(a) Earth's Plane



(b) North-South Axis

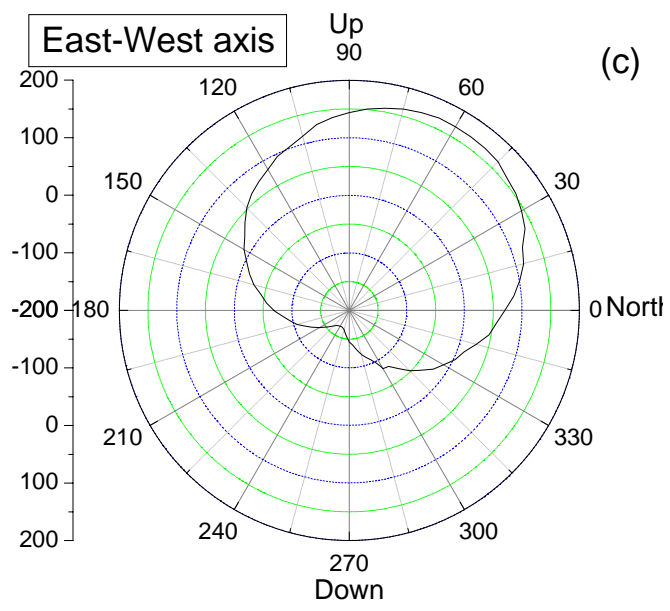


Figure 5.8 Output voltage from the magnetolectric sensor, when it is rotated: (a) in the Earth's plane; (b) along the North-South axis; and (c) along the East-West axis.

along south and north directions in the plane, its output was maximum. This is because the ME sensor is only sensitive along its length direction: thus, when this direction is oriented along the geomagnetic field in Earth's plane, it has only vector components in the north-south axis. Figure 5.8b shows V_{ME} when the sensor is rotated along the north-east axis. Similar to Figure 5.8a, when the sensor was oriented along the east-west direction, V_{ME} was nearly 0mV; whereas the other two directions, up and down, had the largest sensor output. Figure 5.8c shows V_{ME} when the sensor is rotated along the east-west axis. The inclination of our laboratory (Blacksburg, VA) in this plane was $65^{\circ}51'$. The experimental results indicated when the sensor angle was set at 65° and/or 235° that the output voltage was also the largest in this plane.

The sensitivity of the Metglas/PZT-fiber laminates to changes in DC magnetic field was $H_{DC}=0.8nT$, over a range of operations of $\pm 1.5Oe$. These properties are comparable to a fluxgate sensor⁸. Along a set plane, changes in the angle of rotation will result in changes in the geomagnetic field vector. The best angular sensitivity was found along the east-west direction, which was $\approx 3 \times 10^{-6}$ degrees; whereas, the worst sensitivity was found along the north-south direction, which was $\approx 10^{-5}$ degrees. Based on these results, one could develop a three-axis ME sensor unit, where each sensor is perpendicular to the other two. Using said, three-axis ME sensor unit, one could determine the local magnetic field and its inclination, by knowing the geomagnetic field. Accordingly, a small global positioning device could be made with quite good accuracies, by comparing to a grid of values for Earth's field and its spatial/temporal variations.

5.3 Gyrator

In 1948⁴⁴, Bernard Tellegen of Philips Research Laboratories published seminal work on classic passive network elements, in which he theorized that an additional network element based on magneto-electric (ME) interaction should exist – that he designated the gyrator. An ideal gyrator would be unique with respect to the other known four network elements – capacitance, resistance, inductance, and transformer – in that it would not comply with reciprocity, but rather would be non-reciprocal. Well-known microwave gyrators which work on the Faraday effect in ferrites² use another operational principle. However, over the course of many years, the notion/hope of realizing a true passive network component with large gyration effects at lower frequencies has fallen into obscurity.

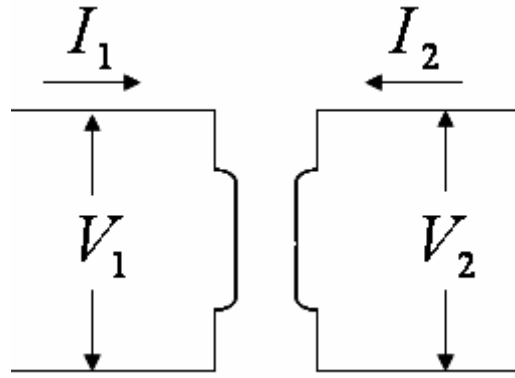
A four-pole circuit is showed in Figure 5.9a, the relations between the voltages and the currents can be expressed as

$$\begin{aligned} V_1 &= Z_{11}I_1 + Z_{12}I_2 \\ V_2 &= Z_{21}I_1 + Z_{22}I_2 \end{aligned} \quad (5.1)$$

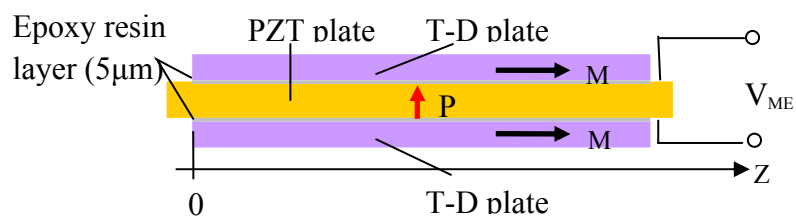
where V is the voltage, I is the current and Z is the impedance that is a function of frequency. When $Z_{12} = -Z_{21}$ and $Z_{11} = Z_{22} = 0$, the equations of (1) simplify to

$$\begin{aligned} V_1 &= -\alpha I_2 \\ V_2 &= \alpha I_1 \end{aligned} \quad (5.2)$$

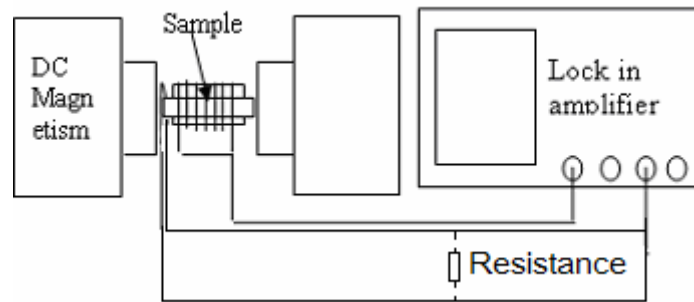
where α is a conversion coefficient between voltage and current. If a four-pole device has this non-reciprocal relation, it is an ideal gyrator as defined by Tellegen¹. He conjectured that a media with both magnetization (M_s) and polarization (P_s) phases



(a)



(b)



(c)

Figure 5.9 (a) Gyrator equivalent circuit; (b) illustration of longitudinal-transverse or L-T mode of a magnetoelastic laminate composite consisting of longitudinally-poled $\text{Pb}(\text{Zr}_x\text{Ti}_{1-x})\text{O}_3$ layer sandwiched between two longitudinally-magnetized Terfenol-D layers, epoxied together with a thin insulating resin layer; and (c) schematic illustrating the experiment setup

could be used to design such a gyrator; however, at that time, no such ferromagneto-electric materials were known.

Since Tellegen's time, ME materials have been found and extensively investigated, as evidenced in reviews¹. Here, I conclusively demonstrate the gyrator capabilities of composites consisting of a $\text{Pb}(\text{Zr}_x\text{Ti}_{1-x})\text{O}_3$ (PZT) or $\text{Pb}(\text{Mg}_{1/3}\text{Nb}_{2/3})\text{O}_3$ -30at% PbTiO_3 (PMN-PT) piezoelectric layer(s) laminated together with magnetostrictive Terfenol-D ones operated under electromechanical resonance (EMR) conditions. In Figure 5.9b, a ME laminate that has a L-T mode configuration was illustrated. Investigations were not limited to this mode, rather only show it as illustrative. Laminates with L-L mode, and a 'push-pull' configuration were studied. The piezoelectric PZT layers were polycrystalline, whereas the PMN-PT ones were (001) oriented crystals.

A ME laminate with a coil wrapped around it is a four-pole device. In this case, the impedances of (1), where the subscript 1 refers to the piezo circuit and the subscript 2 refers to the coil circuit, are given as

$$\begin{aligned}
 Z_{11} &= -i \frac{1}{2\pi f} \frac{d}{\epsilon_{\text{eff}} l w}, \\
 Z_{12} &= N \frac{\alpha_{\text{me}} d}{\epsilon_{\text{eff}} l}, \\
 Z_{21} &= -N \frac{\mu_{\text{eff}} d}{\alpha_{\text{me}} l}, \\
 Z_{22} &= i2\pi f \frac{N^2 d w \mu_{\text{eff}}}{l};
 \end{aligned} \tag{5.3}$$

where Z_{11} , Z_{22} are impedance of piezoelectric phase and coil; and Z_{12} and Z_{21} are equal to a gyrator coefficient or α ; d , l , w are the thickness, length and width of the

ME laminate; N the number of the coil; f the frequency; and ϵ_{eff} , μ_{eff} and α_{me} the effective dielectric, permeability and ME susceptibilities of the ME laminate. An ideal (or Tellegen) gyrator has the following additional imposed restriction between ϵ_{eff} , μ_{eff} and α_{me}

$$\frac{\alpha_{\text{me}}}{\sqrt{\mu_{\text{eff}} \epsilon_{\text{eff}}}} \approx 1; \quad (5.4)$$

which simplifies (3) to

$$Z_{12} = -Z_{21} \quad (5.5a)$$

$$Z_{11} * Z_{22} = -Z_{12} * Z_{21}. \quad (5.5b)$$

It was found for ME laminates, compared to these two criteria for ideal gyrators that (i) the first one of (5.5a), $Z_{12} = -Z_{21}$, is met; but (ii) the second one of (5.5b) is not met: although Z_{12} and Z_{21} can be changed by varying Z_{11} and Z_{22} , and at best either Z_{11} or Z_{22} close to zero can be set.

Measurements were performed by using a dual lock-in amplifier method to calibrate the phase difference of the two signals (i.e., that of both the piezo and magnetic sides of the circuit in Figure 5.9a). A DC magnetic field of 5000e was applied along the length of Terfenol-D; and a 50 turns-coil (tightly wound without gaps) was wrapped around the laminates. The experimental set-up is shown in Figure 5.9c. When exciting the piezo-layer(s), the output BNC connector ($10^7 \Omega$ resistance and 15pF capacitance, which can be considered as an open circuit) of the lock-in (SR850 DSP) was connected to a 1k Ω resistor, which was connected to both sides of the piezo-layer(s); and the input BNC connector (50 Ω) was connected in series with the drive coil. The current of the coil (I_2) was measured by connecting a small

capacitor, via the voltage across the capacitor. The voltage of the coil (V_2) was calculated by that applied from the lock-in, subtracting the resistance of the input BNC connector multiplied by I_2 . The voltage induced across the piezo-layer(s) was directly measured by the lock-in under open circuit conditions, and the induced current (I_1) was measured using a small resistance that short circuited the piezo-layer(s). During the phase measurements, an AC voltage source was used to excite the coils; and a small resistor was connected to the source and used as a reference signal for the lock-in. This reference signal has the same phase as the current of the exciting coil. The lock-in can then give the phase shift ($\Delta\phi$) of the detected signal relative to the reference one, yielding a measure of $\Delta\phi$ between the voltage induced across the piezo-layer(s) (V_1) and the current of the exciting coil (I_2). The phase shift between the induced current of the piezo-layer(s) (I_1) and that of a drive voltage applied to the coils (V_2) has been measured.

In Figure 5.10, the frequency dependence of the phase shifts between voltage and current is presented, taken under different excitation conditions. Also, in the inset of Fig.5.10, the dependence of the gyration coefficient on frequency is shown. As can be seen in Figure 5.9, the required phase difference between open and short circuit conditions is met over a broad bandwidth from $1 < f < 10 \times 10^5$ Hz; but as can also be seen in the inset, the required condition for ideal gyration in (Equation 5.5a) of the L-T mode is fulfilled only at the EMR condition. These results unambiguously demonstrate the existence of an 180° phase shift between I and V. This is the first

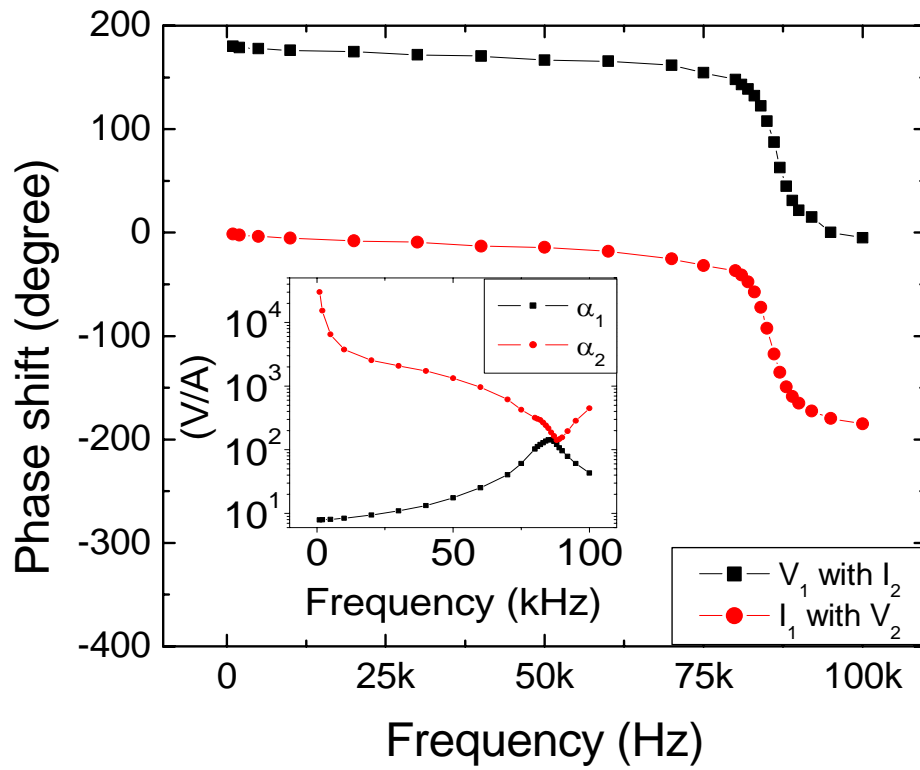


Figure 5.10 Phase difference between open and short circuit conditions for a L-T mode PZT/Terfenol-D laminate as a function of frequency from 1 to 10^5 Hz, where 1 designates the PZT capacitance side of the gyrator, and 2 the inductance side of the coils.

report of such an 180° phase shift at low frequencies ($< \text{GHz}$), and it is distinctly different than the conventional 90° shift between I and V as in the case of usual reactive elements of the circuit (i.e., L or C). At the resonance frequency, the phase of PZT will change rapidly, which will cause a phase shift between V_2 and I_1 , and correspondingly V_1 and I_2 will change rapidly near the resonance frequency. The results in Figure 5.10 establish: (i) the non-reciprocal nature of the couple; and (ii) the non-dissipative nature of the I-V conversion, i.e., current is not generated by a voltage drop at the EMR.

Figure 5.11 shows the impedance inverter property of the ME gyrator, predicted by (5b). The inset is an illustration of the measurement circuit. Here, V is the voltage source; R_1 the output impedance of the voltage source; R_2 is a resistance of 2000Ω that is used to avoid possible open circuit conditions on the piezo-layer side. First, Z was connected in series to the piezo-layers and the voltage induced on R_2 was measured. Then, Z was removed, and Z' was connected in parallel to the coil, selecting a suitable value to let the induced voltage on R_2 be equal to that when it was connected in parallel with Z . The value of α was estimated as that of α_1 and α_2 , as given in the inset of Figure 5.10. The data in Figure 5.11 were measured using the following values of resistances: $Z_{\text{piezo}}=2010\Omega$, $Z_{\text{coil}}=9.8\Omega$ and $\alpha=150\Omega$ all at a resonance frequency of 84kHz . As can be seen in Figure 5.10, this construction exhibited good characteristics as an impedance inverter. Although changing R_1 or R_2 may change α , a linear relation between Z and $1/Z'$ was demonstrated. If Z and Z' are

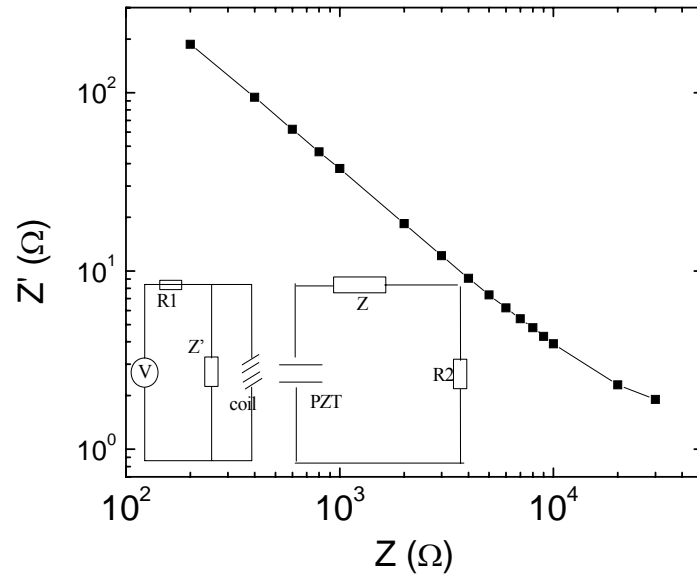


Figure 5.11 Impedance inverter property of the gyrator under different resistance loads. The inset shows the measurement circuit. Z and Z' are not coexisting. Measurement were done near a resonance frequency of 84kHz.

changed to a capacitor and an inductor, but not a pure resistor, similar results can be obtained: except that there will be about a 15° phase change introduced. These findings show that ME gyrator are like an ideal gyrator, but ones that are in reality connected with a capacitor on one side and an inductor on the other side. In the future, by use of other ME laminate configurations, One could hope to decrease the values of the resistances Z_{piezo} and Z_{coil} together, while maintaining the gyration coefficient constant.

This four-pole device is a small, discrete, passive network element that offers solutions of functional electronics to complex networks. Tellegen suggested a bidirectional ideal gyrator, however here it has been shown that ME laminates are a unidirectional gyrator with good gyration characteristics. Accordingly, they could offer new electrical components capable of tuning stray or mutual inductances in a circuit into purely capacitive ones. As a new fundamental network element, they could offer considerably improved and/or simplified solutions to many complex network problems.

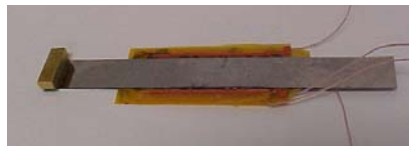
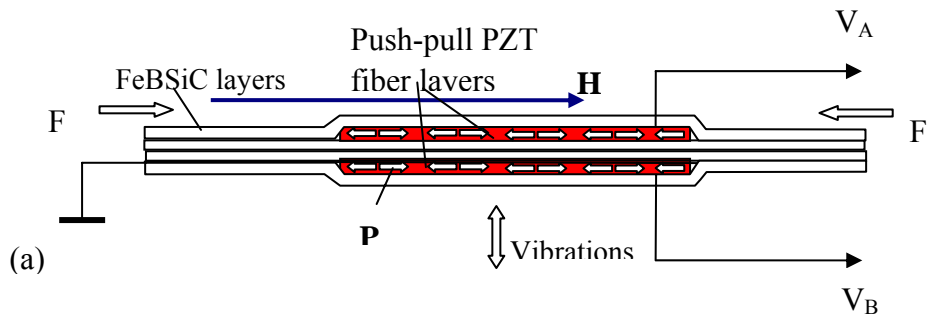
5.4 Energy harvester

There is an increasing demand for energy harvesting (EH) systems in mobile electronics and sensor networks. EH systems are required not only to serve as supplemental power source, but in some cases even to replace the batteries such as in implantable networks. Similarly, periodic replacement of batteries in distributed sensor networks is an expensive and tedious operation, which would benefit from the

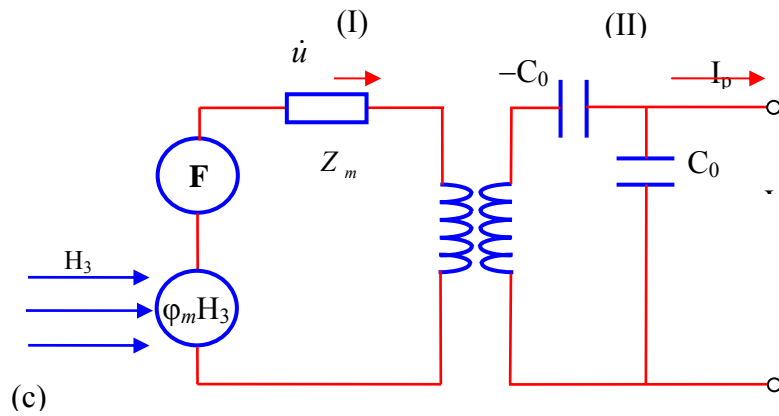
development of EH based recharging mechanisms⁶⁸. Multimodal EH systems which can simultaneously convert magnetic and mechanical energy into electric energy could be developed. These systems could be deployable in undersea conditions to simultaneously capture earth's magnetic field and wave energy. Here, I report an EH device fabricated from high-permeability magnetostrictive FeBSiC alloy ribbons laminated with piezoelectric Pb(Zr,Ti)O₃ (PZT) fibers. My results clearly demonstrate that this laminate composite can synchronously harvest both stray mechanical and magnetic energies. This is a significant advancement towards improving the energy density of current EH systems.

The schematic design of the fabricated energy harvester is illustrated in Figure 5.12a, and a picture of prototype is shown in Figure 5.12b. In this ME laminate configuration, two PZT fiber layers with *push-pull* type symmetric polarization units were laminated together with four magnetostrictive Metglas ribbons. This design allows one to utilize mechanisms simultaneously: (i) the magneto-elasto-electric effect, where a stray magnetic field H can excite longitudinal strain through magnetostrictive effect of Metglas; and (ii) the piezoelectric effect, where mechanical vibrations can create strain. The two responses can be combined together to convert a net composite strain into electricity. Since the conversion occurs through elastic interactions, it is possible to realize this additive effect.

Assuming that an external *ac* magnetic field H_{ac} and an external mechanical force F of frequency ω are synchronously applied to the laminate, longitudinal and/or bending vibration modes will be excited. the energy harvesting can be molded



(b)



(c)

Figure 5.12 Conceptual illustration of the magneto-electric energy harvester: (a) schematic of the ME laminate configuration, (b) photo of the ME laminate prototype, and (c) equivalent circuit model for a bi-mechanism of energy harvesting.

capabilities from excitation of these modes by using an equivalent approach^{27,43,54}, as shown in Figure 5.12c. Correspondingly, the induced voltage ($V_{induced}$) across the dielectric layer under open circuit condition can be given as:

$$V_{induced} = \frac{\varphi_p}{-j\omega p C_0 Z_m} F + \frac{\varphi_p \varphi_m}{-j\omega p C_0 Z_m} H \quad (5.6)$$

where φ_p is the electromechanical coupling factor, φ_m the magneto-elastic coupling factor, C_0 the static capacitance and Z_m the mechanical impedance. The induced voltage in Equation 5.6 can clearly be seen to be a sum effect from two contributions:

(i) a F -induced voltage, via a mechanical-to-electric conversion φ_p , which is the 1st contribution in Equation 5.6; and (ii) a H -induced voltage, via a magneto-elasto-electric conversion $\varphi_m \varphi_p$, which is the 2nd contribution in Eq. (1).

Please note that H - or F - induced voltages are related to the ratio of the capacitive impedance ($Z_c = 1/j\omega p C_0$) of the piezoelectric layer to the mechanical impedance Z_m of the entire ME laminate. This indicates that a large capacitive impedance or a small mechanical one will result in large H - and F - induced voltages.

The ME laminates were mechanically excited by a vibration system. A dSPACE shaker was powered by using the HP Bipolar power amplifier 6826A. The generated mechanical excitation was monitored by accelerometer (PCB Piezotronics Model# U352C22/meter 482A16). Alternating magnetic field H_{ac} was generated by using Helmholtz coils powered by function generator. The voltage generated from the laminate composite was measured by using a digital oscilloscope across an known external load.

Figure 5.13 shows the H induced voltage and the corresponding power as a function of load ($P = V_{\text{rms}}^2/R$). The data was measured at 1st longitudinal resonance frequency of $\sim 21\text{kHz}$ without any mechanical vibration. Under an ac magnetic field of 1Oe , the maximum induced voltage was $\sim 63 \text{ V}_{\text{pp}}/\text{Oe}$; correspondingly, the harvested power output was $420 \mu\text{W}/\text{Oe}$ across a $50 \text{ k}\Omega$ load. By accounting for the ME laminate's volume ($\sim 0.2\text{cm}^3$), the output power density can be estimated to be $2.1\text{mW}/\text{Oe}\cdot\text{cm}^3$. This power density is quite high, compared to other types of energy harvesters⁶⁹.

Figure 5.14 shows the voltage induced by an applied mechanical vibration, via the direct piezoelectric effect. These data were taken at a bending resonance frequency of 40 Hz and under a vibration acceleration of 1g . Measurements were made by mounting the laminate shown in Figure 5.13 on top of a shaker, where it was in a cantilever-like configuration, with its free end attached to a small mass of 1 gram . The two voltage outputs (from the two piezo-layers) generated by an acceleration of 1g were $\sim 60\text{V}_{\text{pp}}$; correspondingly, the calculated power density was $\sim 400\mu\text{W}/\text{g}\cdot\text{cm}^3$ at an external load of $3\text{M}\Omega$. The differential voltage output from these two piezoelectric fiber layers could be as high as 120V_{pp} , as can be seen in Fig.5.14. Practically, the output signal from piezoelectric layers can be separately rectified and conditioned before combining together.

The data presented in Figure 5.13 and 5.14 demonstrates that the ME laminates have capability to harvest both magnetic and mechanical energy. Figure 5.15 shows the combined response of the system. Figure 5.15a shows the voltage

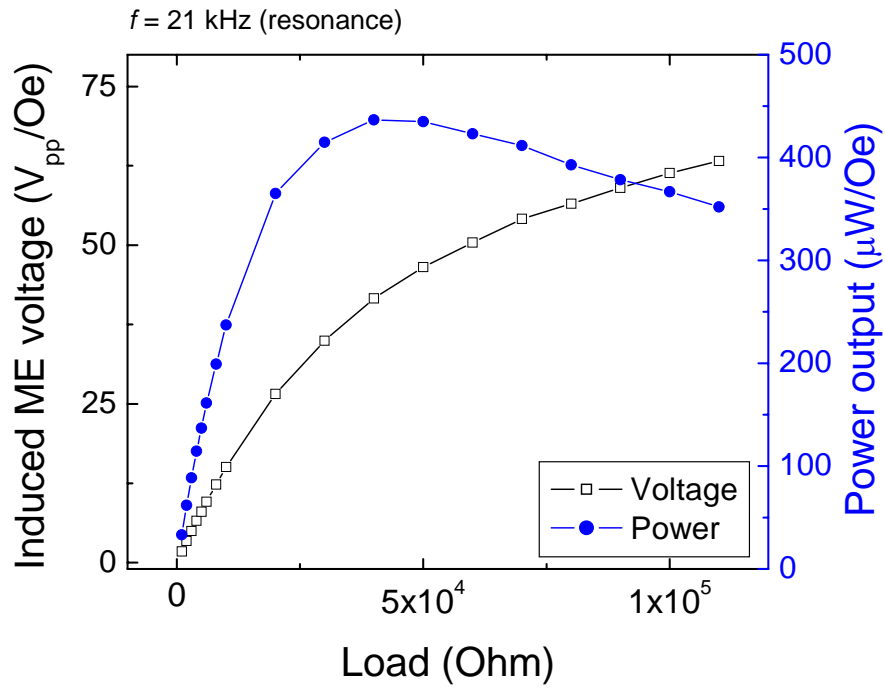


Figure 5.13 Voltage induced by “stray” magnetic field across the prototype as a function of electrical load.

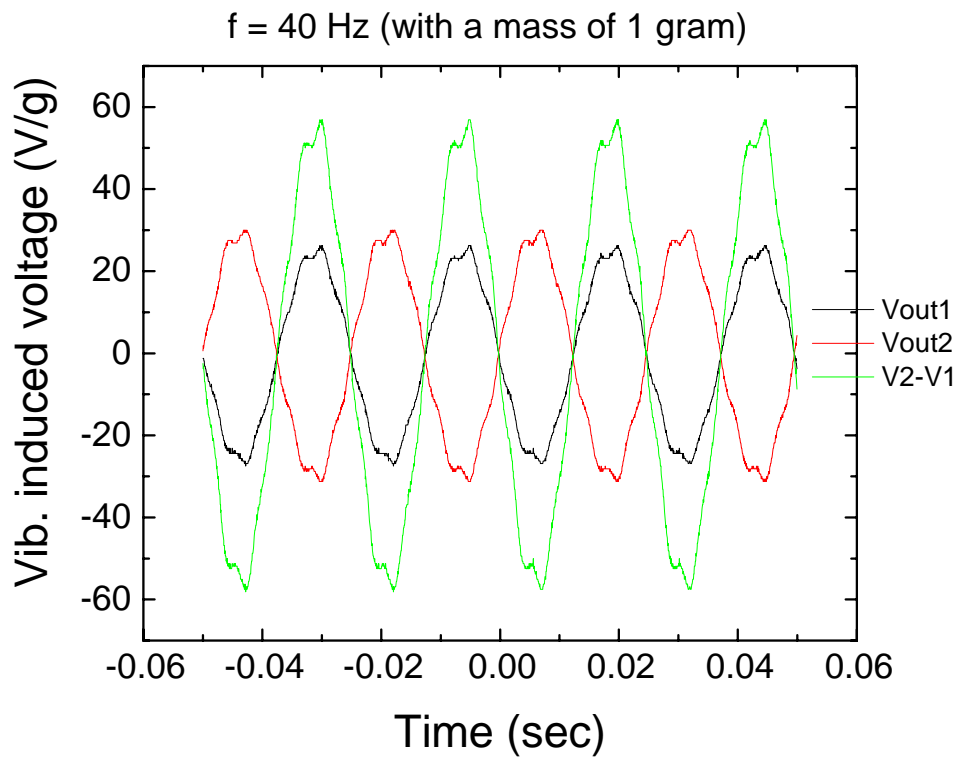


Figure 5.14 Voltage induced by “stray” vibration the prototype as a function of time.

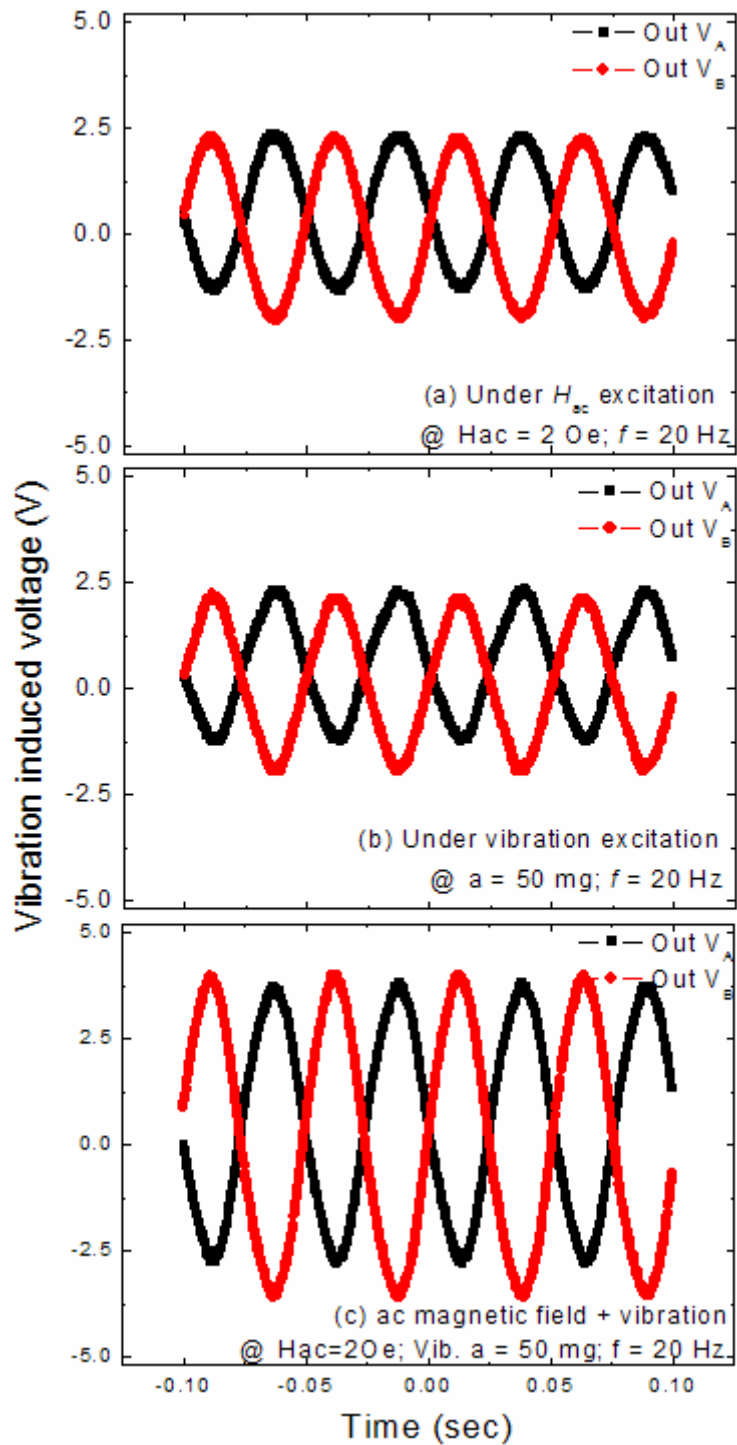


Figure 5.15 Experimental confirmation of the bi-mechanism for magnetic field and mechanical vibration energy harvesting: (a) under only a “stray” magnetic excitation of $H_{ac}=20\text{Oe}$ ($f=20\text{Hz}$), (b) under only a “stray” vibrational excitation of $a=50\text{mg}$ ($f=20\text{Hz}$), and (c) under both “stray” magnetic and vibrational excitations.

induced at the 1st bending mode by $H_{ac} = 2 \text{ Oe}$ ($f = 20 \text{ Hz}$), without any mechanical vibrations. The output voltages V_{out1} and V_{out2} were $\sim 4 V_{pp}$ (or $\sim 2V_{pp}/\text{Oe}$). Figure 5.15b shows the voltage induced at 1st bending mode by a mechanical vibration with an acceleration of 50 mg ($f = 20 \text{ Hz}$) without any applied magnetic field. The voltage V_{out1} and V_{out2} were found to be of the order of $\sim 4 V_{pp}$ (or $\sim 80V_{pp}/\text{g}$) (open circuit voltage). Figure 5.15c shows the voltage induced under a simultaneous magnetic field of $H_{ac}=2\text{Oe}$ and a mechanical vibration of amplitude 50mg ($50 \times 10^{-3} \times 9.8 \text{ m/s}^2$). This figure shows that the output voltages were doubled relative to a single source to $8V_{pp}$. The data clearly illustrate that the laminates responds to both the external magnetic field and mechanical vibrations. In the present investigation, both external inputs were imposed at the same frequency which enhanced the bending stress on the composites, resulting in doubling of the generated electric charge.

5.5 Section summary

In summary, four device applications have been constructed and tested that are based on the giant ME effect of magnetostrictive-piezoelectric laminate composites. The results of this chapter can be summarized, as follows:

- (i) ME laminates offer much potential for low-frequency (10^{-2} to 10^3 Hz) detection of minute magnetic fields (10^{-12}Tesla or below), at room temperature, in a passive mode of operation: such combinations of characteristics are not available in any other magnetic sensor. With a wrapped

active coil, the Metglas/PZT laminates also have a capable to achieve 0.8 nano-Tesla DC magnetic field change without an applied DC bias. For both DC and AC magnetic field sensors, the output voltage was linear to an applied magnetic field.

- (ii) A geomagnetic field sensor have been developed based on the giant magnetoelectric effect in Metglas/PZT-fiber laminates. This sensor does not need a DC bias to achieve an optimum performance, but rather is driven by a small AC current. This geomagnetic sensor was shown to have good anisotropy in the magnetic field direction, and a high sensitivity to variations in Earth's field of $H_{DC}=0.8$ nano-Tesla. Such low cost and low power consuming laminates (with wrapped coil) could offer potential applications in global positioning.
- (iii) While under EMR drive conditions, ME laminates have been shown to have high gyration effect. These findings indicate the potential existence of a fifth fundamental network element.
- (iv) Finally, a multimodal system has been developed for simultaneously harvesting mechanical vibration and magnetic energies. It is shown that the generated electric energy is a sum effect from the magneto-elasto-electric and the piezoelectric contributions. This design has significant promise for new energy harvesting components in environments where there is the presence of both stray vibrational and magnetic fields

VI. Conclusion and future work

6.1 Conclusion

In this dissertation, I have investigated the ME effect in piezoelectric/magnetostrictive laminate composites. This work not only has a material vision, but also has important findings relevant to applications.

It was found that Metglas based laminated composites have a large ME effect due to a large piezomagnetic coefficient. My findings show that besides magnetostriction, the permeability of the magnetic materials is also important for ME laminated composites, which had always been omitted in prior investigations. In addition, by use of large permeability materials, ME laminates can operate at dramatically smaller DC magnetic bias.

Prior work had shown that the structure of laminated composites could change both the ME voltage coefficient and optimum DC bias. In this thesis, I have found that the structure can also be used to reject environmental noise. Symmetric bimorph designs can reject thermal noise, and differential ones can dramatically decrease vibration noise. These findings show that laminated composite design itself can be used to increase the signal to noise ratio, for detection of small low frequency magnetic field variations.

The ME susceptibility is the fundamental property of the ME effect. I have determined the relationship between the ME susceptibility of laminates and the other fundamental properties of piezoelectric and magnetostrictive materials. The maximum

of the ME susceptibility is limited by the permeability and permittivity of the laminates. This finding helps in the select of materials for ME laminate composites.

Due to a shape demagnetization effect, the shape of ME laminates affects the internal magnetization and effective piezomagnetic coefficient. This resulted in significant changes in the ME effect upon changing laminate shape and geometry. A long, narrow and thin shape could enhance the ME effect in composites fabricated from identified materials. Also, the internal magnetization is not uniform along the longitudinal direction of the laminates, in particular, for high permeability materials. In high permeability materials, to achieve large ME effects, the magnetostrictive layer should be longer than the piezoelectric one.

Resonance ME voltage coefficients are known to be enhanced by a factor of 10-100x that at quasi-static frequency. However, the resonance frequency is limited over a narrow frequency range by material parameters and dimensions. I have developed a magnetic field tunable resonance frequency based on the giant magnetostriction of Terfenol-D. The origin of this effect is that the giant magnetostriction can tune the internal stress of the laminate, resulting in a wide tunable resonance frequency bandwidth.

Ultra-sensitivity AC passive and DC active magnetic sensors have been designed based on my advancements in ME materials. In the case of AC sensors, a sensitivity of 10^{-14} Tesla/Hz^{1/2} could be reached under resonance drive. In the case of quasi-static AC sensors, a sensitivity of 0.3Nano-Tesla was achieved. And, for DC ones, a sensitivity of 8NanoTesla is feasible. Furthermore, with a wrapped coil, the

ME laminates can serve as a gyrator, which is a fifth element in electronic circuit design. Finally, I have shown that ME laminates can harvest both stray magnetic and vibrational energy; a bi-mechanism for enhanced energy harvesting capabilities.

6.2 Suggested future work

ME laminates require a DC bias to achieve optimum performance. By using giant permeability materials and proper shape of the laminates, the optimum DC bias can be decreased to as small as 20e. However, a small DC bias is still needed a magnet. An important achievement for future research would be to develop a material that can operate without applied magnetic bias. Alternatively, one might find pre-magnetize the magnetic layer, such as incorporating a magnetic bias layer.

The giant permeability of Metglas not only decreases the required H_{dc} , but also increases the anisotropy of the ME coefficient: it can lens or repel flux, depending on the orientation of the laminate with respect to the field. In Section 3.2.2, it was shown only along the length axis of the laminate that there was a large magnetic-field induced voltage: whereas the other two perpendicular directions had essentially zero voltage response. Thus, one ME laminate can not measure the direction of a magnetic field. A pair of ME laminates, or three, each perpendicular to the other could sense not only intensity but also inclination of the magnetic field. The challenge is .for a set of laminates, in whether the ME effect of one laminate will alter the others? Also, a magnetic target movement can change the environmental magnetic flux. A question for future work is whether a set of ME laminates could measure the

target movement direction? For a fixed target movement direction and distance, it would be important to see whether the shape of the determined?

In this thesis, the laminates are bulk size. It is an interesting question to ask whether size changes to the nano-scale might make any difference to the ME effect? Nano-scale thin films could be deposited on a substrate. The thickness of the substrate is much thicker than that of film. The in-plane strain between each layer is restricted by the substrate, which might dramatically decrease the ME voltage coefficient. One method to solve this problem would be orient the interface out-plane. Another method is to remove the substrate at the bottom of the ME laminates. Also, for nano-scale ME composites, we need to ask if the shape will affect the ME effect? Finally, a small voltage might be used to change the strain of the thin film, realizing electrically tunable resonance frequencies.

REFERENCE

- 1 M. Fiebig, "Revival of the magnetoelectric effect," *J. Phys. D: Appl. Phys.* **38** (8), 123 (2005).
- 2 D.N. Astrov, "Magnetoelectric effect in antiferromagnetic Cr_2O_3 ," *Sov. Phys. JETP* **13**, 2 (1961).
- 3 G.T. Rado and V.J. Folen, "Observation of the Magnetically Induced Magnetoelectric Effect and Evidence for Antiferromagnetic Domains," *Phys. Rev. Lett.* **7**, 310 (1961).
- 4 J. van den Boomgaard and R.A.J. Born, "A Sintered Magnetoelectric Composite Material $\text{BaTiO}_3\text{-Ni}(\text{Co}, \text{Mn}) \text{Fe}_3\text{O}_4$," *J. Mater. Sci.* **13**, 1538 (1978).
- 5 J. van den Boomgaard, A.M.J.G. Van Run, and J. Van Suchtelen, "Magnetoelectricity in piezoelectric-magnetostrictive composites," *Ferroelectrics* **10**, 295 (1976).
- 6 T. G. Lupeiko, S. S. Lopatin, I. V. Lisnevskaya et al., "Magnetoelectric Composite-Materials Based on Lead-Zirconate-Titanate and Nickel Ferrite," *Inorg. Mater.* **30** (11), 1353 (1994).
- 7 M. I. Bichurin, I. A. Kornev, V. M. Petrov et al., "Investigation of magnetoelectric interaction in composite," *Ferroelectrics* **204** (1-4), 289 (1997).
- 8 M. I. Bichurin, V. M. Petrov, Y. V. Kiliba et al., "Magnetic and magnetoelectric susceptibilities of a ferroelectric/ferromagnetic composite at microwave frequencies," *Phys. Rev. B* **66** (13), 134404 (2002).
- 9 J. Y. Zhai, N. Cai, Z. Shi et al., "Magnetic-dielectric properties of $\text{NiFe}_2\text{O}_4/\text{PZT}$ particulate composites," *J. Phys. D: Appl. Phys.* **37** (6), 823 (2004).
- 10 M. I. Bichurin, D. A. Filippov, V. M. Petrov et al., "Resonance magnetoelectric effects in layered magnetostrictive-piezoelectric composites," *Phys. Rev. B* **68** (13), 132408 (2003).
- 11 G. Srinivasan, E. T. Rasmussen, J. Gallegos et al., "Magnetoelectric bilayer and multilayer structures of magnetostrictive and piezoelectric oxides," *Phys. Rev. B* **66** (2), 214408 (2002).
- 12 J. Y. Zhai, N. Cai, Z. Shi et al., "Coupled magnetodielectric properties of laminated $\text{PbZr}_{0.53}\text{Ti}_{0.47}\text{O}_3/\text{NiFe}_2\text{O}_4$ ceramics," *J. Appl. Phys.* **95** (10), 5685 (2004).
- 13 C. W. Nan, "Magnetoelectric Effect in Composites of Piezoelectric and Piezomagnetic Phases," *Phys. Rev. B* **50** (9), 6082 (1994).
- 14 K. Srinivas, G. Prasad, T. Bhimasankaram et al., "Electromechanical coefficients of magnetoelectric $\text{PZT-CoFe}_2\text{O}_4$ composite," *Mod. Phys. Lett. B* **14** (17-18), 663 (2000).

- 15 H. X. Fu and R. E. Cohen, "Polarization rotation mechanism for ultrahigh electromechanical response in single-crystal piezoelectrics," *Nature* **403** (6767), 281 (2000).
- 16 E. Fukada, "History and recent progress in piezoelectric polymers," *Ieee Transactions on Ultrasonics Ferroelectrics and Frequency Control* **47** (6), 1277 (2000).
- 17 L. Sandlund, M. Fahlander, T. Cedell et al., "Magnetostriction, Elastic-Moduli, and Coupling Factors of Composite Terfenol-D," *J. Appl. Phys.* **75** (10), 5656 (1994).
- 18 S. Guruswamy, N. Srisukhumbowornchai, A. E. Clark et al., "Strong, ductile, and low-field-magnetostrictive alloys based on Fe-Ga," *Scripta Materialia* **43** (3), 239 (2000).
- 19 R. Malmhall, G. Backstrom, K. V. Rao et al., "Metglas 2826b - Transport, Magnetic and Thermal-Properties," *J. Appl. Phys.* **49** (3), 1727 (1978).
- 20 S. X. Dong, J. F. Li, and D. Viehland, "Ultrahigh magnetic field sensitivity in laminates of TERFENOL-D and $\text{Pb}(\text{Mg}_{1/3}\text{Nb}_{2/3})\text{O}-3\text{-PbTiO}_3$ crystals," *Appl. Phys. Lett.* **83** (11), 2265 (2003).
- 21 S. X. Dong, J. Y. Zhai, N. G. Wang et al., "Fe-Ga/ $\text{Pb}(\text{Mg}_{1/3}\text{Nb}_{2/3})\text{O}-3\text{-PbTiO}_3$ magnetoelectric laminate composites," *Appl. Phys. Lett.* **87** (22), 222504 (2005).
- 22 K. Mori and M. Wuttig, "Magnetoelectric coupling in terfenol-D/polyvinylidenedifluoride composites," *Appl. Phys. Lett.* **81** (1), 100 (2002).
- 23 J. Y. Zhai, S. X. Dong, Z. P. Xing et al., "Giant magnetoelectric effect in Metglas/polyvinylidene-fluoride laminates," *Appl. Phys. Lett.* **89** (8), 083507 (2006).
- 24 S. X. Dong, J. Y. Zhai, J. F. Li et al., "Near-ideal magnetoelectricity in high-permeability magnetostrictive/piezofiber laminates with a (2-1) connectivity," *Appl. Phys. Lett.* **89** (25), 252904 (2006).
- 25 S. Dong, J. Zhai, F. Bai et al., "Push-pull mode magnetostrictive/piezoelectric laminate composite with an enhanced magnetoelectric voltage coefficient," *Appl. Phys. Lett.* **87** (6), 062502 (2005).
- 26 S. X. Dong, J. F. Li, and D. Viehland, "A longitudinal-longitudinal mode TERFENOL-D/ $\text{Pb}(\text{Mg}_{1/3}\text{Nb}_{2/3})\text{O}-3\text{-PbTiO}_3$ laminate composite," *Appl. Phys. Lett.* **85** (22), 5305 (2004).
- 27 S. X. Dong, J. F. Li, and D. Viehland, "Longitudinal and transverse magnetoelectric voltage coefficients of magnetostrictive/piezoelectric laminate composite: Theory," *Ieee Transactions on Ultrasonics Ferroelectrics and Frequency Control* **50** (10), 1253 (2003).
- 28 S. X. Dong, J. F. Li, and D. Viehland, "Voltage gain effect in a ring-type magnetoelectric laminate," *Appl. Phys. Lett.* **84** (21), 4188 (2004).
- 29 S. X. Dong, J. Y. Zhai, F. M. Bai et al., "Magnetostrictive and magnetoelectric behavior of Fe-20 at. % Ga/Pb(Zr,Ti)O-3 laminates," *J. Appl. Phys.* **97** (10), 103902 (2005).

- 30 S. X. Dong, J. F. Li, and D. Viehland, "Vortex magnetic field sensor based on
ring-type magnetoelectric laminate," *Appl. Phys. Lett.* **85** (12), 2307 (2004).
- 31 S. X. Dong, J. F. Li, and D. Viehland, "Giant magnetoelectric effect in
laminated composites," *Philosophical Magazine Letters* **83** (12), 769 (2003).
- 32 S. X. Dong, J. F. Li, and D. Viehland, "Characterization of magnetoelectric
laminated composites operated in longitudinal-transverse and
transverse-transverse modes," *J. Appl. Phys.* **95** (5), 2625 (2004).
- 33 J. Y. Zhai, Z. P. Xing, S. X. Dong et al., "Detection of pico-Tesla magnetic
fields using magneto-electric sensors at room temperature," *Appl. Phys. Lett.*
88 (6), 062510 (2006).
- 34 S. X. Dong, J. F. Li, and D. Viehland, "Circumferentially magnetized and
circumferentially polarized magnetostrictive/piezoelectric laminated rings," *J.*
Appl. Phys. **96** (6), 3382 (2004).
- 35 S. X. Dong, J. G. Bai, J. Y. Zhai et al., "Circumferential-mode, quasi-ring-type,
magnetoelectric laminate composite - a highly sensitive electric current and/or
vortex magnetic field sensor," *Appl. Phys. Lett.* **86** (18), 182506 (2005).
- 36 J. G. Wan, Z. Y. Li, Y. Wang et al., "Strong flexural resonant magnetoelectric
effect in Terfenol-D/epoxy-Pb(Zr,Ti)O-3 bilayer," *Appl. Phys. Lett.* **86** (20),
202504 (2005).
- 37 Z. P. Xing, S. X. Dong, J. Y. Zhai et al., "Resonant bending mode of
Terfenol-D/steel/Pb(Zr,Ti)O-3 magnetoelectric laminate composites," *Appl.*
Phys. Lett. **89** (11), 112911 (2006).
- 38 M. Avellaneda and G. Harshe, "Magnetoelectric Effect in Piezoelectric
Magnetostrictive Multilayer (2-2) Composites," *J. Intell. Mater. Syst. Struct.* **5**
(4), 501 (1994).
- 39 G. Harshe, J. P. Dougherty, and R. E. Newnham, "Magnetoelectric Effect in
Composite-Materials," *Mathematics in Smart Structures* **1919**, 224 (1993).
- 40 Y. K. Fetisov and G. Srinivasan, "Electrically tunable ferrite-ferroelectric
microwave delay lines," *Appl. Phys. Lett.* **87** (10), 103502 (2005).
- 41 G. Srinivasan, A. S. Tatarenko, and M. I. Bichurin, "Electrically tunable
microwave filters based on ferromagnetic resonance in ferrite-ferroelectric
bilayers," *Electronics Letters* **41** (10), 596 (2005).
- 42 G. Srinivasan, R. Hayes, and M. I. Bichurin, "Low frequency and microwave
magnetoelectric effects in thick film heterostructures of lithium zinc ferrite
and lead zirconate titanate," *Solid State Communications* **128** (6-7), 261
(2003).
- 43 S. X. Dong and J. Y. Zhai, "Equivalent circuit method for static and dynamic
analysis of magnetoelectric laminated composites," *Chinese Science Bulletin*
53 (14), 2113 (2008).
- 44 B.D.H. Tellegen, "Gyrator," *Phillips Research Reports* **3**, 81 (1948).
- 45 L. X. Bian, Y. M. Wen, P. Li et al., "Magnetostrictive/Piezoelectric
magnetoelectric transducer with an elastic substrate," *2007 Ieee Sensors* **1-3**,
892 (2007).

- 46 X. H. Wu, Y. P. Shen, and Q. Sun, "Lamb wave propagation in
magnetoelastic plates," *Applied Acoustics* **68** (10), 1224 (2007).
- 47 N. Tiercelin, V. Preobrazhensky, P. Pernod et al., "Enhanced magnetoelectric
effect in nanostructured magnetostrictive thin film resonant actuator with field
induced spin reorientation transition," *Appl. Phys. Lett.* **92** (6), 062904 (2008).
- 48 Z. Kossowski and K. Kopias, "Magnetolectric driving device for
displacements of a guide needle bar in a weaving loom," *Fibres & Textiles in
Eastern Europe* **14** (2), 76 (2006).
- 49 R. E. Newnham, D. P. Skinner, and L. E. Cross, "Connectivity and
Piezoelectric-Pyroelectric Composites," *Materials Research Bulletin* **13** (5),
525 (1978).
- 50 S. X. Dong, J. Y. Zhai, Z. P. Xing et al., "Extremely low frequency response
of magnetoelectric multilayer composites," *Appl. Phys. Lett.* **86** (10), 102901
(2005).
- 51 Z. P. Xing, J. Y. Zhai, S. X. Dong et al., "Modeling and detection of
quasi-static nanotesla magnetic field variations using magnetoelectric laminate
sensors," *Measurement Science & Technology* **19** (1), 015206 (2008).
- 52 J. Y. Zhai, J. F. Li, S. X. Dong et al., "A quasi(unidirectional) Tellegen
gyrator," *J. Appl. Phys.* **100** (12), 124509 (2006).
- 53 Y. Yan, M. B. Liu, H. M. Jin et al., "Effects of shape and number of grains on
the demagnetization curve calculated for nanocrystalline Nd₂Fe₁₄B magnets,"
Physica B-Condensed Matter **364** (1-4), 273 (2005).
- 54 S. X. Dong, J. F. Li, and D. Viehland, "Magnetolectric coupling, efficiency,
and voltage gain effect in piezoelectric-piezomagnetic laminate composites,"
Journal of Materials Science **41** (1), 97 (2006).
- 55 H. Yu, M. Zeng, Y. Wang et al., "Magnetolectric resonance-bandwidth
broadening of terfenol-D/epoxyPb(Zr,Ti)O-3 bilayers in parallel and series
connections," *Appl. Phys. Lett.* **86** (3), 032508 (2005).
- 56 R. Salmelin, R. Hari, O. V. Lounasmaa et al., "Dynamics of Brain Activation
during Picture Naming," *Nature* **368** (6470), 463 (1994).
- 57 T.R. Clem, *Naval Research Reviews* **3**, 29 (1997).
- 58 J. Vrba and S. E. Robinson, "SQUID sensor array configurations for
magnetoencephalography applications," *Superconductor Science &
Technology* **15** (9), 51 (2002).
- 59 J. Vrba and S. E. Robinson, "Signal processing in magnetoencephalography,"
Methods **25** (2), 249 (2001).
- 60 L. Hao, J. C. Macfarlane, P. Josephs-Franks et al., "Inductive superconducting
transition-edge photon and particle detector," *Ieee Transactions on Applied
Superconductivity* **13** (2), 622 (2003).
- 61 H. J. Barthelmeß, M. Halverscheid, B. Schiefenhovel et al., "Low-noise
biomagnetic measurements with a multichannel dc-SQUID system at 77 K,"
Ieee Transactions on Applied Superconductivity **11** (1), 657 (2001).

- ⁶² M. N. Baibich, J. M. Broto, A. Fert et al., "Giant Magnetoresistance of (001)Fe/(001) Cr Magnetic Superlattices," *Phys. Rev. Lett.* **61** (21), 2472 (1988).
- ⁶³ M. Pannetier, C. Fermon, G. Le Goff et al., "Femtotesla magnetic field measurement with magnetoresistive sensors," *Science* **304** (5677), 1648 (2004).
- ⁶⁴ P. D. D. Schwindt, S. Knappe, V. Shah et al., "Chip-scale atomic magnetometer," *Appl. Phys. Lett.* **85** (26), 6409 (2004).
- ⁶⁵ W. W. Cochran, H. Mouritsen, and M. Wikelski, "Migrating songbirds recalibrate their magnetic compass daily from twilight cues," *Science* **304** (5669), 405 (2004).
- ⁶⁶ K. J. Lohmann, C. M. F. Lohmann, L. M. Ehrhart et al., "Animal behaviour - Geomagnetic map used in sea-turtle navigation," *Nature* **428** (6986), 909 (2004).
- ⁶⁷ S. X. Dong, J. Y. Zhai, J. F. Li et al., "Small dc magnetic field response of magnetoelectric laminate composites," *Appl. Phys. Lett.* **88** (8), 082907 (2006).
- ⁶⁸ R. C. White, T. Long, and T. W. Schneider, "Development of miniature electro-mechanical pressure sensor arrays (MEMPSA) for high resolution thermospheric and mesospheric neutral wind measurement," *Advanced Environmental and Chemical Sensing Technology* 4205, 248 (2001).
- ⁶⁹ H. A. Sodano, J. Lloyd, and D. J. Inman, "An experimental comparison between several active composite actuators for power generation," *Smart Structures and Integrated Systems* 5390, 370 (2004).